UNIVERSITÀ DEGLI STUDI DI PADOVA

Dipartimento di Agronomia Animali Alimenti Risorse Naturali E Ambiente

Dipartimento di Biologia

CORSO DI LAUREA MAGISTRALE IN SCIENZE E TECNOLOGIE PER L'AMBIENTE E IL TERRITORIO

Tesi di laurea magistrale

Stress granules as a post-transcriptional regulation tool of antioxidant defenses in *Squalius cephalus* chronically exposed to PFAS in the rivers of the Veneto region

Relatore:

Prof. Gianfranco Santovito

Correlatrici:

Dr.ssa Sara Pacchini

Dr.ssa Laura Drago

Laureanda:

Martina Cortese

Matricola n. 2079298

Anno accademico: 2023/2024

INDEX

RIASSUNTO (Versione italiana)

Le sostanze poli- e per-fluoroalchile (PFAS) sono dei contaminanti che si sono diffusi in tutto il mondo a causa del loro ampio utilizzo e delle loro caratteristiche chimico-fisiche, che li rendono estremamente persistenti in ambiente. Nel 2013 un'importante contaminazione da PFAS fu individuata nelle acque della regione Veneto, in Italia. Da allora numerose ricerche si sono concentrate nel capire l'effetto di queste sostanze sulla salute umana, ma le PFAS possono possono anche bioaccumularsi nei tessuti animali, influenzando la fauna che vive nelle acque dolci contaminate da questi.

Studi precedenti hanno analizzato le risposte fisiologiche della specie *Squalius cephalus* (cavedano) in seguito ad un'esposizione cronica alle PFAS nei fiumi del Veneto. I risultati hanno evidenziato un effetto di questi inquinanti sul sistema antiossidante dei pesci. Inoltre, l'azione degli stress granules (SGs, foci citoplasmatici contenenti mRNA e proteine, solitamente formatisi durante condizioni di stress per proteggere l'mRNA da eventuali danni) è stata ipotizzata come strumento post-trascrizionale. Questi foci possono infatti dissasemblarsi in caso di stress per rendere disponibile il trascritto per la traduzione in proteine anti-stress, ad esempio gli enzimi antiossidanti.

Individui di *S. cephalus* sono stati pescati, tramite elettropesca, in quattro siti della provincia di Vicenza aventi concentrazioni crescenti di PFAS. Varie analisi sono state effettuate su campioni di fegato e di rene caudale. In particolare sono state quantificate l'espressione dell'mRNA e l'attività tissutale di glutatione perossidasi selenio dipendente e catalasi, e confrontate con l'espressione dell'mRNA di tre proteine legate agli SGs: tritrestrapolin (*ttp*), Stress Granule Assembly Factor (*g3bp*), e TIA-1 related nucleolysin (*tiar*). Le analisi dell'espressione dell'mRNA sono state effettuate mediante qRT-PCR, mentre l'attività degli enzimi è stata studiata mediante saggi biochimici.

Un'alta presenza di messagero è stata rilevata per *gpx4* e *cat* sia nel fegato che nel rene caudale del sito altamente inquinato. Inoltre, *ttp* sembra avere un ruolo importante nella regolazione dei trascritti nel rene, probabilmente tramite la formazione degli SGs.

I risultati ottenuti rappresentano un punto di partenza nello studio della correlazione tra stress ossidativo indotto dagli PFAS e assemblaggio/disassemblaggio degli SGs. Ricerche future si concentreranno sullo studio di altri componenti sia del sistema antiossidante, sia degli SGs, per avere un quadro più completo delle risposte fisiologiche indotte negli organismi esposti a stress cronico e meglio capire l'interazione tra gli SGs e gli enzimi antiossidanti.

SUMMARY (English version)

Poly- and perfluoroalkyl substances PFAS are pollutants that have spread worldwide due to their extensive use and chemical-physical characteristics, which make them extremely persistent in the environment. Since the discovery of a major contamination in 2013 in the freshwater of the Veneto region (Italy), extensive research has been conducted to evaluate the damage entity and understand the effect of these compounds on human health. Nevertheless, they can also bioaccumulate into animal tissues, affecting fauna that live in contaminated freshwater habitats, such as fish.

Previous studies have analysed the physiological responses of *Squalius cephalus* (chub) following chronic exposure to PFAS in the Veneto rivers. The results highlighted these pollutants' effect on the fish's antioxidant system. Furthermore, the action of stress granules (SGs, cytoplasmic foci containing mRNA, typically formed under stress conditions to protect mRNA from damage) was also hypothesized as a post-transcriptional regulation tool. These foci can disassemble and make mRNA available for translation; this can be helpful in stress conditions because it can increase the formation of anti-stress proteins, such as antioxidant enzymes.

Specimens of *S. cephalus* were collected by electrofishing in four different rivers of the Vicenza province, each presenting a different concentration of total PFAS. Analyses were conducted on those specimens' caudal kidney and liver samples. The mRNA expression and the tissue activity of selenium-dependent glutathione peroxidase and catalase were investigated and then compared to the mRNA expression of three SG components: tritrestrapolin (*ttp*), Stress Granule Assembly Factor (*g3bp*), and TIA-1 related nucleolysin (*tiar*). The mRNA expression analyses were done through qRT-PCR while the enzyme activity was investigated through biochemical essays.

A major *gpx4* and *cat* transcript presence was discovered in the highly-polluted site for both organs. Furthermore, *ttp* seems to have an important role in caudal kidney transcript regulation, probably through the formation of SGs.

The obtained results represent a starting point in studying the correlation between oxidative stress induced by PFAS and the assembly/disassembly of SGs. Further

research will focus on studying other components of both the antioxidant system and SGs to have a complete picture of the physiological responses induced in organisms exposed to chronic stress and better understand the interaction between stress granules and antioxidant enzymes.

ACRONYMS USED IN THE TEXT

ANOVA	One-way variance analysis
ARPAV	Regional Agency for Environmental Prevention and Protection of Veneto
CAT	Catalase protein
cat	Catalase gene
CDS	Coding sequences
ECF	Electro Chemical Fluorination
eIF	eukaryotic Initiation Factor
ER	Endoplasmic Reticulum
ETC	Electron-Transport Chain
FCF	Fulton's Condition Factor
f_{OC}	Fraction of organic carbon in solid
G3BP	Stress Granule Assembly Factor
GCN2	General control nonderepressible 2
GPx	Glutathione peroxidases protein
gpx	Glutathiona peroxidases gene
GR	Glutathione Reductase
GSH	Glutathione
GST	Glutathione-S-transferase protein
HIS	Hepatosomatic Index
HRI	Heme- regulated inhibitor
IDRs	Intrinsically disordered regions
K_D	Adsorption-desorption distribution coefficient
K_{OC}	Organic carbon-water distribution coefficient
K_{OW}	n-Octanol/Water partition coefficient
LOQ	Limit Of Quantification
LPO	Lipid Peroxidation
mRNP	Non-translating messenger ribonucleoprotein
NOM	Natural Organic Matter
PBs	Processing Bodies

PERK	PKR endoplasmic reticulum kinase
PFAAs	Perfluoroalkyl acids
PFAS	Per- and poly-fluoroalkyl substances
PFOA	Perfluorooctanoic acid
PFOS	Perfluorooctane sulfonic acid
PFSAs	Perfluoroalkane sulfonic acids and sulfonates
PKR	Protein kinase R
Prdx	Peroxiredoxins protein
prdx	Peroxiredoxin gene
PxxP	Proline-rich motif
ROS	Reactive Oxygen Species
RRM	RNA recognition motif
SE	Standard Error
Se-GPx	Selenium-dependent GPx
SGs	Stress Granules
SOD	Superoxide dismutase protein
sod	Superoxide dismutase gene
SSI	Spleen Somatic Index
TIA	T-cell-restricted intracellular antigen
TIAR	TIA-1 related nucleolysin
TTP	Tritrestrapolin

1 INTRODUCTION

Since the beginning of civilisation, populations have always settled near waterways, as water is an essential element in human and animal life. However, the relationship between humans and this vital element has changed in the past few centuries. With the advent of the Industrial Revolution, many substances have been dumped in rivers, lakes, and marine waters, causing large-scale pollution. The problem was that people (who drank the water) and ecosystems living within these waters were affected.

At some point, it became clear that creating a system capable of monitoring what was being poured into the waters and what was in them became necessary. Since then, a series of regulatory systems have been introduced in Italy, and thanks to the evolution of scientific knowledge, each new method has enabled scientists to find new substances and detect lower concentrations. However, a problem remains: while some compounds are identifiable, many other substances are more difficult to identify, and their presence in the water we drink and the habitats animals live in is not always known.

Constant analyses are performed on drinking, fresh, and marine waters, but they focus only on known analytes regulated by specific values, such as EQS (environmental quality standards) and threshold concentrations. This system only considers “emerging contaminants” partially, with this term intended to indicate those pollutants that are not commonly monitored but can cause damage to the environment and humans. It is therefore important to find these substances through non-target analysis and research them to answer questions like where they came from, their effect on the environment and human health, and how they can be analyzed and removed. Once an emerging contaminant has been identified and its characteristics have been studied, it becomes an official pollutant. The next step is the regulation of its threshold values, which can be modified if new scientific information is discovered.

1.1 THE PFAS

These pollutants are per- and poly-fluoroalkyl substances (PFAS), synthetic compounds characterized by multiple fluorine atoms bound to an alkyl chain.

The first PFAS appearance dates back to the 1930s, and due to their special/unique industrial characteristics, they have been used worldwide since then. To better understand the extent of the PFAS phenomenon, it is worth noting that Teflon®, produced by DuPont, was used during World War II. Since then, PFAS production has grown steadily. In particular, perfluorooctanoic acid (PFOA) and perfluorooctane sulfonic acid (PFOS) have been employed in a wide range of fields, from carpeting to dental floss (Renfrew and Pearson, 2021).

As a result of the widespread use of these substances, PFAS have started to be found not only in several environmental compounds, such as water and sediments (Zareitalabad et al., 2013), but also in living organisms, especially the ones that live in industrialized regions (Giesy and Kannan, 2001).

Therefore, the effect of PFAS on human health has raised public interest. In particular, long-chain PFAS (those with seven or more fluorinated carbon, such as the PFOA and PFOS mentioned above) have attracted attention since the late 1990s. As a result, PFOA has been added to Annex A of the Stockholm Convention (2001) and is now considered a Persistent Organic Pollutant (POP). However, there are many more PFAS that need to be studied and about which very little is known (Wang et al., 2017).

As previously mentioned, PFAS have a wide range of uses. This peculiarity makes them challenging to substitute, as alternatives are not always available. Understanding the most important uses of these compounds can help evaluate which ones are essential, which can't be eliminated due to the lack of satisfying alternatives, and which can be easily replaced (Glüge et al., 2020).

1.1.1 PFAS chemistry and properties

As mentioned, PFAS are characterized by multiple fluorine atoms bound to an alkyl chain. They contain one or more C atoms on which all H atoms are substituted with F atoms, resulting in the formula C_nF_{2n+1} (Buck et al., 2011). Therefore, they must contain at least one perfluorinated methyl group or one perfluorinated methylene group. It is worth mentioning that there isn't a general definition of PFAS, and their classification is always evolving.

PFAS can generally be divided into two main groups: non-polymeric and polymeric molecules. The second group can be further subdivided into perfluoroalkyl substances (characterised by a hydrophobic carbon chain that is wholly fluorinated except for the terminal end) and poly-fluoroalkyl substances (in which some C atoms are partially fluorinated and bond to an O or H atom). PFOA and PFOS (Figure 1.1), probably the most well-known among these substances, are included in the perfluoroalkyl acids (PFAAs) group, a subgroup of the perfluoroalkyl category.

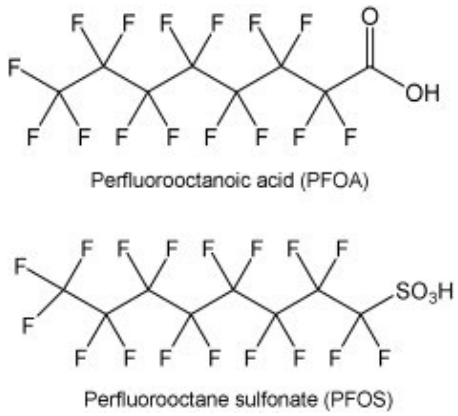

Figure 1.1) Chemical structure of PFOA and PFOS

The non-polymeric PFAS are also divided into groups: fluoropolymers (where most of the H atoms are replaced with F), side-chain fluorinated polymers (with a non-fluorinated carbon chain), and perfluoropolyether (where O and F are bound to the C atoms of the main chain) (Panieri et a., 2022). The general structure of these non-polymeric PFAS is depicted in Figure 1.2, and the subgroups in Table 1.1.

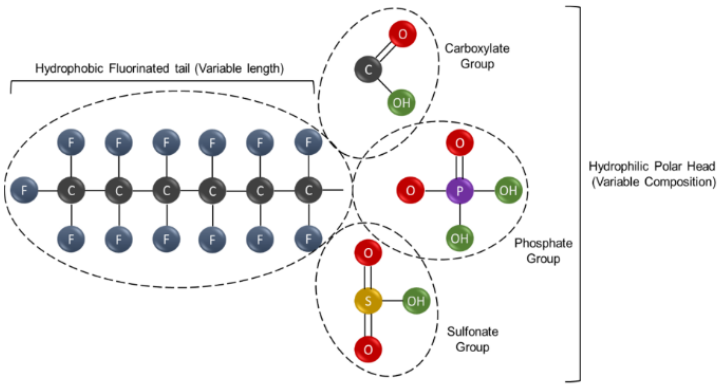

Figure 1.2) General structure of non-polymeric PFAS (Panieri et al., 2022)

Table 1.1 List and categorization of the main PFAS

Non-Polymeric PFAS		Polymeric PFAS
Perfluorinated PFAS	**Polyfluorinated PFAS**	-
-Perfluoroalkyl acids (PFAAs) -Perfluoroalkane sulfonic acids and sulfonates (PFSAs) -Perfluoroalkane sulfonic acids (PFSIAs) -Perfluorocarboxylic acids & carboxylates (PFCAs) -Perfluoroalkyl phosphonic acids (PFPAs) -Perfluoroalkyl phosphinic acids (PFPIAs)	Fluorotelomer compounds (FT)	Fluoropolymers
Perfluoroalkane sulfonamides (PFEAs)	Perfluoroalkane sulfonamido compounds (Me/Et/Bu-FASAs)	Side-chain Fluorinated Polymers
Perfluoroalkane sulfonamides (FASA)		Perfluoropolyethers (PFPEs)
Perfluoroalkane sulfonyl fluorides (PASFs)		
Perfluoroalkyl iodides (PFAIs)		
Perfluoroalkanoyl fluorides (PAFs)		
Perfluoroalkyl aldehydes (PFALs)		

PFAS are characterized by persistence, mobility, and bioaccumulation potential, all of which derive from their chemical composition. Generally, two factors evaluate persistence and mobility: the half-life threshold ($t_{1/2}$) and the organic carbon-water distribution coefficient (K_{OC}).

$$K_D = C_{solid}/C_{water}$$

$$K_{OC} = K_D/f_{oc}$$

It is worth mentioning that half-lives depend on various factors such as temperature, pH, oxygen level, and bioavailability. Consequently, another factor can be considered to evaluate the persistence of a pollutant, the overall persistence (P_{OV}), as it accounts for interactions between compartments (Arp and Hale, 2022).

Persistence

In general, PFAS are considered highly persistent under natural conditions. They are very resistant to environmental and metabolic degradation due to perfluoroalkyl moieties. Some are non-degradable, while others may be degraded into highly stable products like PFAAs. This group includes PFCAs, perfluoroether carboxylic acids (PFECAs), perfluoroether sulfonic acids (PFESAs), and PFSAs (Wang et al., 2017).

The presence of the C-F bond, the strongest bond in organic chemistry, makes PFAS persistent. This bond is even stronger when there is more than one on the same germinal carbon. Combined with the high electronegativity of fluorine, the C-F bond prevents reactions between PFAS and nucleophile elements. In addition, the presence of fluorines in perfluoroalkyl moieties reinforces the C-C bond in the chain.

As said before, the half-life of a chemical is typically used to describe its persistence. However, it is sometimes difficult to quantify this value. This is not the case for PFAS, considered the "forever chemicals" and show the highest persistent level among all organic substances. For example, under the European Chemical Agency's REACH regulation (Registration, Evaluation, Authorisation and Restriction of CHemicals), PFAS are classified as very persistent.

The main problem with persistent pollutants is that they accumulate inside matrices over time, increasing exposure. This way, when the adverse effects of the contaminants are discovered, the contamination is too widespread to be efficiently controlled (Cousins et al., 2020).

Mobility

In general, PFAS are considered mobile compounds which can be found worldwide, including in Antarctica (Xie and Kallenborn, 2023). On a global scale, PFAS distribution occurs due to atmospheric transport, while on a terrestrial scale, the transport of those compounds happens through aqueous advection. In this case, PFAS mobility depends on the presence of NOM (natural organic matter), minerals, and the fluid-fluid interface (air-water) interaction.

Some experiments have shown that the K_{OC} of PFOA and PFOS is, respectively, 3,7 and 4,2 (Zareitalabad et al., 2013). The n-Octanol/Water Partition Coefficient (K_{OW}) can be used to express the tendency of a substance to be adsorbed into organic matter. The higher the value, the more the substance will tend to be absorbed. Furthermore, K_{OC} depends on K_D (distribution coefficient), which describes the tendency of a substance to divide between liquid and solid phases. A lower K_D favours a higher environmental mobility, as a lower K_D value corresponds to a lower K_{OC} value, which means that the substance tends to be absorbed into organic matter. Therefore, the mobility of PFAS doesn't strictly depend on aqueous advection but more on the presence of NOM.

Bioaccumulation

The other important characteristic of PFAS is their tendency to bioaccumulate within organisms. PFAS bioaccumulation depends not only on various environmental factors but also on the unique chemical characteristics of PFAS. More specifically, the presence of fluorine and its polar hydrophobic nature make PFAS particularly affine with proteins. They also tend to remain inside the body for a long time due to the presence of halogens.

PFAS bioaccumulation depends on the chemical characteristics of each single compound so that different PFAS can accumulate in various body parts. Regarding humans, the highest concentrations of perfluorobutanoic acid are found in the kidneys and lungs, which also tend to accumulate more PFAS. In contrast, perfluorohexanoic acid is mainly concentrated in the liver and brain (Pérez et al., 2013).

Fish are positioned at a high level of the trophic chain, so they tend to accumulate more PFAS due to biomagnification. It is, therefore, logical that carnivorous fish accumulate more PFAS than omnivorous fish, especially the long-chain ones (likely because the PFAS sources for herbivorous fish are plants).

Some studies revealed that in fish, PFAS accumulate more in the blood and liver tissues and less in other tissues such as kidney, gills, and intestine; the muscle accumulation is very low. Different kinds of PFAS accumulate in humans and fish in various body parts. Furthermore, PFAS do not bind with just any proteins; they prefer specific ones, such as liver fatty acids binding proteins and serum albumin.

Long-chain PFAS tend to be more bioaccumulated in fish, with PFOS supremacy. However, bioaccumulation is also influenced by the function groups. For example, carboxyl acid groups form two bonds with binding sites, while sulfonic acids form three (Lewis et al., 2022).

1.1.2 PFAS in the Veneto region, a study case

During the summer of 2013, a significant PFAS contamination of shallow waters, groundwaters and drinking waters was discovered in the Veneto region in Italy (Figure 1.3).

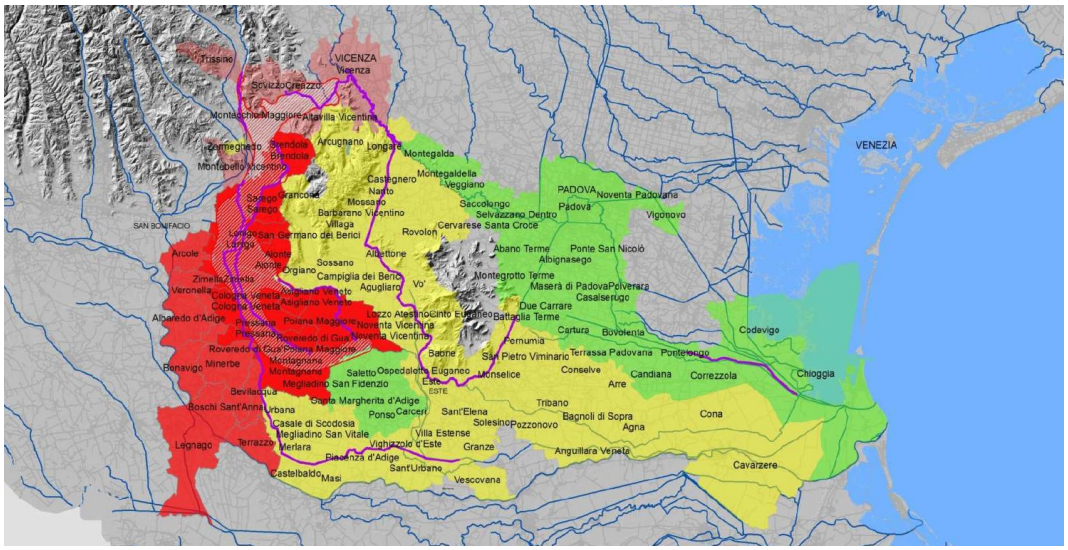

Figure 1.3. Map of the contaminated area in Veneto region (DGR n. 691/2018) Adapted from Technical report of the PFAS contamination in drinking water (August 2022).

Analyses of the emerging contaminants were conducted by the CNR (National Research Council) and ISPRA (Higher Institute for Environmental Protection and Research) at the request of the Ministry of the Environment. The 2013 research was prompted by the growing interest of the European Union in the perfluorinated compounds (PFC) present in Italian rivers, with the Po River being the most polluted.

A chemical plant that has been active since 1968 has produced herbicides, pharmaceuticals, and PFAS in the contaminated area. PFAS were made through electrochemical fluorination (ECF), a technique that forms a mixture of linear and branched isomers. ECF replaces the hydrogen atoms bound to organic carbon with fluorine atoms. This reaction leads to the fragmentation and rearrangement of the

carbon chain, forming several isomers. This outcome is even more emphasised when long-chain elements are used.

The PFAS contamination in the Veneto region included a mixture of isomers with different chemical properties, such as bioaccumulation, mobility, and, most importantly, toxicity (Pellizzaro et al., 2018). Some research had already been conducted in 1977, and a trifluorobenzene contamination was discovered in the area. Later analyses ascertained that the source of that contamination was the same as the current PFAS one (World Health Organization, 2017). There were two causes of pollution: first, the wastewater from the factory percolated into the groundwater, and second, the factory was directly connected to a wastewater treatment plant.

To contain the extensive damage, it was decided to add granular active carbon to the water treatment plants in the area, and the concentration of PFAS decreased (World Health Organization, 2017).

Since the discovery of the contamination, several epidemiological studies have been made to understand the effect of PFAS on human health. For example, the serum level of PFAS was studied, and the concentration was 27 times higher than that of the average non-exposed residents of the region (Pitter et al., 2020).

1.1.3 PFAS effect on health

A crucial aspect of PFAS is that they can damage both human and animal health. This, combined with their status as persistent pollutants present worldwide, makes them a very urgent topic, and extensive research has already been carried out. The effects of PFAS on health depend on various factors, such as the dose, duration, and route of exposure, as well as the age, sex, and health status of the exposed individuals.

Between 2005 and 2006, the first important/significant epidemiological study on the effects of PFAS was made/conducted in the United States of America. It was called the “C8 Health Project”, and, on that occasion, blood samples from 69,000 people living near the 3M plant in Mid-Ohio Valley were collected. The C8 study found that the average concentration of PFOS in the tested subjects was 500% higher than that of the rest of the country. Since then, several studies have been conducted/carried out on people who had been chronically exposed to that contaminant (Bonato et al., 2020).

Some of the main effects of PFAS exposure are: alteration of the immune function and interference with the vaccine's effect/efficacy; "probable link" between PFOA exposure and thyroid disease (hyperthyroidism in women and general thyroid disease in children); liver disease, including cancer caused by the induction of steatosis (as long-chain PFAS tend to storage inside this organ); alteration of lipids and insulin concentration, which may be associated with diabetes; kidney disease and cancer (liver long-chain PFAS, tend to accumulate in this organ); and finally, PFAS can interfere with fertility and may cause growth deficit (Fenton et al., 2021).

1.2 PFAS AND OXIDATIVE STRESS

1.2.1 What oxidative stress is

Oxidative stress occurs when there is an excessive production of reactive oxygen species (ROS) in cells, which is not well counterbalanced by the action of the antioxidant system. Therefore, a cellular redox imbalance occurs, leading to a disruption of homeostasis and an alteration of the physiological condition.

Oxygen is an important molecule for organisms. Its reactivity allows it to be a part of the electron transfer chain and concur with the ATP production process in mitochondria (Burton and Jauniaux, 2011). Generally, 6% of the O_2 used by cells forms ROS. However, in some specific cases, this percentage can increase and overwhelm the cell's ability to counteract them (Santovito et al., 2005). Various factors can increase ROS production, such as physical activity, ageing, cardiovascular disease, cancer, mechanical stress, thermal stress, hypoxia, high pO_2, and xenobiotics (Poli et al., 2018).

The opposite phenomenon of oxidative stress is called "reductive stress", which consists of an elevated concentration of reductants in the cells. This condition is not as discussed as oxidative stress but is frequent in certain environmental conditions. For example, reductive stress is typical of Black Sea deep water, with high concentrations of hydrogen sulphide (Lushchak, 2016).

1.2.2 Reactive oxygen species (ROS)

ROS are free radicals, meaning they have an unpaired electron in their external core. This characteristic makes them particularly reactive as atoms tend to complete their

octet to form more stable compounds. In the biological field, oxygen and nitrogen are the two most common types of free radicals; concerning oxygen, there are various kinds of ROS, including superoxide anion ($\bullet O_2^-$), hydrogen peroxide (H_2O_2), and hydroxyl radical (•OH) (Storey, 1996). Among these, •OH is the most reactive compound, followed by $\bullet O_2^-$, with H_2O_2 being the least reactive. It is worth mentioning that ROS have a short life span, so they do not accumulate inside the cell but are continuously produced and degraded (Lushchak, 2016).

Despite being a dangerous by-product of aerobic metabolism, ROS also play a pivotal role as secondary messengers in cells (Burton and Jauniaux, 2011). Signalling is essential for cells as it allows them to monitor changes in the inner and outer environment. Secondary messengers have a role in this pattern. They are small molecules formed after the receptor activation to amplify and spread the signal inside the cells. ROS can act as secondary messengers when they induce a physiological response through a redox reaction. This process should not be confused with redox modulation, a mechanism where ROS alter a redox-sensitive target, thus activating physiological or pathophysiological responses (such as oxidative stress). (Li et al., 2016).

In aerobic conditions, inside eukaryotic cells, over 90% of oxygen is reduced to water by cytochrome oxidase in the mitochondria's electron-transport chain (ETC). Therefore, most of the O molecule is used to produce ATP. Consequently, less than 10% of the O_2 that cells use is reduced via one-electron chain reactions. Initially, oxygen is reduced to $\bullet O_2^-$, then this molecule is reduced to H_2O_2 first, and then to •OH, the final product of these reactions being water (Lushchak, 2016).

$$O_2 + e^- \rightarrow \bullet O_2^- + e^- \rightarrow H_2O_2 + e^- \rightarrow \bullet OH + e^- \rightarrow H_2O$$

However, the one-electron chain can be “interrupted”, leading to the formation of intermediates and thus enhancing the ROS concentration.

ROS production is mainly due to the electron escaping from the ETC in mitochondria, which then reacts with molecular oxygen. The amount of this electron depends on the organism's physiological state (Lushchak, 2016). However, ROS can also be produced in oxidase reactions involving xanthine oxidase,

cytochrome P450 reductase, glucose oxidase, etc. (Lushchak and Bagnyukova, 2006).

In general, ROS can be produced inside mitochondria, where ROS are primarily generated due to the loss of electrons from the electron transport chain and in the endoplasmic reticulum (ER) for the action of cytochrome P_{450} and phagocytosis. Additionally, some other minor sources are apoptosis, autooxidation of small molecules like dopamine and flavones, the generation of hydrogen peroxides carried out by peroxisomes, and the action of lysosomes (Noori et al., 2012).

Superoxide anion radical ($\bullet O_2^-$) is the most common type of ROS and is mainly found inside mitochondria. It forms when the electrons of the complex I and III of the respiratory chain leak and bind with oxygen. The more electrons are present, the more radical is formed. Also, hypoxia leads to radical formation. When there is a lack of oxygen inside the cell, oxygen can't act as the final acceptor for complex IV; thus, electrons accumulate. Due to its charge, the mitochondrial membrane can't let $\bullet O_2^-$ exit, causing it to accumulate inside the cell. However, superoxide can also form in other processes, such as during an electron shortage in the short electron transport chain in the ER (Burton and Jauniaux, 2011).

Additionally, $\bullet O_2^-$ can be formed by reducing O_2 via NAD(P)H oxidase and xanthine oxidase. Xanthine oxidase typically transfers electrons to NAD, becoming uric acid, but in some cases, it can also reduce oxygen. This way of ROS formation is linked to several human diseases, such as atherosclerosis and ischemia (Valko et al., 2007).

Hydroxyl radical ($\bullet OH$), as previously mentioned, is the most reactive species of ROS, and its production is linked to the iron redox couple Fe^{2+}/Fe^{3+}. Under stress conditions, $\bullet O_2^-$favors the release of iron Fe^{2+} from the [4Fe-4S] cluster. The ion, then, can participate in the Fenton reaction, thus producing the hydroxyl radical:

$$Fe^{2+} + H_2O_2 \rightarrow Fe^{3+} + \bullet OH + OH^-$$

Another important reaction not only for hydroxyl but also for other radicals is the Haber-Weiss one:

$$\bullet O_2^- + H_2O_2 \rightarrow O_2 + \bullet OH + OH^-$$

This reaction is where the $\bullet O_2^-$ reacts with hydrogen peroxide within a combination of the Fenton reaction and the reduction of Fe^{3+} mediated by $\bullet O_2^-$ ($Fe^{3+} + \bullet O_2^- \rightarrow Fe^{2+} + O_2$) (Valko et al., 2007).

Hydrogen peroxide (H_2O_2) is the less reactive of the three radicals and is important in producing hydroxyl radicals. Under physiological conditions, H_2O_2 is produced by peroxisomes, where the major amount of oxygen is consumed. Hydrogen peroxide is produced to oxidate other molecules. Within the peroxisome, catalase is also used to prevent the accumulation of radicals. Anyway, when organelles are damaged, the regulation of H_2O_2 production becomes out of control, causing the molecule to be released into the cytosol (Valko et al., 2007).

Peroxyl radicals (ROO•) are another group of reactive species that can form after the reaction between a radical and oxygen.

$$R\bullet + O_2 \rightarrow ROO\bullet$$

The simplest one is the protonated form of superoxide, peroxyl radical HOO•; generally, those compounds have an important role in lipid peroxidation (see Chapter 1.2.4) (Valko et al., 2007).

Oxidative stress can be divided into four intensity classes based on the organism's response to ROS levels. The classes are basal oxidative stress (BOS), low-intensity oxidative stress (LOS) when there is a slight enhancement of the antioxidant response, intermediate-intensity oxidative stress (IOS) and high-intensity oxidative stress (HOS). There is also another classification of oxidative stress, which divides it into two categories: mild oxidative stress (MOS), when the activity of antioxidant defences overwhelms the level of ROS-modified components, and strong oxidative stress (SOS) when the activity of antioxidant defences is not enough (Lushchak, 2016).

1.2.3 ROS sources

As mentioned in the previous chapter, reactive oxygen species can have different sources. They can be divided into three general groups: endogenous sources, exogenous sources, and pathological sources (Noori et al., 2012).

Endogenous sources are described in the previous chapter, including essential metabolic processes that are regularly going on in the organism, like the loss of electrons in the electron chain reaction and the production of ROS inside the ER. They can also be divided into enzymatic and non-enzymatic: among the latter the earlier described Fenton's and Harber's reactions, while enzymatic sources on a subcellular level are xanthine oxidase, lipoxygenases, NO synthases, and mitochondrial oxidases.

Exogenous sources are those that increase ROS concentration for reactions that don't occur directly inside the cell but are stimulated by external factors, for example, mechanical and thermal stress, ionizing radiations, viral and bacterial infections, hypoxia and hyperoxia, biotransformation of xenobiotic compounds, exposure to industrial waste products, asbestos fibres, cigarette smoke etc. Dioxins and heavy metals are the primary environmental contaminants that can cause oxidative stress, but exposure to PFOS and PFOA has also been shown to enhance ROS production (Bonato et al., 2020).

Pathological sources refer to ROS production due to diseases, such as when the organism is under radiation, inflammation, ischemia, cancer infection, etc. When produced in excess, ROS can cause tissue injury, which can cause further ROS generation, which may (or may not, depending on the situation) contribute to worsening the injury (Aruoma, 1998).

1.2.4 Effect of ROS

ROS can interact with all cell components like carbohydrates, proteins, nucleic acids, lipids, etc; for example, when ROS reacts with lipids and carbohydrates, they can be transformed into toxic products. An example of the damage produced by ROS is lipid peroxidation (LPO). It consists of an oxidant attack on lipids with a C-C double bond, particularly polyunsaturated fatty acids. During the lipids peroxidation, the oxidants (especially •OH and $\bullet O_2^-$) and hydrogen bind to carbon

and are substituted with oxygen; the target of this reaction can also be glycolipids, phospholipids, and cholesterol. Other enzymes can oxidize lipids, for example, lipoxygenases, cyclooxygenases, and cytochrome P450.

In response to lipid peroxidation, the cell can react in two ways: promoting survival or inducing death. The first occurs when the damage is minor, and the cell activates antioxidant defences. In the case of medium and high lipid peroxidation, the cell results are overwhelmed, and the damage is irreparable, possibly leading to the development of various pathologies.

The process of lipid peroxidation is divided into three phases: initiation, where the prooxidants remove the hydrogen, forming a carbon-centred lipid radical (•L); propagation, where the lipid radical reacts to oxygen and forms a lipid peroxy radical (•LOO) that remove hydrogen from another lipid forming a lipid radical and lipid hydroperoxide (LOOH); and termination, where the antioxidants donate an H to •LOO; in this way the chain is interrupted (Ayala et al., 2014).

LPO produces several compounds, but the most mutagenic one is malondialdehyde, and the most toxic is 4-hydroxynonenal (4-HNE). 4-HNE can rapidly react with thiols and amino groups, and it's considered the major biomarker of LPO.

Peroxyl radicals have an important role in lipid peroxidation; they can induce it with two different pathways: one is LOOH-independent, and the other is LOOH-dependant. In this process, ROO• is peroxidized first to endoperoxides and then to MDA (Valko et al., 2007).

The opening of the ion channels is another effect caused by excessive ROS production. In normal conditions, the calcium concentration inside the ER lumen is higher than in the cytosol: when ROS concentration is altered, the Ca^{2+} channels are activated, and ions are released. This altered cell homeostasis by activating processes that depend on calcium concentration. Furthermore, Ca^{2+} inside ER is necessary for protein-folding activity, so a lack of this ion can lead to misfolded proteins inside the lumen. Finally, mitochondrial functions are negatively affected by the increased concentration of calcium cation, and they raise the production of ROS with an alteration of pores permeability that ends with the collapse of ATP synthesis (Burton and Jauniaux, 2011).

Two other ROS effects should be discussed: the alteration of protein structure and DNA oxidation. In the first one, carbonyl groups like aldehydes and ketones are formed due to the oxidation of the side chains of amino acids and hydrogen ions are removed from the thiol group with the consequence of disulfide bond formation and irregular protein folding. This can lead to protein loss of function, aggregation and cell death.
The second effect is predominant in mitochondrial DNA because it's close to the $\bullet O_2^-$ source, and the repair mechanism is barely absent; this can lead to impaired energy production and a consequent further leak of electrons (Burton and Jauniaux, 2011).

1.2.5 Antioxidant defenses

Animals have a complex antioxidant system that eliminates ROS and ROS-modified molecules but also prevents their formation to maintain cellular homeostasis in which the production of ROS is balanced by the presence of antioxidants (Iqbal et al., 2024).

There is a difference between acute oxidative stress and chronic oxidative stress. Usually, in the first case, the antioxidant potential is enough for the organism to return ROS concentration to normal values without important consequences. Conversely, if the stress is chronic, the antioxidant potential can't be enough to contrast with the enhanced ROS level. In this particular case, there are two possible ways: the ROS level decreases thanks to the antioxidant system action, or a new steady-state concentration of ROS is established, which leads to the development of specific pathologies and chronic inflammation (Lushchak, 2016).
The antioxidant defences can be divided into enzymatic and non-enzymatic (see Table 1.2). The latter divides into molecules biosynthesized by the organism (GSH and MT) and compounds acquired by the diet (Poli et al., 2018; Valko et al., 2007).

Table 1.2) List of the main antioxidants.

Enzymatic	Non-enzymatic
Superoxide dismutase (SOD)	Carotenoids
Catalase (CAT)	Flavonoids
Glutathione peroxidases (GPx)	Vitamin E
Glutathione-S-transferase (GST)	Vitamin C
Peroxiredoxins (Prdx)	Glutathione (GSH)
Aldokheto -reductase	Metallothionein (MT)
Aldehyde dehydrogenase	

1.2.6 GPx

Glutathione peroxidases (GPxs) are a group of enzymes, some of which contain selenium, capable of reducing organic and inorganic peroxides into hydroxyl compounds using GSH (glutathione) or other equivalent. There are eight isoforms; three are monomeric proteins (GPx 4, 7, and 8) with several amino acids between 186 and 209, and the other five are homotetramers. The various isoforms are sites in different cellular compartments: GPx-3, GPx-6, and GPx-7 are extracellular. At the same time, the others are located inside the cell (isoform number 4 is the only one present inside mitochondria) (Poli et al., 2018).

The first four isoforms are the selenium-dependent ones: they present a selenocysteine (Sec) residue, usually codified from the stop codon TGA. Its insertion inside the protein needs a particular translation factor, Sec-tRNA and the presence of the Sec insertion sequence (SECIS) element in the 3' untranslated region, which permits the insertion of selenocysteine (SeCys). If there is a lack of selenium, TGA is recognized as a standard STOP codon protein translation ends there.

Regarding SecGPxs, during the catalytic cycle of GPx (showed in Figure 1.4), H_2O_2 oxidates selenol (SeH), and the product of this reaction (maybe SeOH, selenenic acid) is subsequently reduced by the electron acceptor (GSH). During these reactions, the oxidation level of the enzyme depends on the concentrations of GSH and H_2O_2. The GPx activity leads to a decrease in the GSH concentration and an increase in its oxidative form (GSSG). The reduced form can be restored from GSSG thanks to a reaction catalyzed by glutathione reductase (GR), the contemporary oxidate NADPH produced by the pentose phosphates cycle. When selenium becomes limiting, not all proteins are uniformly supplied; there is a

hierarchy used to describe this phenomenon, and it's linked to the stability of the proteins: the ones that disappear fast in a selenium-deficient condition are the ones ranked lower (Poli et al., 2018; Brigelius-Flohé and Maiorino, 2013).

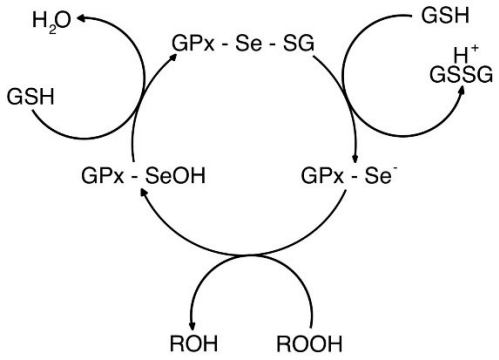

Figure 1.4) Se-dependent GPx catalytic cycle (Poli et al., 2018)

$$GPx - Se^- + H_2O_2 \rightarrow GPx - SeOH + OH^-$$

$$GPx - SeO^- + H^+ + GSH \rightarrow GPx - Se - SG + H_2O$$

$$PGx - Se - SG + GSH \rightarrow GPx - Se^- + H^+ + GSSG$$

From the kinetics of this reaction, it could be stated that GPx is 100% oxidized if the concentration of H_2O_2 and GSH are similar, but, in reality, the second one is typically 1-10Mm concentrated. The first one is not even in the micromolar range, so the enzyme is almost entirely reduced. Accordingly, a slight change in the GSH concentration doesn't influence how hyperoxide is removed (Brigelius-Flohé and Maiorino, 2013).

Phylogenetic studies pointed out that the diversity between organisms, regarding GPxs, is very high. Molecular evolution increased their complexity until those proteins could not be considered ROS scavengers. Initially, the enzyme was monomeric; in plants and fungi, this gene was duplicated, and different isoforms of the protein were developed. The most recently evolved GPxs have a dimeric/tetrameric domain with a preference for GSH and H_2O_2 as substrates (Trenz et al., 2021).

GPx1

GPx1 is a selenium-dependent protein and was the first to be identified; it is considered the prototype of glutathione peroxidase because it contains all five amino acids involved in the reaction with GSH, and it ranks lowest in the hierarchy

of selenium-dependent proteins. This enzyme reacts with H_2O_2 and soluble hydroperoxides with low molecular mass but not with more complex lipids. When GSS (GSH synthetase) is absent, for example, in the brain mitochondria, GPx1 can reduce H_2O_2 by using γ-glutamylcysteine.

Some mice experiments show that other selenium-dependant proteins cannot replace GPx1 in the presence of oxidative stress, and it functions as the primary antioxidant response in vivo.

Although GPx1 protects organisms from oxidative stress and prevents oxidative DNA mutations and so cancer, in the long run, overexpression of this protein can lead to the development of some diseases like hyperglycemia and hyperinsulinemia (Brigelius-Flohé and Maiorino, 2013).

GPx4

GPx4 has first been detected as a lipid peroxidation inhibiting protein because it can reduce not only H_2O_2 but also hydroperoxides in complex lipids. It's the only GPx capable of reducing hydroperoxides located inside membranes. There are three different GPx4 isoforms: a cytosolic one, a mitochondrial one, and a sperm nuclear one; all derivates from the same gene with seven exons.

GPx4 is an antioxidant enzyme important for some essential life functions; the disposal of cytosolic GPx4 is embryonically lethal (Brigelius-Flohé and Maiorino, 2013).

1.2.7 CAT

The first catalase from an eukaryotic individual was purified in 1948, and many studies have been conducted to understand the activity of CAT. It was discovered that the protein is linked to mutagenesis, inflammation, and apoptosis, all associated with oxidative stress (Nandi et al., 2019).

Unlike GPx, catalase has only one isoform and has been isolated from prokaryotic and eukaryotic. With its activity, it can break down two molecules of H_2O_2 into two molecules of water and one of molecular oxygen:

$$2H_2O_2 \rightarrow 2H_2O + O_2$$

This reaction is divided into two different steps; in the first one, a molecule of hydrogen peroxide is reduced while oxyferryl ($Fe^{IV}O$) is produced, this complex is reduced to O_2 by the second hydrogen peroxide (Jomova et al., 2023).
There are three different types of CAT, based on the difference in their sequence: a monofunctional one that contains a heme group and is the most common, a bifunctional one that also contains a heme group and has a catalase-peroxidase activity, and finally, one that doesn't contain a heme but a Mn (Nandi et al., 2019). The absence of CAT is linked to different diseases like neurological disorders, metabolic diseases, cancer, and anaemia.

1.2.8 Oxidative stress induced by PFAS in fish

Aquatic environments are very heterogeneous regarding the oxygen content; the amount of this molecule depends on temperature, salinity, flows, eutrophication, and many other water characteristics. Fish species are adapted to various environmental conditions. For example, cyprinids can survive from low to high O_2 concentrations, so those organisms evolved a complex antioxidant system (Lushchak and Bagnyukova, 2006).
Oxidative stress can be induced by many factors, including pollution caused by human activity. In the case of fish, pollutants can affect the animals directly or indirectly by altering the environment.
The stress can be further divided into direct, if the pollutant directly interacts with the redox cycle of the cell, altering it (for example, metal ions), and indirect, if the pollutant has a stable redox state but, for example, alters the energy or the substrate resource of the cell (Lushchak et al., 2016).

Recent studies have shown that PFAS contamination in the rivers of the Veneto region leads to a significant mRNA expression of *gpx4* and *sod2* in liver tissues of two species, *Squalius cephalus* and *Padagobius bonelli.* Furthermore, the lipid peroxidation levels were slightly lower in the two contaminated sites. On the other hand, the total antioxidant capacity assay did not show any statistically significant difference between the organisms exposed to the various concentrations. Those data suggest that PFAS contamination and chronic exposure in fish could lead to an increase of ROS production in the organism, which, however, gets successfully controlled by an increased expression of the genes encoding for the antioxidant

response enzymes like GPx and SOD (Piva et al., 2022). Afterwards, other analyses were performed on the same samples, specifically the *Squalius cephalus* caudal kidney. The gene expression and the activity of GPx1, GPx4 CAT, and many other antioxidant enzymes were investigated; it was pointed out that the expression of *gpx1* increased in the highly polluted site while the one of *gpx4* in the low polluted one. At the same time, increased activity of the Se-GPxs in the low polluted site doesn't fit with an increase in *gpx4* mRNA expression. The hypothesis of a post-transcriptional regulation carried out by Stress Granules was made, but no analyses were performed to confirm that. The same situation was found in gene expression and activity of catalase (Vanzan, 2024).

1.3 STRESS GRANULES

The first evidence of stress granules (SGs) formation was observed by Nover et al. (1989) in the cytoplasm of tomato cells subjected to heat shock. For this reason, SGs were first named "heat shock granules".

SG are membranless foci of 0.1-2 μm in diameter, forming in the cytoplasm of eukaryotic cells. SGs comprise non-translating messenger ribonucleoproteins (mRNPs), i.e. complexes of silenced mRNAs and mRNA-binding proteins, such as TTP, G3BP, and TIAR, acting as translational repressors.

Other SG components are ribosomal subunit 40S (but not the 60S subunit), eukaryotic initiation factors (eIF4E, eIF4G, eIF4A, eIF4B, eIF3, eIF2) and additional proteins (e.g. post-translation modification enzymes, metabolic enzymes, proteins for RNA remodeling), which can affect SG assembly and disassembly (Kedersha et al., 2002). The small subunit 40S has an essential role in the mechanism of initiation of protein synthesis when it combines with the ternary complex the eIF2-GTP-$tRNA^{Met}$ which also contains the guanosine triphosphate (GTP) and the transfer RNA (tRNA) loaded with the amino acid methionine. Initiation factors and mRNAs form the 48S preinitiation complex (Buchan and Parker, 2009).

The assembly of SGs is mainly induced by stress conditions, such as exposure to xenobiotics, UV light, thermal shock, and oxygen radicals (Anderson and Kedersha, 2006; Hirose et al., 2023). Inside these complexes, the protection of mRNAs stalled in translation is guaranteed, allowing the cell to direct its energy into translating

mRNAs excluded from SGs useful for cell viability, such as those encoding the heat shock proteins (Warris et al., 2014).

The structure of SGs is not uniform: there is an internal part called “core”, where proteins and mRNAs are more concentrated and molecular interactions are more robust, and an external part called “shell”, where interactions between proteins and mRNAs are weaker. The shell confers a dynamic structure to SGs that allows the rapid response to stress conditions through the rapid assembly/disassembly of SGs (Jain et al., 2016).

SGs, together with processing bodies (PBs), another example of membranelles foci in which mRNAs undergo degradation, could explain the discrepancy between levels of transcripts and those of the relative proteins found in the cell (Anderson and Kedersha, 2009; Lavut and Raveh, 2012).
Much work was dedicated to studying the presence of SGs in response to acute stress conditions, but little is known about their formation under chronic stress conditions. Until now, data suggest that SGs forming during acute and chronic stress differ in composition (Reineke and Neilson, 2019).

1.3.1 The formation of SGs

The assembly/disassembly of SGs depends on the amount of mRNAs not translated inside the cell: when this concentration increases, it leads to SG formation; when it decreases, it leads to SG disassembly (Ivanov et al., 2019). An important role in the formation of SGs is given by the destabilization of the polysomes, complexes made by mRNA, and ribosomes active in translation. There is a dynamic balance between polysomes and SGs: when the first one gets destabilized by specific drugs, like emetine, the second one assembles and vice versa (Kedersha et al., 2000).
When a cell is under stress, the phosphorylation of eIF2α causes a decrease in the availability of the eIF2-GTP-$tRNA^{Met}$ complex, reducing translation processes (Kedersha et al., 2002).
The phosphorylation of eIF2α at serine 51 subunit, stabilized by the bind with eIF2B, can be induced by the activation of four different kinases: protein kinase R (PKR), heme-regulated inhibitor (HRI), PKR endoplasmic reticulum kinase (PERK), and general control nonderepressible 2 (GCN2) (Figure1.5). Each

responds to a specific stressor, but the stimuli sometimes overlap (Donnelly et al., 2013).

PRK is mainly activated during viral infections: phosphorylating eIF2α blocks mRNA translation from the virus. PKR is typically located in the cytosol and the nucleus, where it stays latent before being activated by double-strand RNA, which specifically binds with one of its domains.

HRI is important during development but also responds to stress conditions like proteasome inhibition and arsenite exposure. The activation of this kinase depends on heme concentrations: when low, the HRI binds with heme and creates dimers because of intermolecular autophosphorylation; when the concentration of heme is high, the dimer formation is inhibited, and HRI phosphorylates eIF2α.

PERK is activated when there is an accumulation of misfolded proteins inside the ER. With eIF2α phosphorylation, the kinase blocks the synthesis of polypeptides and gives the time to ER to refold the misfolded proteins.

GCN2 is activated under amino acid or glucose deprivation, viral infection, and UV irradiation. Its activation occurs when uncharged tRNAs bind to its His/RS domain, which tends to accumulate when there is a lack of essential amino acids.

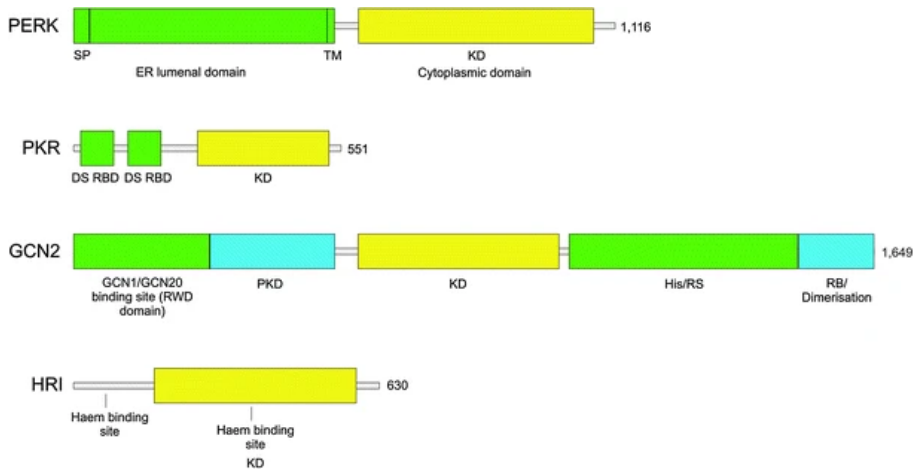

Figure 1.5) Domain organization of kinases acting in the phosphorylation of eIF2α to regulate SG formation (Donnelly et al., 2013).

eIF2α is not a component of newly ensembled SGs, unlike other initiation factors (e.g. eIF3, eIF4E and eIF4G, which forms the 48S subunit), so probably the assembly of SGs is not directly due to its phosphorylation but to the decrease in the availability of eIF2-GTP-tRNAi^{Met} complex. The translation can occur when the

48S complex, without eIF2α, meets the ternary complex (Figure 1.6) (Kedersha et al., 2002).

The phosphorylation of eIF2α is not the only mechanism that leads to SG formation. For example, eIF4A, if disturbed or inhibited, can lead to SG formation because the translation process is compromised. This happened because the recruitment of mRNAs by ribosomes decreases, and the initiation factor doesn't bind with mRNAs (Mazroui et al., 2006).

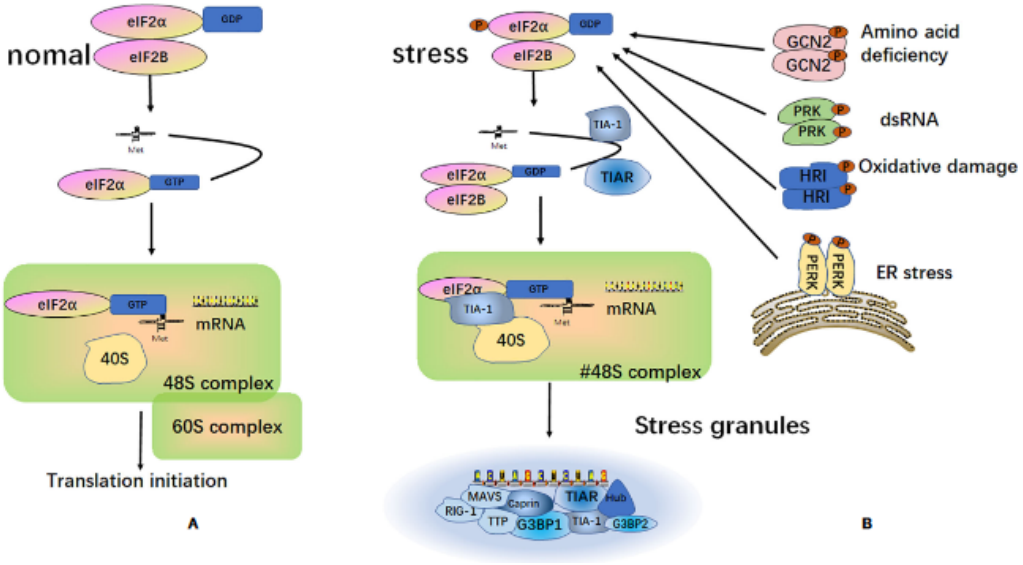

Figure 1.6) (A) Under normal conditions, the eIF2-GTP-tRNA^{Me} complex binds to mRNA and the 40S and 60S ribosomal subunits to participate in the translation process. ***(B)*** *Under stress conditions, kinases can be activated to induce phosphorylation of the α subunit of eIF2, which binds to eIF2B, preventing eIF2B from catalyzing GDP into GTP; the level of eIF2-GTP-tRNA^{Met} decreases, not allowing the formation of a functional 48S initiation complex; a non-canonical 48S initiation complex is produced, under the action of TIA-1 and TIAR for example, and recruited into SGs (Kang et al., 2021).*

1.3.2 Stress granule components: TTP, G3BP, AND TIAR

Tristetrapolin (TTP), also known as ZFP36 Ring Finger Protein, is a nucleic acid binding protein containing two zinc-finger domains, able to bind nucleic acids and, in this way, alter the gene transcription (Klug, 1999). These two domains can recognize adenine (A) and uridine (U)-rich regions of some mRNAs, such as mRNA for the tumour necrosis factor, at their 3'/5'-untranslated regions (Hall, 2005), thus promoting their deadenylation and so conservation inside SGs or

degradation inside PBs (Lai et al., 1999; Chen et al., 2001; Gamsjaeger et al., 2007; Stocklin et al., 2004).

TTP moves typically between the nucleus and the cell's cytoplasm thanks to its TIS11 domain, N-terminal (Murata et al., 2002); during stress conditions, TTP accumulates in the cytoplasm.

The presence of TTP inside SGs depends on the type of stress. For example, TTP can colocalize with T-cell-restricted intracellular antigen (TIA) proteins inside SGs during energy starvation but not during arsenate-induced oxidative stress (Stocklin et al., 2004).

Stress Granule Assembly Factor 1/2 (**G3BP 1/2**) is an endoribonuclease phosphorylation-dependent which interacts with the Ras-GTPase activating protein through its SH3 domain (Parker et al., 1996).

There are three homologous proteins of G3BP: G3BP1, G3BP2a, and G3BP2b, each containing one C-terminal RNA recognition motif (RRM), responsible for the recognition of A/U-rich mRNAs (Figure 1.7) (Kang et al., 2021). They can be distinguished by their number of proline-rich (PxxP) motifs: G3BP1 has one PxxP motif, while G3BP2 has four/five PxxP motifs. These motifs are essential for assembling SGs and recruiting PKR to activate G3BP during viral infections. The alteration of the PxxP motifs reduces the antiviral activity of G3BP (Reineke and Lloyd, 2014).

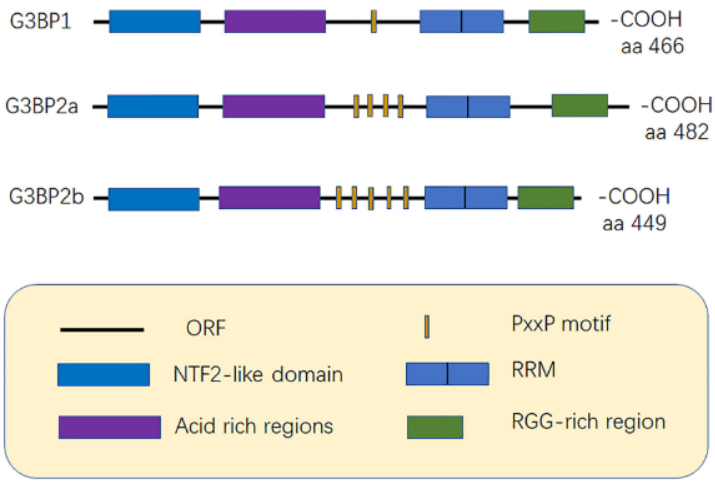

Figure 1.7) G3BP isoforms (Kang et al., 2021).

G3BP1 and G3BP2 are both components of SGs (Matsuki et al., 2013), which can multimerize the mRNA molecules and induce the formation of SG (Tourrière et al., 2001, 2023).
G3BP has an essential role in SG assembly, in the liquid-liquid phase separation: when the RNA concentration in the cell rises, G3BP works as a condensation nucleus for the RNA aggregation; in particular, the three intrinsically disordered regions (IDRs) of G3BP permit this phenomenon (Yang et al., 2020).
In non-stress conditions, G3BP is found in the compact form inside the cytoplasm, which sizes the arginine (R) and glycine (G)-rich regions by electrostatic relations with IDR. When the cell is under stress conditions, the mRNA from the polysomes competes with these intramolecular relationships. It promotes the G3BP expansion, thus leading to an association between the protein and mRNA in a condensate structure (Guillén-Boixet et al., 2020).

Also, TIA proteins, T-cell-restricted intracellular antigen 1 (TIA-1) and TIA-1-related nucleolysin (**TIAR**) can bind A/U-rich mRNAs. TIA proteins have three N-terminal RRMs and a C-terminal glutamine (G)-rich prion-related domain, the last one essential for the assembly of SGs.
For both, the proteins exist two different isoforms that result from varying splicing: the TIA-1 isoforms differ for 11 amino acids, and the TIAR isoforms differ for 17 amino acids (Warris et al., 2014).
In normal conditions, TIA proteins shift between the nucleus and cytoplasm, but when the cell is under stress conditions, they tend to accumulate in the second one following the phosphorylation of eIF2α (Kerdasha et al., 1999; Lopez de Silanes et al., 2005; Kim et al., 2013). Their RRM2 domains are essential for the recognition of A/U-rich mRNAs, whereas RRM3 domains are essential in maintaining the protein-mRNA interaction in the case of C-rich mRNAs, typically encoding ribosomal protein and translation factors (Cruz-Gallardo et al., 2014).

1.3.3 Oxidative stress and stress granules

When stress occurs, cells can react in two ways: induce apoptosis or inhibit the stress and repair the stress-induced alterations. SGs play an important role in this mechanism since they can inhibit apoptosis in some situations, for example,

hypoxia, heat shock, and arsenite exposure), but if their formation is not induced, for example, after exposure to x-ray irradiation and genotoxic drugs, the cell goes through apoptosis. The mechanism through which this happens is not still well understood. One study pointed out the relationship between SGs and ROS, with these cytoplasmic foci being able to exert an antioxidant effect by the synergic action of two components: G3BP and USP10 (Takahashi et al., 2013).

Generally, SGs can explain the inconsistencies observed in protein expression levels of antioxidant enzymes, such as gene expression levels of the relative genes. This phenomenon was found on different occasions, as in the case of Antarctic fish, where the glutathione peroxidase (GPx) activity didn't correlate with the mRNA levels (Sattin et al., 2015). This probably happened because, in stress conditions, mRNAs were stored inside SGs to preserve them from damage and make them rapidly available to be translated if necessary. So, high levels of gene expression didn't correspond to high levels of enzymatic activity since the gene was blocked in translation inside SGs.

2 AIM OF THE THESIS

In the last decade, poly- and perfluoroalkyl substances (PFAS) have significantly raised public interest due to their widespread presence in Italy across the country and their harmful effects on human health. One of the most significant PFAS contamination events occurred in the Veneto region, where wastewater produced by the Miteni factory in Trissino (VI) polluted freshwaters and groundwater in Vicenza, Padova, and Verona provinces since the 1970s. This contamination event was discovered in 2013, thanks to the efforts of the Regional Agency for Environmental Prevention and Protection of Veneto (ARPAV) in its biomonitoring activities.

Even though more than ten years have passed since the discovery of PFAS pollution in Veneto, their chronic effects on freshwater organisms remain unknown. PFAS are persistent and tend to bioaccumulate in organisms, two characteristics that make them harmful to fauna, even in small quantities, especially in prolonged exposures. How PFAS influence organisms' metabolism is still unknown. One plausible hypothesis is that they may alter physiological conditions by interfering with cellular substrates or altering the redox balance condition, leading to the excessive formation of ROS.

The present research aims to verify the effects of PFAS, at different environmental concentrations, on freshwater fish, focusing on physiological responses activated in the liver and caudal kidney as a consequence of chronic exposure. Due to its ubiquitous presence in the Veneto region rivers, *Squalius cephalus* was chosen as the target species. Sampling occurred in June and July 2024 at four different sites around Vicenza. A non-contaminated site, with PFAS concentration < 5 ng/l, was chosen as a control, while the other three sites were selected as "low-polluted", "medium-polluted", and "highly-polluted" by PFAS.

One previous research highlighted several effects on *S. cephalus* from Veneto, chronically exposed to PFAS, particularly in the liver and caudal kidney. Concerning the latter organ, an increase in the selenium-dependent GPx
(Se-GPx) activity was observed in fish collected ed from medium-polluted areas (582.6 ng/l), and an increase in the CAT activity was observed in fish collected from low-polluted areas (5.64 ng/l) (Vanzan, 2024). However, this was not always

correlated to an increase in the gene expression, suggesting a possible involvement of SGs in the regulation of translation of selected mRNAs, temporarily blocked inside SGs by specific proteins.

Different analyses were performed on the sampled fish. Gene expression of *gpx1, gpx4, cat, ttp, g3bp,* and *tiar* was quantified by qRT-PCR. These genes were chosen to investigate the effects of PFAS on the antioxidant system and evaluate the relationship between them and SGs, possibly formed by the mRNA-binding proteins TTP, G3BP, and TIAR. In the case of the three SGs-related genes codifying the above proteins, no genetic sequences were available. In the present thesis, I characterized *S. cephalus ttp*, *g3bp*, and *tiar* sequences for the first time. Biochemical analyses were performed to evaluate the antioxidant enzymes Se-GPx and CAT activity. Specifically, these analyses evaluated possible mismatches between the enzyme activity and gene expression. In addition, morphological aspects were investigated through the calculation of Fulton's Condition Factor (FCF), the Hepatosomatic Index (HSI), and the Spleen Somatic Index (SSI) to evaluate fat accumulation, organ development, and general adaptation to the environment.

3 MATERIALS AND METHODS

3.1 TARGET SPECIES

In the present study, one single species was considered, *S. cephalus* (Linnaeus, 1758), commonly known as European chub or "Cavedano" in Italian. The taxonomy is shown in Table 3.1.

Table 3.1) S. cephalus taxonomy.

Domain	Eukaryota
Kingdom	Animalia
Phylum	Chordata
Class	Actinopterygii
Order	Cypriniformes
Family	Cyprinidae
Genus	*Squalius*
Species	*S. cephalus*

Cyprinids are widely distributed in European freshwaters due to human introductions. European chub is the most common species of this family, including 34 species in total. Chubs have been introduced in Italy over time, so it's difficult to understand the original distribution. Anyway, this fish is considered native to north and central parts of Italy (Balestrieri et al., 2016).

S. cephalus (Figure 3.1) is a pelagic species; generally, it prefers warm waters but has a broad ecological plasticity (Balestrieri et al., 2016). The average size is 25 cm, but it can reach a maximum of 60 cm. The body is thick with a cylindrical shape; it can be recognized thanks to a marked distinction between the head and the trunk on the dorsal profile, the presence of black pigments along the margins of the scales, which are almost entirely colourless and, lastly, the anal and the pelvic fins have an orange-red colouration. The mouth is large with plump lips. The sexual dimorphism is generally not evident.

Chub has a diversified diet and includes invertebrates, insect larvae, and worms. During adult life, large individuals eat predominantly little fish. The reproduction occurs in fast-flowing waters with a gravel bottom, more rarely among vegetation. Juveniles move in groups, while adults are solitary.

S. cephalus specimens generally live 15 years; males become fertile at 2-4 years old, while females at 4-6 years old. They spawn in spring/summer, when the

temperature overcomes 12°C, and females can produce eggs several times a year. The eggs get deposited into the gravel, so it is more common to find this species in rivers with a gravel bottom.

Figure 3.1) S. cephalus body structure.

Despite little economic interest, *S. cephalus* is commonly a target species in ecotoxicological studies. This is because of the population's abundance and the ubiquitous presence throughout Europe (Collard et al., 2018).

3.2 SAMPLING ACTIVITY AND TISSUE PREPARATION FOR LABORATORY ANALYSES

The fieldwork activity occurred on the 6th of June and the 11th of July, 2024. Four watercourses were chosen as target sites, each presenting a different PFAS concentration.

ARPAV data collected in 2022 and 2023 were analysed to choose the sampling sites. Since the discovery of PFAS pollution in 2013, ARPAV has conducted constant analyses of environmental contaminants. The four chosen rivers, according to the monitoring data, have different PFAS concentrations and have been classified as: “control site”, “low-polluted site”, “medium-polluted site”, and “highly-polluted site”. This classification was based on the total PFAS concentration without distinguishing between specific compounds, such as PFOA or PFOS (Table 3.2).

Sites were then geolocalized with qGIS (version 3.22) (Figure 3.2), and for each ARPAV station, the concentration of other contaminants in water, different from PFAS compounds, was also evaluated. Sites with no high concentration of metals, pesticides, and other pollutants were chosen to minimize their effect on the analysis. The Gauss-Boaga reference system was selected because it’s the one with which

ARPAV provides us the data. It is commonly used in Italy because it was proposed here in 1940; its identification codes are EPSG 3003 and EPSG 3004.

Table 3.2) Total PFAS concentration in freshwater from sampling sites (ARPAV).

SITE	Water sampling period	Average concentration of total PFAS (ng/l)	Highest concentration	Detection date of the highest concentration
Roggia Moneghina	02/07/2023 11/14/2023	**<5 - <10**	<10	11/14/2023
Fosso Brenta	02/09/2022 11/15/2023	**185.263**	304.91	08/18/2022
Scolo Togna	02/21/2022 11/29/2023	**855.704**	1629.06	08/23/2022
Torrente Poscola	01/11/2022 04/10/2023	**1116.14**	6932.81	01/23/2023

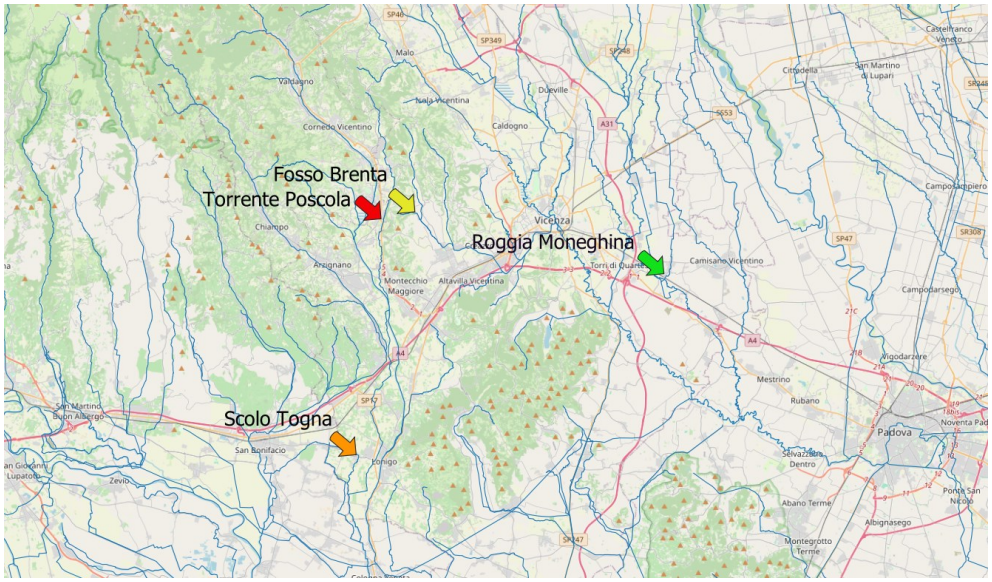

Figure 3.2) Geolocation of the sampled sites operated with qGIS (version 3.22) using the Gauss-Boaga reference system.

3.2.1 Sampling sites

The first site was Roggia Moneghina (Figure 3.3) (drainage basin of Bacchiglione), located in Grumolo delle Abbadesse (VI) (X GAUSS BOAGA: 1707494.771; Y GAUSS BOAGA: 5043242.570). The sampling activity was performed on the 11th

of July, 2024. This site has been chosen as the “control” because the total PFAS concentration in the last few years was <10 ng/l.
Since October 2017, the limit of quantification (LOQ) for PFAS has been 5 ng/l.

Figure 3.3) Photo of the “control site” in Roggia Moneghina.

The second site was Fosso Brenta (Figure 3.4) (drainage basin of Bacchiglione), located in Sovizzo (VI) (X GAUSS BOAGA: 1688840.326; Y GAUSS BOAGA: 5047241.734). The sampling activity was performed on the 6th of June, 2024. This site has been chosen as the “low-polluted site” because of the total PFAS concentration detected in freshwater in the last few years, from 10 ng/l to 500 ng/l.

Figure 3.4) Photo of the “low-polluted site” in Fosso Brenta.

The third site was Scolo Togna (Figure 3.5) (drainage basin of Fratta Gorzone), located in Lonigo (VI) (X GAUSS BOAGA: 1685003,474; Y GAUSS BOAGA: 5029108,091). The sampling activity was performed on the 11th of July, 2024. This

site has been chosen as the “medium-polluted site” because of the total PFAS concentration detected in freshwater in the last few years, from 500 ng/l to 1000 ng/l.

Figure 3.5) Photo of the “medium-polluted site” in Scolo Togna.

The last site was Torrente Poscola (Figure 3.6) (drainage basin of Fratta Gorzone), located in Trissino (VI) (X GAUSS BOAGA: 1686344.594; Y GAUSS BOAGA: 5046652.211). The sampling activity was performed on the 6th of June, 2024. This site has been chosen as the “highly-polluted site” because the total PFAS concentration detected in freshwater in the last few years is higher than 1000 ng/l.

Figure 3.6) Photo of the "highly-polluted site" in Torrente Poscola.

3.2.2 Electrofishing

Ten/fifteen specimens were sampled from each of the four rivers by electrofishing, performed by Aquaprogram staff. Five will be used in the future for the PFAS quantification, while ten will be used for the laboratory analysis. In particular, eight specimens were used for gene expression quantification. Acquaprogram is a research company in Luca Della Robbia, 48 (Vicenza, Italy) that deals with environmental analysis, fishing, and aquaculture. They perform various practical activities like electrofishing, water analysis, ecological DNA analysis, etc., but they also work in environmental education for schools.

The electrofishing device has three elements: a generator (or a battery), a transformer, and two electrodes (cathode and anode). The generator produces alternating current that the transformer converts into direct current. The optimal voltage depends on various factors like the type of the riverbed, the mean depth, and the conductivity of the water. To set the optimal voltage, some characteristics need to be considered, particularly the size of the species. Longer fishes respond better to the electric field since the fish behave like a dipole of the electric field generated in the water (Bohlin et al., 1987). An example of an electrofishing device is shown in Figure 3.7.

Figure 3.7) Acqauprogram staff during sampling activity. A red arrow indicates the generator, and the cathode and the anode are marked with yellow arrows.

After being sampled, fish were anaesthetized with essential clove oil, an anaesthetic generally used in fieldwork, obtained from *Syzygium aromaticum* and diluted in ethyl alcohol. A few drops of clove (0.0070 ml/l) were added to a basket of water. Once the fish stopped moving, a cut was performed at the level of the spinal cord behind the head. Fish were then put in plastic bags, stored in boxes filled with ice and dry ice, and immediately transferred to the Department of Biology of the University of Padova.

3.2.3 Fish dissection

All the specimens were weighed and measured for total body length before proceeding with dissection. The liver, caudal kidney, intestine, gills, gonads, spleen, heart, brain, white muscle, and tail were removed from the fish, frozen with liquid nitrogen and stored at –80°C for molecular and biochemical analysis. The sex of the individuals was assigned through macroscopic observation of the gonads. The liver and spleen were weighed to calculate the SSI (spleen somatic index) and the HIS (hepatosomatic index).

3.2.4 Calculation of indexes

To calculate the Hepato somatic index (HSI), the Spleen somatic index (SSI), and the Fulton's Condition Factor (FCF), the total body weights (g) and lengths (cm) of all specimens were measured, together with the weight of liver and spleen.
Indices were calculated using the following equations:

- Fulton's Condition Factor

$$FCF = \frac{TW}{L^3} * 100$$

- Hepato somatic index

$$HSI = \frac{LW}{TW} * 100$$

- Spleen somatic index

$$SSI = \frac{SW}{TW} * 100$$

Where:

- TW = total weight of the individual (g)
- L = total length of the individual (cm)
- LW = liver weight (g)
- SW = spleen weight (g)

3.3 RNA EXTRACTION

Total RNA was extracted from the liver and caudal kidneys, collected from nine specimens from each sampling site, to be used in preparation for gene expression analysis.
As lysis buffer, 1 ml of PRImeZOLTM (Canvax) was added to 100 mg of tissue, and samples were homogenized using sterile pestles. PRImeZOL^{TM} keeps the RNA intact while destroying cells and dissolving cellular components; it contains 25-50% phenol to denature proteins and 10-25% guanidinium thiocyanate to protect RNA from RNase degradation. After keeping samples at room temperature for 5 minutes, 200 µl of chloroform were added to the homogenized to improve protein denaturation and enhance lipids' solubilization and recovery of total RNA. Samples were rigorously agitated manually, kept at room temperature for 3 minutes, and then centrifuged at 13000 ×g for 15 minutes at 4°C.

The centrifugation leads to the separation of the sample into three phases: the first on the bottom (red coloured) contains organic substances, like proteins and lipids, the second in the middle (white coloured) contains DNA and denatured proteins, and the last one, i.e. the supernatant (colourless), includes the total RNA. The supernatant was collected from each sample and transferred to a new Eppendorf tube; in this step, it is important not to touch the other phases.

In the next step, the RNA was precipitated by adding 500 µl of isopropyl alcohol. Samples were kindly agitated manually, incubated for 10 minutes at room temperature, and then centrifugated at 13000 ×*g* for 30 minutes at 4°C. At the end of this step, a white pellet formed on the bottom of the Eppendorf tube. It was washed twice with 1 ml of 75% ethanol and centrifuged at 7600 ×*g* for 5 minutes at 4°C. In the last steps, pellets were air-dried under the laminar flow hood for about 10 minutes, and then 30-70 µl of RNasi-free water was added to each pellet, depending on their size. Samples were incubated at 55°C for 10 minutes until the pellets were dissolved entirely.

3.3.1 RNA purification

This step eliminates peptides and carbohydrates remaining in the samples after total RNA extraction. The purification was performed only on RNA extracted from livers, which was not incubated at 55°C for 10 minutes, as described in the previous paragraph. Instead, it was incubated at 40°C for 5 minutes and centrifuged at 13000 ×*g* for 15 minutes to promote the precipitation of remaining carbohydrates and peptides. Then, 8M lithium chloride (LiCl) was added to each sample (1 volume of LiCl: 3 volumes of RNAase-free water) to induce the precipitation of total RNA. Samples were kept at 4°C overnight and then centrifuged at 13000 ×*g* for 20 minutes. This step again leads to the pellet forming on the bottom of the Eppendorf tubes.

Pellets were washed twice with 200 µl of 75% cold ethanol, samples were air-dried, and RNA was resuspended in RNAase-free water.

3.3.2 RNA quantification

After RNA extraction, its concentration was evaluated spectrophotometrically by a NanoDrop™ 2000c, which works in a range of concentration between 2000 and 15000 ng/µl.

This instrument can quantify the absorbance of small volumes (1 µl). The absorbance was measured at 230, 260, and 280 nm for each sample to evaluate the $A_{260/230}$ and $A_{260/280}$ ratios. The first is used to assess phenolic contamination (the absorbance peak of phenols is at 230 nm), indicated by a ratio lower than 1.8.

The $A_{260/280}$ must be included between 1.8 and 2.2; values lower than 1.8 indicate a possible protein contamination of the sample, and higher than 2.2 indicate a possible DNA contamination.

3.3.3 Assessment of RNA integrity

Electrophoresis was performed on a 1% agarose gel with intercalating FluoroVue Nucleic Acid Gel Stain (SMOBIO) to evaluate the integrity of total RNA and the absence of genomic contamination. The concentration of loaded in RNA was adjusted at 500 ng/µl; for electrophoresis, a 6x loading dye (Biotechrabbit) was used. mRNA represents only 1-3% of total RNA and is not visible on the agarose gel. So, to evaluate the integrity of the samples, ribosomal RNA was visualized, representing 80% of the total RNA. If the bands corresponding to 18S rRNA and 28S rRNA are visible, without smir, the RNA is intact. The absence of genomic contamination was verified by visualizing the absence of a high band in the gel.

3.4 cDNA SYNTHESIS

The total RNA samples were reverse transcribed into cDNA to quantify gene expression of *gpx1, gpx4, cat, ttp, tiar* and *g3bp* by quantitative real-time PCR (Polymerase Chain Reaction).

A cDNA Synthesis Kit (Biotechrabbit™) was used to obtain cDNA samples. This kit is highly efficient with long cDNAs (≥19 kb). 1000 ng/µl of total RNA were retrotranscribed, according to mix preparation:

Component	Volume (µl)
dNTPs mix (10 mM of each nucleotide base	2
RNase Inhibitor (40 U/µl)	0.5
5X Reverse Transcriptase Buffer	4
RNA Template (1000 ng/µl)	1
RevertUP™ II Reverse Transcriptase (200 U/µl)	1
Oligo (dT) primer (10 µM)	0.5
Nuclease-Free Water	11
Total volume	20

The RevertUP™ II Reverse Transcriptase enables highly efficient reverse transcription with increased thermostability, RNase Inhibitor is a potent inhibitor of RNAses, and Oligo (dT) promotes the synthesis of cDNA from poly(A) tailed mRNA.

Every test tube was then incubated into a PCR thermocycler (Applied Biosystems™ SimpliAmp™ Thermal Cycler) at 50° for 60 minutes and at 99°C for 5 minutes for the enzyme inactivation, as indicated in Figure 3.8.

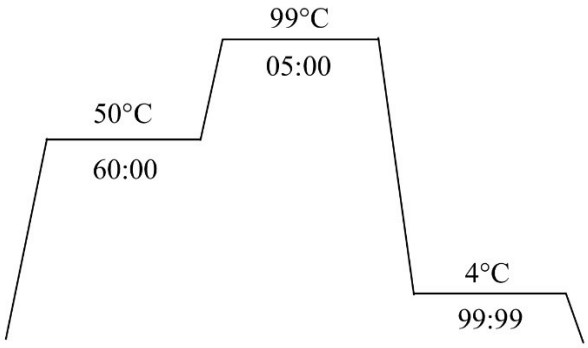

Figure 3.8) T*hermal profile for cDNA synthesis.*

3.5 CARACTERIZATION OF *ttp*, *tiar* AND *g3bp* SEQUENCES

To characterize nucleotide sequences of stress granules-related genes of *S. cephalus,* primers for PCR amplification were designed on conserved regions in multi-aligned orthologous coding sequences (CDS). These sequences, belonging to phylogenetically related species to *S. cephalus* (Table 3.3), were collected from the

NCBI database (https://www.ncbi.nlm.nih.gov/) and multi-aligned with the Clustal OMEGA program (https://www.ebi.ac.uk/jdispatcher/msa/clustalo).

Table 3.3) GeneBank accession numbers of nucleotide sequences used in multi-alignment for primer design.

Gene	Species	Accession numbers
ttp	*Carassius carassius*	XM_059513162.1
	Cyprinus carpio	XM_019126099.2
	Onychostoma macrolepis	XM_058756884.1
	Puntigrus tetrazona	XM_043220012.1
tiar	*Carassius auratus*	XM_026223905.1
	Cyprinus carpio	XM_042736949.1
	Onychostoma macrolepis	XM_058795710.1
	Sinocyclocheilus rhinocerous	XM_016536653.1
g3bp	*Carassius carassius*	XM_059554058.1
	Onychostoma macrolepis	XM_058778972.1
	Puntigrus tetrazona	XM_043248942.1

3.5.1 Primer design for PCR amplification

The following primer parameters were checked with the IDT OligoAnalyzer tool (https://eu.idtdna.com/pages/tools/oligoanalyzer):

- Primer size 18-23 nucleotides (nt)
- Melting temperature (Tm) 50-60°C, with the difference between melting temperature of forward primer and reverse primer no more than 2°C GC content 50-60%, with the absence of G and C at 3' end
- ΔG< -3.61 kcal/mol in the evaluation of hairpin and self-dimer structure
- ΔG< -3.61 kcal/mol in evaluation of hetero-dimer structure

Table 3.4) Primer sequences and relative Tm, used in stress granules-related genes characterization.

PRIMER	Sequences 5' → 3'	Tm (°C)
TTP_Seq_forward3	TACAGTCTGTCCCCACCA	60.70
TTP_Seq_reverse3	CGCTCCATCTTGTTGAAG	59.00
TIAR_Seq_forward2	CGTGGGGAATCTTTCAAG	58.00
TIAR_Seq_reverse4	CATGTCAGGTGACTCTTTGC	60.00
G3BP_Seq_forward1	CTGGTAGGGCGGGAGTT	62.20
G3BP_Seq_reverse4	GATGACTGTCTGGATACCTG	60.00

3.5.2 PCR amplification and amplicon purification

cDNA obtained by reverse transcription from RNA extracted from the liver was PCR-amplified using the primers reported in Table 3.4, according to 2X YourTaq™ PCR Master Mix (BiotechRabbit™) kit instructions. The following reagents were used in preparing the PCR mix:

Component	Volume (µl)
2X YourTaq PCR Master Mix	12.5
Primer forward (10 µM)	1
Primer reverse (10 µM)	1
cDNA (50 ng/l)	1
Nuclease-Free Water	9.5
Total volume	**25**

The thermal amplification profile used to promote the PCR reactions is reported in Figure 3.9.

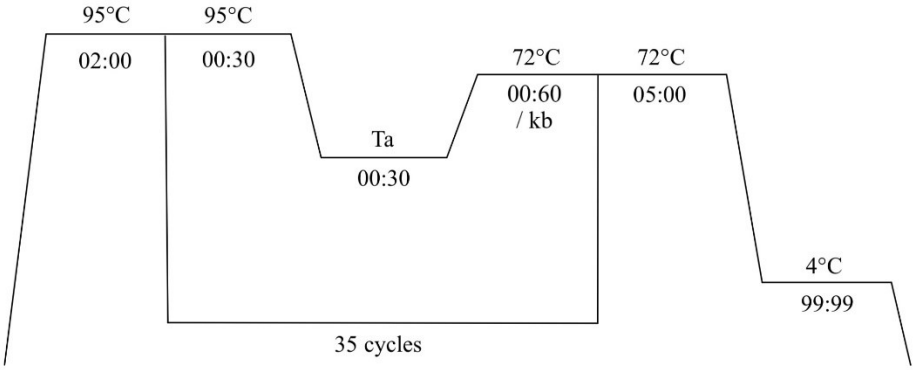

Figure 3.9) Thermal profile for PCR.

Electrophoresis was performed on 1.5% agarose gel to visualize the amplicons; those on bands that showed high light intensity and the expected size on the transilluminator were gel-purified according to Wizard® SV Gel and PCR Clean-Up System (Promega) kit instructions.

Gel slices were transferred in an Eppendorf tube with Membrane Binding Solution (10 µl per 10 mg of gel slice) and incubated at 60°C until completely dissolved. The obtained solution was applied to a minicolumn from the kit, and after 1 minute of incubation, it was all centrifuged at 16,000 ×*g* for 1 minute. After the flowthrough

was discarded, 700 µl of Membrane Wash Solution was added to the minicolumn and centrifugated at 16,000 ×*g* for 1 minute. The wash was repeated twice, the second time with 500 µl of Membrane Wash Solution, then centrifuged at 16,000 ×*g* for 5 minutes. One last centrifuge was performed to allow complete evaporation of residual ethanol. The Minicolumn was transferred to a new Eppendorf tube, and 30 µl of Nuclease-Free Water were added to elute the purification product after 1 minute at room temperature and centrifugation at 16,000 ×*g* for 1 minute.

3.5.3 Cloning: ligation, transformation, miniprep

Gel-purified amplicons, referring to *ttp*, *tiar*, and *g3bp,* were ligated in pGEM-T Easy Vector (Promega) (Figure 3.10) and cloned in chemo-competent DH-5α *E. coli* cells. To verify the transcription of the genes in *S. cephalus* and to obtain the sequences for the design of specific primers for quantitative real-time PCR (qRT-PCR), plasmid DNA was extracted from positively screened colonies using the UltraPrep (AHN Biotechnologie GmbH) kit and sequenced by Eurofins Genomics.

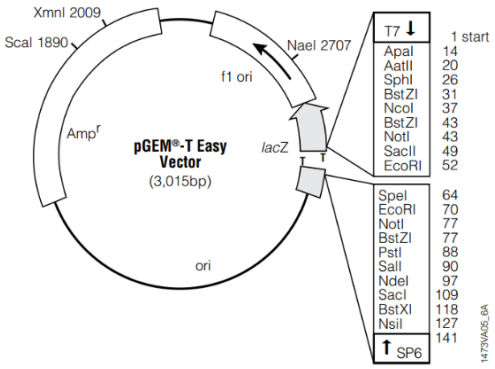

Figure 3.10) pGEM-T Easy Vector.

pGEM-T Easy Vector is an open vector with protruding ends with a single T, which is suitable for ligating amplicons with protruding ends with a single A, obtained with the PCR kit previously described. The ligation reaction was prepared as follows:

Component	Volume (µl)
2X Rapid Ligation Buffer	2.5
pGEM-T Easy Vector (50 ng/ µl)	0.5
PCR product (15-150ng/l)	1.5
T4 DNA Ligase (3 U/µl)	0.5
Total volume	**5**

Ligation reactions were then kept at 4°C overnight.

For transformation, 2 µl of ligation product, with *ttp*, *tiar* or *g3bp* amplicon inside, were added to 17 µl of *E. coli* bacteria and kept in ice for 30 minutes. The solution was incubated at 42°C for 90 seconds, then at 4°C for 2 minutes to induce thermal shock and the consequent perforation of the bacterial cell membrane to enter the ligation product. 150 µl of sterile LB-BROTH (Sigma Aldrich) medium (20 g/l) were added, and the solutions were kept at 37°C in an orbital shaker for one hour for bacteria growth. Bacteria were then distributed in sterile agarose (32 g/l) plates containing 50 mg/ml of ampicillin, 50 mg/ml of x-gal (5-bromo-4-chloro-3-indolyl-β-d-galactopyranoside) and 100 mM of IPTG (Isopropil-β-D-tiogalattopiranoside). Plates were kept at 37°C overnight for bacterial colony growth.

Two types of colony growth. Blue colonies are those in which ligation did not occur. This is evident because bacteria have the lacz gene vector not interrupted by the target gene sequence to produce β-galactosidase and break x-gal molecules producing 5-bromo-4-chloro-3-hydroxyindole (blue-coloured). White colonies are where ligation occurs; in this case, the target gene interrupts *lacz*, which does not permit its expression.

Some white colonies, the biggest and the most isolated inside the agarose plates, were used as DNA sources and amplified by PCR with the kit previously described. Commercial M13 primers (Invitrogen) were used to select the portion of the p-GEM vector where the *ttp*, *tiar* or *g3bp* insert could be present. PCR-verified colonies were cultured in sterile LB-BROTH medium, with 50 mg/ml ampicillin, overnight at 37°C in an orbital shaker.

PureYield™ Plasmid Miniprep System (Promega) was used to extract and purify the plasmid DNA; the term miniprep indicates the extraction of small quantities of plasmid DNA from transformed bacteria.

600 µl of bacterial culture were mixed with 100 µl of Cell Lysis Buffer, and then 350µl of cold (4–8°C) Neutralization Solution was added. The solution was centrifuged at maximum speed for 3 minutes, and the supernatant was then transferred to a PureYield™ Minicolumn. This was placed on a Collection tube and centrifuged at maximum speed for 15 seconds. The flowthrough was discarded. The column was then washed by adding 200µl of Endotoxin Removal Wash and centrifuged for 15 seconds, then 400 µl of Column Wash Solution were added, and the tubes were centrifuged for 30 seconds. Finally, 30 µl of nuclease-free water were added to the minicolumn and collected in a clean tube.

The purification products were sent to Eurofins Genomics™ for Sanger sequencing. For this purpose, 5 µl of plasmid DNA (50-100 ng/µl) were added to 5 µl of primers with a concentration of 5 pmol/µl (5 µM). The total volume was mixed into a Mix2Seq tube and sent to sequencing.

3.5.4 Gene and protein organization analysis

Stress granules-related gene sequences of S. *cephalus*, obtained by sequencing, were firstly verified by the BLAST tool (https://blast.ncbi.nlm.nih.gov/Blast.cgi), by evaluating similarity and identity to other sequences and then translated *in silico* with the Expasy translate tool (https://web.expasy.org/translate/). The deduced amino acid sequences were analyzed using the SMART program (http://smart.embl-heidelberg.de/) to visualize their domain composition.

3.6 QUANTITATIVE REAL-TIME PCR (qRT-PCR)

Reverse transcription-quantitative PCR (RT-qPCR) is based on identifying and quantifying the fluorescence emitted by a reporter molecule (in this case, the SYBRGreen intercalating dye). The measurement takes place in real-time during the accumulation phase of the PCR product and at each amplification cycle, thus allowing us to monitor the amplification during the initial phase and especially during the exponential phase of the PCR reaction.

3.6.1 Primer design for qRT-PCR

Specific primers for *ttp*, *tiar*, *g3bp*, *cat*, *gpx1,* and *gpx4* quantification were designed in CDS of sequences of *S. cephalus* verified by sequencing (Table 3.5)

(for the sequence of *cat, gpx1* and *gpx4* see Piva, 2021 and Vanzan, 2024). Primers were designed considering 60°C as the optimal melting temperature, 100-200 nt as product size, and GC clamp < 2 according to Beacon Designer (https://www.premierbiosoft.com/qOligo/Oligo.jsp?PID=1).

Table 3.5) Primer sequences, and relative Tm, used in qRT-PCR.

PRIMER	Sequences 5' → 3'	Tm (°C)
TTP_RT_forward2new	CAGTCTCAAGATGGAAGGCTCGG	66.00
TTP_RT_reverse2	TGGCTGTTTCCGTTGGCACT	67.00
TIAR_RT_forward3	CGTCTGTCGCATAAGGTGTTCT	64.20
TIAR_RT_reverse3	GGACTAACTGGGCTACTCGGA	64.50
G3BP_RT_forward4	GAAGCAGTCTATGGGCAAGC	62.90
G3BP_RT_reverse3	AGCCTCAGAGTCCCCAAAG	63.40
1_CAT_P.promelas_F	GCGTCCTGAATCGTTGCACCA	67.20
1_CAT_P.promelas_R	TGACCCTCAGCGTTGACCAGT	67.50
1_GPX1b_P.promelas_F	GCAAGGCATCGGGGTTGGA	67.00
1__GPX1b_P.promelas_R	TCGTTCCTCAAAGAGAAGCGACA	65.70
2_GPX4_S.cephalus_F	CGGGACAGAAGCGGACATCAA	66.20
2_GPX4_S.cephalus_R	TCCCAGAGTTCCCTTGCCTTTG	66.30
GAPDH_RT_forward	ATCACAGCCACACAGAAGAC	62.10
GAPDH_RT_forward	AGGAATGACTTTGCCCACAG	62.50

3.6.2 Gene expression quantification

Nine specimens of *S. cephalus* per site, each in technical triplicate, were evaluated by qRT-PCR for gene quantification in the liver and caudal kidneys. Transcription levels were normalized according to the housekeeping gene *gapdh* to compensate for variations in the amounts of cDNA.

First of all, primer amplification efficiency (about -3.3) was verified by absolute quantification (calibration line) on scalar diluted cDNAs (100, 50, 25 and 12.5 ng/μl).

qPCRBIO SyGreen Blue (PCRBIOSYSTEM) kit, containing 100 nM ROX as a quencher, was used for qRT-PCR on A7500 Real-Time PCR System (Applied Biosystems). The mix was prepared as follows:

Component	Volume (µl)
2x qPCRBIO SyGreen Mix	5
Forward Primer (10 µM)	0,4
Reverse Primer (10 µM)	0,4
cDNA (50 ng/ul)	1
Nuclease-Free Water	3,2
Total volume	**10**

The qRT-PCR thermal parameters were set as follows:

- 2 minutes at 95°C (initial denaturation)
- 95°C for 20 seconds and 60°C for 1 minute for 38 cycles (primer annealing and amplification)
- 15 seconds at 95°C, 1 minute at 60°C, 15 seconds at 95°C and 15 seconds at 60°C (melting profile). A dissociation curve represents the melting profile, evaluated to verify the absence of genomic contamination

Relative values were obtained using the $2^{-\Delta\Delta Ct}$ mathematical model presented by PE Applied Biosystems (Perkin Elmer, Forster City, CA) (Pfaffl, 2001). Ct for each sample was normalized, subtracting the Ct of the housekeeping gene *gapdh*; this way, the first ΔCt was obtained. For the very low-polluted site (control site), an average of the ΔCt of the samples was made for each analysed gene. The ΔCt of each sample from all three sites were normalized, subtracting the highest mean to obtain a second ΔΔCt. All gene expression values were normalized using the same reference, making it possible to compare different enzymes and sampling sites.

$$\Delta C_T = Ct\,(sample) - Ct\,(gapdh)$$

$$\Delta\Delta C_T = \Delta C_T\,(sample) - \Delta C_T\,(calibration\ sample)$$

3.7 BIOCHEMICAL ANALYSES

To perform biochemical analyses, liver and caudal kidney tissue samples were homogenized using an aqueous saline solution. The so-called homogenization buffer contains the following:

- Tris-HCl, 10 mM (pH 7,6).

- EDTA, 1 mM.
- DTT (Dithiothreitol), 1 mM.
- Sucrose, 0.5 M.
- KCl, 0,15 M.

Initially, 400 µl of buffer were added per 100 mg of tissue. Then, every sample was homogenized using a high-speed mixer-homogenizer (Polytron PT 3000, Kinematica AG, Homogenizer Mixer). After that, the samples were centrifuged at 13000 ×*g* for 60 minutes at 4°C, and the supernatant was then transferred to new Eppendorf, divided into different aliquots, and stored at -20 °C.

3.7.1 Total protein quantification

To evaluate the protein content of the cell extract it has been used the phenolic reagent Folin-Ciocalteau based on the method by Lowry et al., 1951. The procedure allows the determination of a protein quantity between 5 and 100 µg in 0,2 ml of sample.

The protein concentration of each sample, expressed in mg/ml, is calculated by linear regression between known and increasing amounts of standards (Bovine serum albumin, BSA) and their absorbance values at 750 nm.

The following solutions were prepared:

- A solution: Na_2CO_3 2% NaOH 0,1 M. 4 g NaOH + 20 g Na_2CO_3 in 1 l of H_2O milliQ.
- B solution: $CuSO_4x5H_2O$ 0,5% in sodium citrate 1%. 1 g tri-sodium citrate + 0,5 g $CuSO_4x5H_2O$.
- C solution: 25 ml of A solution + 0,5 ml of B solution (ratio 1:50).
- D solution: 1,36 ml of H_2O + 1 ml FOLIN
- Standard solution: 1 mg of BSA/ml in 0.15 M NaCl

A standard curve was constructed to evaluate the sample concentration, using increasing quantities of albumin as standards. For each measurement, a different volume of albumin was added to milliQ H_2O up to a total volume of 200 µl. The measurement was repeated twice for each dilution, and the solution was prepared in different tubes.

The dilution scheme is shown in Table 3.6.

Table 3.6) Dilution scheme for standard curve for Lowry assay

Dilution	1	2	3	4	5	6
Albumin (µl)	0	10	30	50	70	100
milliQ H_2O (µl)	200	190	170	150	130	100

For the samples test, albumin was substituted with 4 µl of cell extract to which 196 µl of H_2O were added. A series of tubes was set up so that each sample was duplicated. The sample was replaced with an identical volume of homogenization buffer for blanks.

For each measurement (standard curve and samples), 1 ml of solution C was added to each tube and vortexed. After 10 minutes, 100 µl of solution D were added and the vortexed. The samples were kept in the dark for 30 minutes, being vortexed halfway through. After that, the absorbance at a wavelength of 750 nm was read.

The standard curve has a linear equation y = bx + a, where y represents the absorbance and x represents the protein concentration to be determined (x=(y-a)/b). The average was calculated and normalized for each double by subtracting the blank mean. Then, the result was divided by the sample volume (to obtain the result in µg/ml) and then multiplied by 0,001 to obtain a protein concentration in mg/ml

$$\text{mg proteins/ml} = \frac{0{,}001\ \left(\frac{y-a}{b}\right)}{sample\ volume}$$

3.7.2 GPx activity assay

The GPx assay was carried out indirectly.

GSH is the reducing factor GPx uses to convert hydroperoxides, being oxidated into GSSG. Meanwhile, GSSG is reduced to GSH by GR in a reaction that uses NADPH as a reducing factor. NADPH oxidates to $NADP^+$, causing the solution to change colour and decrease its absorbance. GPx activity is proportional to the decrease in NADPH. Where GPx is not present, NADPH does not get oxidate. Therefore, in this case, only a slight variation in absorbance is recorded.

The change of absorbance occurring during those reactions was measured with a spectrophotometer. Hydrogen peroxide was used as the substrate; therefore, the activity of only selenium-dependent GPx was evaluated.

The following solutions were prepared:

- Stock solution: 0,0062 g of NADPH (0,15 mM) + 0,019 g of GSH (2,5 mM) + 0,002 g of NaN_3 (1,25 mM) + 52,5 µl of GR in 25 ml of phosphate buffer (125mM);
- H_2O_2 solution: 14 µl of stock H_2O_2 (30%) in 50 ml of H_2O (absorbance at 240 nm > 0,106).

Samples were analyzed in two replicates; two blank measurements were carried out. Quartz cuvettes were set up as in Table 3.7.

Table 3.7) Composition of cuvettes for GPx assay.

		Sample - Liver	Sample – Caudal kidney	Blank
REAGENTS	Stock solution	800 µl	800 µl	800 µl
	Phosphate buffer	98,5 µl	95 µl	100 µl
	Sample	1,5 µl	5 µl	-
	H_2O_2 solution	100 µl	100 µl	100 µl
Total volume		1 ml	1 ml	1 ml

Absorbance was read at a wavelength of 340 nm for 5 minutes at regular intervals of 60 seconds. The delta of absorbance in the total 5-minute trace was considered. To calculate GPx units per mg of total proteins, the following calculations were performed:

- Firstly, the absorbance values of the samples were normalized by subtracting the blank;
- The enzymatic activity of GPx was then calculated with the Lambert-Beer law, per minute, per unit of volume:

$$U\ gpx/mL\ = \left[\frac{Ai\ -\ Af}{\Delta t/6{,}22}\right] \cdot \frac{100}{sample\ volume}$$

- Lastly, the result was normalized to the mg of total protein present in the sample:

$$U\ GPx/mg\ proteins\ = \frac{(U\ GPx/ml)}{(mg\ proteins/ml)}$$

3.7.3 CAT activity assay

Aebi's (1984) protocol was used to quantify catalase activity. This method exploits the reaction between catalase and H_2O_2, which leads to a decrease in the absorbance at 240nm. The reaction is so detectable with a spectrophotometer.

The following solutions were prepared:

- Phosphate buffer Na_2HPO_4 - NaH_2PO_4 (50 mM, pH 7,5);
- H_2O_2 solution: 170 µl of stock H_2O_2 (30%) in 50 ml of H_2O (absorbance > 1,18).

Samples were analyzed in two replicates; two blank measurements were carried out. Quartz cuvettes were set up as in Table 3.8.

Table 3.8) Composition of cuvettes for CAT assay.

		Sample - Liver	Sample – Caudal kidney	Blank
REAGENTS	Phosphate buffer	1990 µl	1990 µl	1990 µl
	homogenization buffer	8 µl	-	10 µl
	Sample	2 µl	10 µl	-
	H_2O_2 solution	1000 µl	1000 µl	1000 µl
Total volume		2 ml	2 ml	2 ml

Enzymatic kinetics were followed every 5 seconds for a total time of 1 minute.

To calculate GPx units per mg of total proteins, the following calculations were performed:

- Firstly, the enzymatic activity of CAT was calculated with the Lambert-Beer law; the value was multiplied by the dilution factor and normalized per minute

$$U\ CAT/mL\ = \left[\frac{Ai\ -\ Af}{40/0{,}833}\right] \cdot \frac{Total\ volume}{Sample\ volume} \cdot 1000$$

- Then, the result was normalized to the mg of total protein present in the sample.

$$U\ CAT/mg\ proteins\ = \frac{(U\ CAT/ml)}{(mg\ proteins/ml)}$$

3.8 STATISTICAL ANALYSIS

For each site, the mean values (n= 9) ± Standard Deviation (SD) were calculated for both qRT-PCR and enzyme activity results. The JASP program (Version 0.19) was used for the statistical analysis of the data. After checking the variance's uniformity with Levene's test, a one-way variance analysis (ANOVA) was applied, followed by Tukey's test to analyze significant ($p < 0.05$) differences between the means.

4 RESULTS

4.1 INDICES (HSI, SSI, and FCF)

Three somatic indices were calculated to have a complete and more accurate evaluation of the sampled specimens: the Hepatosomatic Index (HSI), the Spleen Somatic Index (SSI), and the Fulton's Condition Factor (FCF). All the specimens were weighed, and the total length was measured before the dissection activity; after that, the liver and the spleen were weighed for each fish.

The graphs in Figures 4.1, 4.2, and 4.3 refer to results obtained for every index compared between the four sites.

4.1.1 Hepatosomatic Index (HSI)

The comparison between the HSI of *S. cephalus,* obtained for the four sites at different PFAS levels, is illustrated in Figure 4.1. Levene's test didn't indicate a significant difference between the variances of the sites; therefore, the ANOVA test was performed (Table 4.1 and Table 4.2). In the graph relative to HSI, different letters indicate a significant (p-value < 0.05) difference between the means of the sites; the categorization was based on the posthoc Tukey test (Table 4.3). The HSI for the medium-polluted site shows an increase of 47% compared to HIS for the control site. In the highly-polluted site, the increment of HIS is about 176% with respect to HIS for the control site.

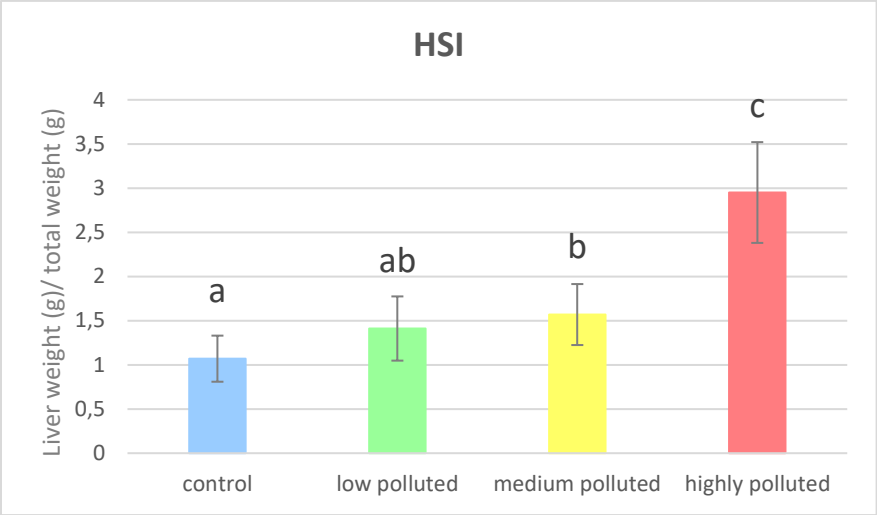

Figure 4.1) Means and standard deviations of the HSI for the four evaluated sites (control site n=10, low-polluted site n=7, medium-polluted site n=9, highly-polluted site n=6). Different letters indicate a significant difference between the means (p<0.05).

Table 4.1) Levene's test result, referred to HSI. Variances show no statistically significant difference (p > 0.05) among sites.

Test for Equality of Variances (Levene's)

F	df1	df2	p
1.624	3.000	28.000	0.206

Table 4.2) ANOVA test result, referred to HSI. Means show statistically significant differences (p < 0.001) among sites.

ANOVA - Hepatosomatic index

Cases	Sum of Squares	df	Mean Square	F	p
Column 2	13.972	3	4.657	32.769	< .001
Residuals	3.979	28	0.142		

Table 4.3) Tukey's test results, referred to HSI. Means for all the sites were compared to each other (SE is the standard error while t is the fraction between the mean difference and SE).

Post Hoc Comparisons - Site

		Mean Difference	SE	t	p_{tukey}
Control	(Low-polluted)	−0.341	0.186	−1.838	0.278
	(Medium-polluted)	−0.499	0.173	−2.883	0.035*
	(Highly-polluted)	−1.881	0.195	−9.662	< .001***
(Low-polluted)	(Medium-polluted)	−0.158	0.190	−0.832	0.839
	(Highly-polluted)	−1.540	0.210	−7.340	< .001***
(Medium-polluted)	(Highly-polluted)	−1.382	0.199	−6.953	< .001***

4.1.2 Spleen Somatic Index (SSI)

The comparison between the SSI of *S. cephalus*, obtained for the four sites at different PFAS levels, is illustrated in Figure 4.2. Levene's test didn't indicate a significant difference between the variances of the sites; therefore, the ANOVA test was performed (Table 4.4 and Table 4.5). In the graph relative to SSI, different letters indicate a significant (p-value < 0.001) difference between the means of the sites; the categorization was based on the posthoc Tukey test (results in Table 4.6). The SSI showed an increase of 87% for the low-polluted site with respect to the control one. No significant difference resulted between the medium-polluted site and the control site; the highly-polluted site showed a decrease in the SSI of 57% compared to the control site.

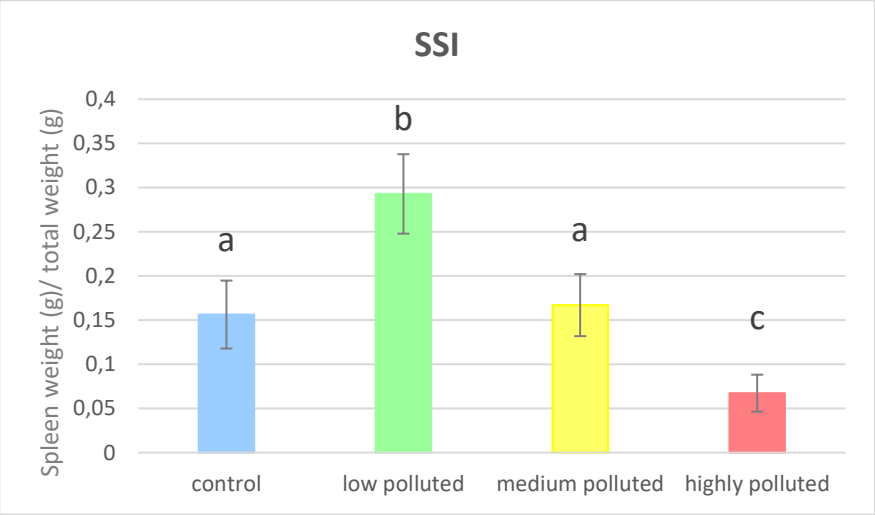

Figure 4.2) Means and standard deviations of the SSI for the four evaluated sites (control site n=8, low-polluted site n=7, medium-polluted site n=9, highly-polluted site n=9). Different letters indicate a significant difference between the means (p-value <0.001).

Table 4.4) Levene's test results, referred to SSI. Variances show no statistically significant difference (p-value> 0.05) among sites.

Test for Equality of Variances (Levene's)

F	df1	df2	p
2.126	3.000	29.000	0.119

Table 4.5) ANOVA test result, referred to SSI. Means show statistically significant differences (p-value < 0.001) among sites.

ANOVA - Spleen somatic index ▼

Cases	Sum of Squares	df	Mean Square	F	p
Site	0.204	3	0.068	55.444	< .001
Residuals	0.036	29	0.001		

Table 4.6) Tukey's test results, referred to SSI. The means for all the sites were compared to each other. (SE is the standard error while t is the fraction between the mean difference and SE).

Post Hoc Comparisons - Site

		Mean Difference	SE	t	p_{tukey}
(Low-polluted)	(Medium-polluted)	0.127	0.018	7.224	< .001***
	(Highly-polluted)	0.227	0.018	12.876	< .001***
	Control	0.138	0.018	7.622	< .001***
(Medium-polluted)	(Highly-polluted)	0.100	0.016	6.042	< .001***
	Control	0.011	0.017	0.626	0.923
(Highly-polluted)	Control	−0.089	0.017	−5.236	< .001***

4.1.3 Fulton's Condition Factor (FCF)

The comparison between the FCF of *S. cephalus,* obtained for the four sites at different PFAS levels, is illustrated in Figure 4.3. Levene's test didn't indicate a significant difference between the variances of the sites; therefore, the ANOVA test was performed (Table 4.7 and Table 4.8). In the graph relative to FCF, different letters indicate a significant (p-value < 0.001) difference between the means of the sites; the categorization was based on the posthoc Tukey test (results in Table 4.9). The FCF showed no significant difference between the low-polluted and control sites. Conversely, an increase in the value of FCF for the medium-polluted and highly-polluted sites, compared to the control one (30% and 31%, respectively), was observed.

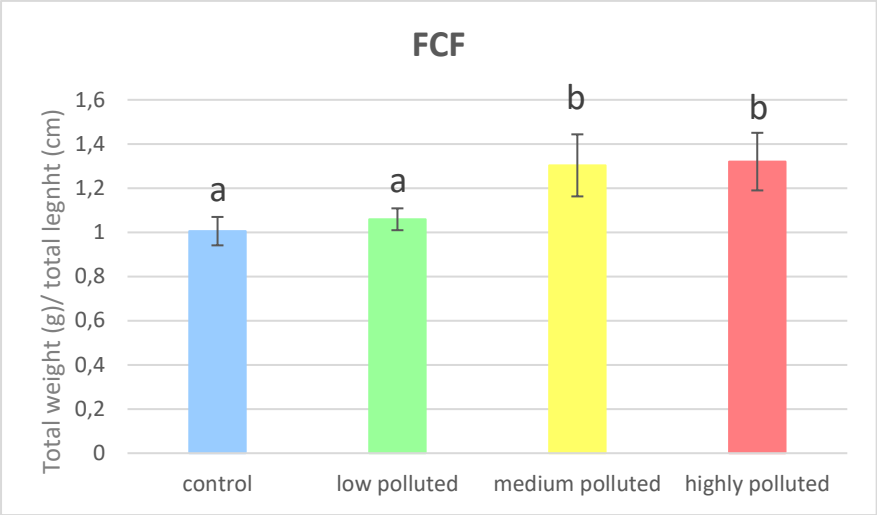

Figure 4.3) Means and standard deviations of the FCF for the four evaluated sites (control site n=9, low-polluted site n=9, medium-polluted site n=9, highly-polluted site n=8). Different letters indicate a significant difference between the means (p-value <0.001).

Table 4.7) Levene's test result, referred to FCF. Variances show no statistically significant difference (p > 0.05) among sites.

Test for Equality of Variances (Levene's) ▼

F	df1	df2	p
2.073	3.000	31.000	0.124

Table 4.8) ANOVA test result, referred to FCF. Means show statistically significant differences (p < 0.001) among sites.

ANOVA - Fulton's Condition Factor ▼

Cases	Sum of Squares	df	Mean Square	F	p
Site	0.695	3	0.232	21.869	< .001
Residuals	0.328	31	0.011		

Table 4.9) Tukey's test results, referred to FCF. The means for all the sites were compared to each other. (SE is the standard error while t is the fraction between the mean difference and SE).

Post Hoc Comparisons - Site

		Mean Difference	SE	t	p_{tukey}
(Highly-polluted)	(Medium-polluted)	0.017	0.050	0.340	0.986
	(Low-polluted)	0.261	0.050	5.226	< .001***
	Control	0.315	0.050	6.295	< .001***
(Medium-polluted)	(Low-polluted)	0.244	0.049	5.036	< .001***
	Control	0.298	0.049	6.137	< .001***
(Low-polluted)	Control	0.053	0.049	1.102	0.691

4.2 CHARACTERIZATION OF STRESS GRANULES-RELATED GENES IN *S. cephalus*

Primers reported in Table 3.4 allowed me to obtain amplicons corresponding to partial nucleotide sequences of the CDS of *ttp*, *tiar* and *g3bp* of *S. cephalus*.

As regards *ttp*, a sequence of 562 nt was characterized, encoding a putative protein of 186 amino acids (aa) (Figure 4.4). The nucleotide sequence showed the highest similarity (100%) and identity (98.22%) to the sequence of "zinc finger protein 36, C3H type-like 1b (*zfp36l1b*)", alias *ttp*, of *Rhinichthys klamathensis goyatoka* (GeneBank accession number: XM_056262707.1; complete CDS: 1056 nt), a fish of the Cyprinidae family. The amino acid sequence showed the highest similarity (100%) and identity (97.31%) to the sequence of "mRNA decay activator protein ZFP36L1b", alias TTP, always of *Rhinichthys klamathensis goyatoka* (GeneBank accession number: XP_056118682.1; complete protein: 351 aa).

```
tacag tct gtc ccc acc acc ggt gcc agt acc ccc ttt acc ccc acc ggg tcc ctg ctg gac
   Q   S   V   P   T   T   G   A   S   T   P   F   T   P   T   G   S   L   L   D
agg aag gtg gtg ggt acc cct tca atg gga ctc tac cag cgt cgc cac tct gtg tcc gtt
 R   K   V   V   G   T   P   S   M   G   L   Y   Q   R   R   H   S   V   S   V
acc agc tcc aaa tct atg cag aac caa tat att aac agt ctc aag atg gaa ggc tcg gtt
 T   S   S   K   S   M   Q   N   Q   Y   I   N   S   L   K   M   E   G   S   V
tcc atg aat ggg agc agt aac aac aag gag aac cgc ttt cgt gac cgg tcc ttc tct gaa
 S   M   N   G   S   S   N   N   K   E   N   R   F   R   D   R   S   F   S   E
act ggg gag cgt cta agg ccg agc aac atc acg tgc att agt gcc aac gga aac agc cag
 T   G   E   R   L   R   P   S   N   I   T   C   I   S   A   N   G   N   S   Q
atc aac tca agc cgc tat aaa acc gaa ctc tgc aga ccc ttc gag gag aac ggc act tgt
 I   N   S   S   R   Y   K   T   E   L   C   R   P   F   E   E   N   G   T   C
aaa tat ggt gac aag tgc cag ttt gcc cac ggg atg cac gag ctt cgt agt cta aat cgc
 K   Y   G   D   K   C   Q   F   A   H   G   M   H   E   L   R   S   L   N   R
cac ccc aag tat aag acc gag ctc tgt cgc aca ttc cac agc att ggt tac tgc ccg tat
 H   P   K   Y   K   T   E   L   C   R   T   F   H   S   I   G   Y   C   P   Y
ggg ccg cgt tgc cac ttc atc cac aac gca gag gag cgc cgc gga ccc cct ccg ctc tct
 G   P   R   C   H   F   I   H   N   A   E   E   R   R   G   P   P   P   L   S
gcc ttc aac aag atg gag cg
 A   F   N   K   M   E
```

Figure 4.4) Partial ttp cDNA sequence of S. cephalus, resulting from amplicon sequencing, and, in bold, deduced amino acid sequence, showing the main TTP domains (Tis11 domain in yellow, ZnF domains in green).

Figure 4.5 shows the typical domain organization of TTP, which is well-known in mammals (Blackshear et al., 2003), according to the deduced partial amino acid sequence of *S. cephalus* shown in Figure 4.4. The two Zinc finger (Znf) domains contain multiple finger-like protrusions, zinc sensing can establish tandem contacts with target molecules (DNA, RNA, protein or lipid substrate), in this way functioning in the regulation of gene transcription and translation, mRNA trafficking, cytoskeleton organisation, epithelial development, cell adhesion, protein folding, and chromatin remodelling. The Butyrate response factor 1 (Tis11B) domain is thought to be involved in the response to growth factors.

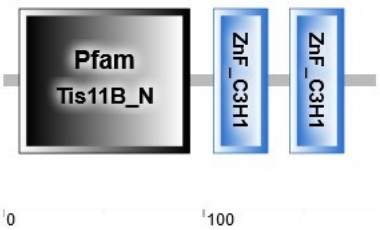

Figure 4.5) Domain organization of partial TTP of S. cephalus.

As regards *tiar*, a sequence of 647 nt was characterized, encoding a putative protein of 215 aa (Figure 4.6). The nucleotide sequence showed the highest similarity (100%) and identity (98.45%) to the sequence of "TIA1 cytotoxic granule-associated RNA binding protein-like 1 (*tial1*)", alias *tiar*, of *Rhinichthys klamathensis goyatoka* (GeneBank accession number: XM_056257075.1; complete CDS: 1164 nt), as resulted for *ttp*. The amino acid sequence showed the highest similarity (100%) and identity (100%) to the sequence of "nucleolysin TIAR", alias TIAR, always of *Rhinichthys klamathensis goyatoka* (GeneBank accession number: XP_056113049.1; complete protein: 388 aa).

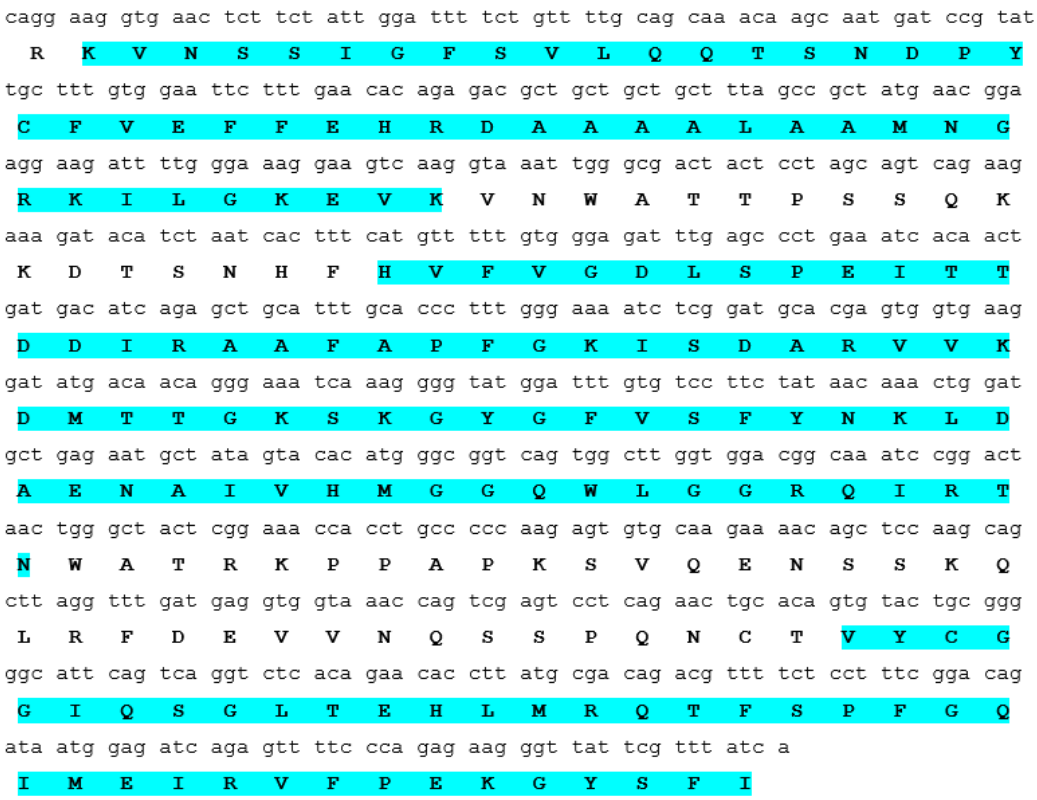

Figure 4.6) Partial tiar cDNA sequence of *S. cephalus*, resulting from amplicon sequencing, and, in bold, deduced amino acid sequence, showing the main TIAR domains (RRM domains in blue).

Figure 4.7 shows the typical domain organization of TIAR, which is well-known in mammals (Warris et al., 2014), according to the deduced partial amino acid sequence of *S. cephalus* shown in Figure 4.6. The three RNA Recognition Motifs (RRMs) are responsible for specific binding to single-strand RNA.

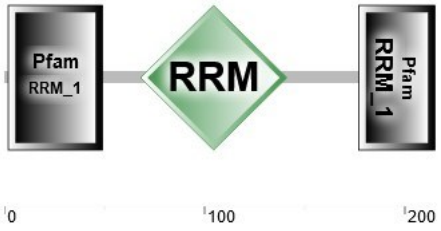

Figure 4.7) Domain organization of partial TIAR of S. cephalus.

As regards *g3bp*, a sequence of 379 nt was characterized, encoding a putative protein of 126 aa (Figure 4.8). The nucleotide sequence showed the highest similarity (99%) and identity (97.8%) to the sequence of "G3BP stress granule assembly factor 2a (*g3bp2a*)", alias *g3bp*, of *Rhinichthys klamathensis goyatoka* (GeneBank accession number: XM_056265135.1; complete CDS: 1524 nt), as resulted for *ttp* and *tiar*. The amino acid sequence showed the highest similarity (82%) and identity (99.4%) to the sequence of "ras GTPase-activating -binding 2", alias G3BP, of *Labeo rohita* (GeneBank accession number: RXN30156.1; complete protein: 431 aa), another fish of the Cyprinidae family.

```
taac ttc tcg ata aag cgc cag act ttc tgc aca gat ttt atg gac gaa act cat cat atg
  N   F   S   I   K   R   Q   T   F   C   T   D   F   M   D   E   T   H   H   M
tcc atg gcc gga ctg gat tcg aat gga aag ctt tca gaa gca gtc tat ggg caa gct gag
 S   M   A   G   L   D   S   N   G   K   L   S   E   A   V   Y   G   Q   A   E
ata cat aag aag gta atg tcc ctg caa ttc agt gag tgc cac aca aaa atc cgg cat gtg
 I   H   K   K   V   M   S   L   Q   F   S   E   C   H   T   K   I   R   H   V
gat gcc cat gcc act ttg agt gat ggt gtg gtt gtc cag gtc atg gga gaa ctt tcc aat
 D   A   H   A   T   L   S   D   G   V   V   V   Q   V   M   G   E   L   S   N
aat gga cag ccc atg agg aag ttc cta cag aca ttt gtg ctg gct cca gag ggt tct gtg
 N   G   Q   P   M   R   K   F   L   Q   T   F   V   L   A   P   E   G   S   V
gca aat aag ttt tat gtt cac aac gac atc ttt cga tat gaa gat gag gtc ttt ggg gac
 A   N   K   F   Y   V   H   N   D   I   F   R   Y   E   D   E   V   F   G   D
tct gag gct gag ctt gat
 S   E   A   E   L   D
```

Figure 4.8) Partial *g3bp* cDNA sequence of *S. cephalus*, resulting from amplicon sequencing, and, in bold, deduced amino acid sequence, showing the NTF2 domain (in purple) of G3BP.

Unlike the characterized sequences of *ttp* and *tiar*, the obtained *g3bp* sequence of *S. cephalus* did not allow to deduce an amino acid sequence long enough to identify all the major domains of G3BP, well-known in mammals (Parker et al., 1996). Only the Nuclear Transport Factor 2 (NTF2) domain is shown in Figures 4.8 and 4.9; it

is a homodimer that stimulates the efficient nuclear import of a cargo protein. The domain that still needs to be identified is the RRM domain.

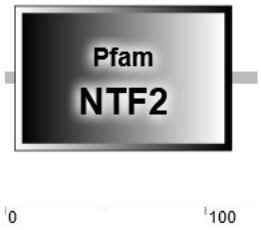

Figure 4.9) Domain organization of partial G3BP of S. cephalus

4.3 GPx1, GPx4, CAT, TTP, G3BP, AND TIAR mRNA EXPRESSION LEVELS

The *gpx1, gpx4, cat*, *ttp, g3bp,* and *tiar* transcription levels were evaluated by qRT-PCR. Data were normalized with respect to the *gapdh* housekeeping gene. The mRNA accumulation was evaluated for specimens of *S. cephalus* sampled in the four sites at different PFAS levels. All the genes were quantified in the liver and the caudal kidney.

4.3.1 *gpx1*

Figure 4.10 shows the expression levels of *gpx1* in the liver of *S. cephalus.* Levene's test didn't indicate a significant difference between the variances of the sites; therefore, the ANOVA test was performed (Table 4.10 and Table 4.11). No statistically significant difference between the control site and the three polluted sites is shown in Table 4.12; conversely, a statistically significant difference ($p < 0.05$) was detected between the *gpx1* mRNA expression level for the medium-polluted site and those for the low/highly-polluted sites.

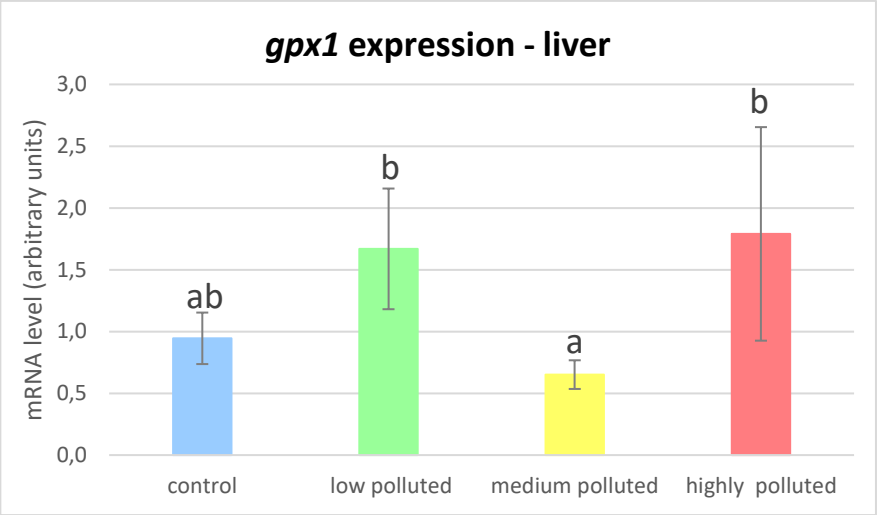

Figure 4.10) gpx1 mRNA expression in the liver of specimens from the four sites, with relative standard deviations (control site n=6, low-polluted site n=7, medium-polluted site n=5, highly-polluted site n=5). Different letters indicate statistically significant differences (p-value < 0.05) among sites.

Table 4.10) Levene's test results refer to gpx1 mRNA expression levels in the liver. Variances show no statistically significant difference (p-value > 0,05) among sites.

Test for Equality of Variances (Levene's)			
F	df1	df2	p
2.569	3.000	19.000	0.085

Table 4.11) ANOVA test result, referred to gpx1 mRNA expression levels in the liver. Means show statistically significant differences (p-value < 0.01) among sites.

Cases	Sum of Squares	df	Mean Square	F	p
Site	5.009	3	1.670	6.766	0.003
Residuals	4.689	19	0.247		

Table 4.12) Tukey's test results refer to gpx1 mRNA expression levels in the liver. The means for all the sites were compared to each other. (SE is the standard error while t is the fraction between the mean difference and SE).

Post Hoc Comparisons - Site

		Mean Difference	SE	t	P_{tukey}
Control	(Low-pollution)	−0.724	0.276	−2.619	0.073
	(Medium-pollution)	0.294	0.301	0.976	0.764
	(Highly-pollution)	−0.845	0.301	−2.810	0.050
(Low-pollution)	(Medium-pollution)	1.018	0.291	3.498	0.012*
	(Highly-pollution)	−0.121	0.291	−0.417	0.975
(Medium-pollution)	(Highly-pollution)	−1.139	0.314	−3.625	0.009**

No statistically significant differences among the sites were observed regarding gpx1 transcription levels in the caudal kidney (Figure 4.11), according to Levene's test and ANOVA test (Table 4.13 and Table 4.14*)*.

It can be noticed in the graph that the standard deviation for each site is very high, indicating high variance levels for each site.

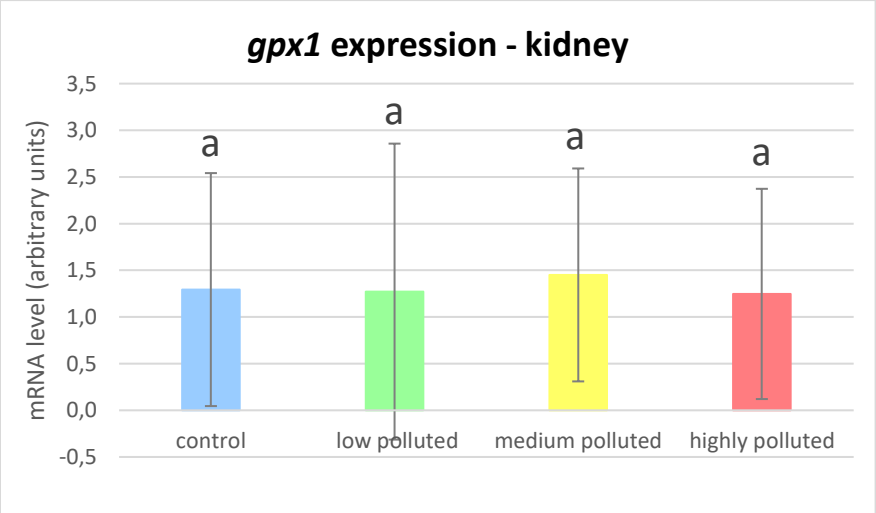

Figure 4.11) gpx1 mRNA expression in the caudal kidney of specimens from the four sites, with relative standard deviations (control site n=5, low-polluted site n=5, medium-polluted site n=5, highly-polluted site n=5). Different letters indicate statistically significant differences (p-value > 0.05) among sites.

Table 4.13) Levene's result, referred to gpx1 mRNA expression levels in the caudal kidney. Variances show no statistically significant difference (p-value > 0.05) among sites.

Test for Equality of Variances (Levene's)

F	df1	df2	p
2.261	3.000	21.000	0.111

Table 4.14) ANOVA test result, referred to gpx1 mRNA expression levels in the caudal kidney. Means show no statistically significant difference (p-value > 0.05) among sites.

ANOVA - 2^-△△Ct

Cases	Sum of Squares	df	Mean Square	F	p
Site	2.407	3	0.802	0.272	0.845
Residuals	61.835	21	2.945		

4.3.2 *gpx4*

For *gpx4,* expression levels in the liver are reported in Figure 4.12. Also, in this case, Levene's test didn't indicate a significant difference between the variances of the sites; therefore, the ANOVA test was performed (Table 4.15 and Table 4.16). The graph shows that gene expression levels are similar for the control site and the low-polluted one; a statistically significant difference ($p < 0.01$) between the control site and the medium-polluted one, with a decrease of 57%, was measured. The highly-polluted site showed an increase of 164% in *gpx4* levels in the liver of *S. cephalus* compared to those measured for the control site (Table 4.17).

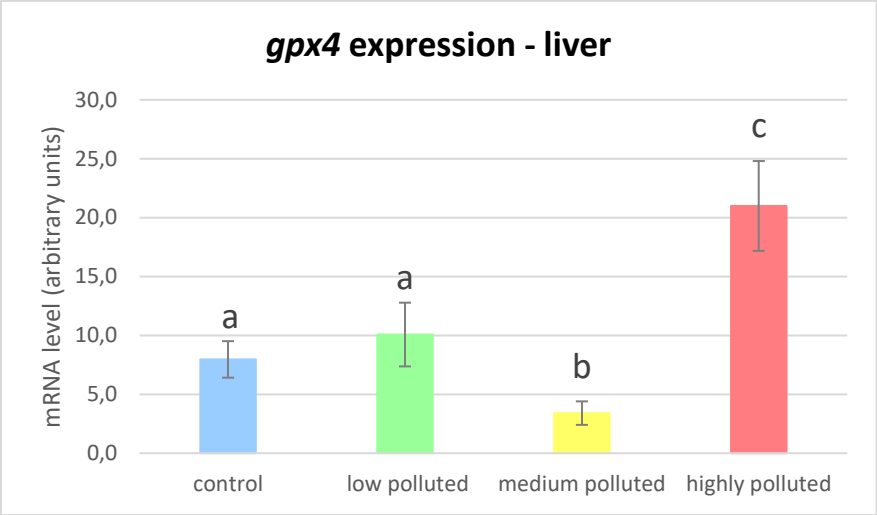

Figure 4.12) gpx4 mRNA expression in the liver of specimens from the four sites, with relative standard deviations (control site n=7, low-polluted site n=5, medium-polluted site n=7, highly-polluted site n=5). Different letters indicate statistically significant differences (p-value < 0.01) among sites.

Table 4.15). Levene's test result refers to gpx4 expression levels in the liver. Variances show no statistically significant difference (p-value > 0.05) among sites.

Test for Equality of Variances (Levene's) ▼

F	df1	df2	p
2.515	3.000	20.000	0.088

Table 4.16) ANOVA test result, referred to gpx4 mRNA expression levels in the liver. Means show statistically significant differences (p-value < 0.001) among sites.

ANOVA - 2^-ΔΔCt ▼

Cases	Sum of Squares	df	Mean Square	F	p
Site	936.484	3	312.161	57.884	< .001
Residuals	107.857	20	5.393		

Table 4.17) Tukey's test results referred to gpx4 mRNA expression levels in the liver. The means for all the sites were compared to each other. (SE is the standard error while t is the fraction between the mean difference and SE).

Post Hoc Comparisons - Site

		Mean Difference	SE	t	P_{tukey}
Control	(Low-polluted)	−2.112	1.360	−1.553	0.426
	(Medium-polluted)	4.560	1.241	3.674	0.008**
	(Highly-polluted)	−13.026	1.360	−9.580	< .001***
(Low-polluted)	(Medium-polluted)	6.672	1.360	4.907	< .001***
	(Highly-polluted)	−10.914	1.469	−7.431	< .001***
(Medium-polluted)	(Highly-polluted)	−17.587	1.360	−12.934	< .001***

In the case of the caudal kidney (Figure 4.13), there is a significant difference ($p < 0.01$) between the *gpx4* mRNA expression levels for the control site and those for the low/highly-polluted sites, showing an increase of 109% and 147% in expression levels, respectively. No statistically significant difference was detected between the control and medium-polluted sites (Table 4.18). Also, in this case, Levene's test indicated no significant difference between variances for each site; therefore, the ANOVA test was performed (Table 4.19 and Table 4.20).

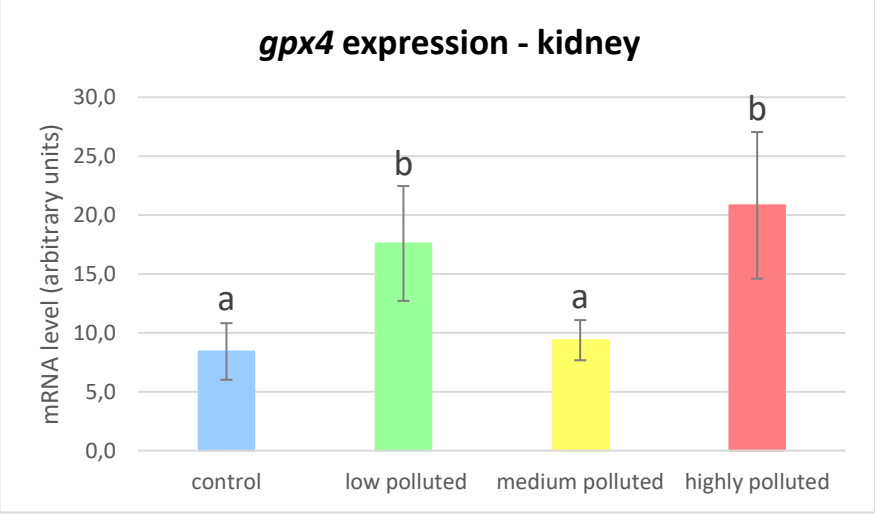

Figure 4.13) gpx4 mRNA expression in the caudal kidney of specimens from the four sites, with relative standard deviations (control site n=5, low-polluted site n=7, medium-polluted site n=7, highly-polluted site n=5). Different letters indicate statistically significant differences (p-value < 0.01) among sites.

Table 4.18). Levene's test result referred to gpx4 mRNA expression levels in the caudal kidney. Variances show no statistically significant difference (p-value > 0.05) among sites.

Test for Equality of Variances (Levene's)

F	df1	df2	p
2.387	3.000	20.000	0.099

Table 4.19) ANOVA test result, referred to gpx4 mRNA expression levels in the caudal kidney. Means show statistically significant differences (p-value < 0.001) among sites.

ANOVA - 2^-ΔΔCt

Cases	Sum of Squares	df	Mean Square	F	p
Site	628.250	3	209.417	12.380	< .001
Residuals	338.315	20	16.916		

Table 4.20) Tukey's test results referred to gpx4 mRNA expression levels in the caudal kidney. The means for all the sites were compared to each other. (SE is the standard error while t is the fraction between the mean difference and SE).

Post Hoc Comparisons - Site

		Mean Difference	SE	t	p_{tukey}
Control	(Low-polluted)	−9.168	2.408	−3.807	0.006**
	(Medium-polluted)	−0.959	2.408	−0.398	0.978
	(Highly-polluted)	−12.407	2.601	−4.770	< .001***
(Low-polluted)	(Medium-polluted)	8.209	2.198	3.734	0.007**
	(Highly-polluted)	−3.238	2.408	−1.345	0.547
(Medium-polluted)	(Highly-polluted)	−11.447	2.408	−4.753	< .001***

4.3.3 *cat*

The *cat* mRNA expression levels in the liver are shown in Figure 4.14. Also, in this case, Levene's test didn't indicate a significant difference between the variances of the sites; therefore, the ANOVA test was performed (Table 4.21 and Table 4.22). For the low-polluted site, a statistically significant ($p < 0.05$) decrease of 39% in *cat* transcription levels resulted from the comparison to those for the control site; the highly-polluted site presented, in transcription levels, a statistically significant (p-value < 0.05) increase, of 46%, if compared to the control site (Table 4.23).

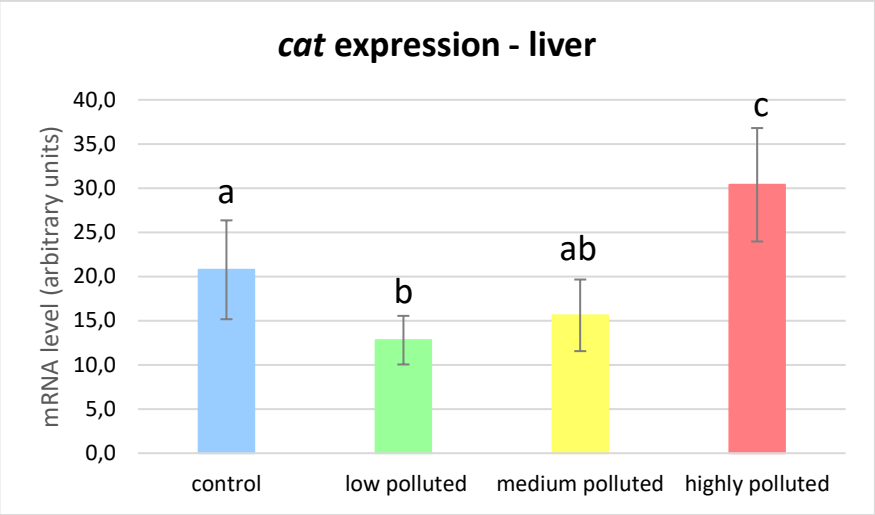

Figure 4.14) cat mRNA expression in the liver of specimens from the four sites, with relative standard deviations (control site n=6, low-polluted site n=8, medium-polluted site n=6, highly-polluted site n=6). Different letters indicate statistically significant differences (p-value < 0.05) among sites.

Table 4.21) Levene's test result referred to cat mRNA expression levels in the liver. Variances among sites show no statistically significant difference (p-value > 0.05).

Test for Equality of Variances (Levene's) ▼

F	df1	df2	p
1.162	3.000	22.000	0.347

Table 4.22) ANOVA test result, referred to cat mRNA expression levels in the liver. Means show statistically significant differences (p-value < 0.001) among sites.

ANOVA - 2^-△△Ct ▼

Cases	Sum of Squares	df	Mean Square	F	p
Site	1170.327	3	390.109	17.240	< .001
Residuals	497.813	22	22.628		

Table 4.23) Tukey's test results referred to cat mRNA expression levels in the liver. The means for all the sites were compared to each other. (SE is the standard error while t is the fraction between the mean difference and SE).

Post Hoc Comparisons - Site

		Mean Difference	SE	t	P_{tukey}
Control	(Low-polluted)	7.967	2.569	3.101	0.025*
	(Medium-polluted)	5.155	2.746	1.877	0.266
	(Highly-polluted)	−9.623	2.746	−3.504	0.010*
(Low-polluted)	(Medium-polluted)	−2.812	2.569	−1.095	0.696
	(Highly-polluted)	−17.590	2.569	−6.847	< .001***
(Medium-polluted)	(Highly-polluted)	−14.777	2.746	−5.381	< .001***

For the *cat* mRNA expression levels in the caudal kidney, Levene's test didn't indicate a significant difference between the variances of the sites; therefore, the ANOVA test was performed (Table 4.24 and Table 4.25). Results are shown in Figure 4.15, with no statistically significant differences between the control site and the low/medium-polluted ones; conversely, a statistically significant (p-value < 0.05) increase of 56% in *cat* mRNA expression levels is shown in the graph for the highly-polluted site. No statistically significant difference resulted between the control and medium-polluted sites (Table 4.26).

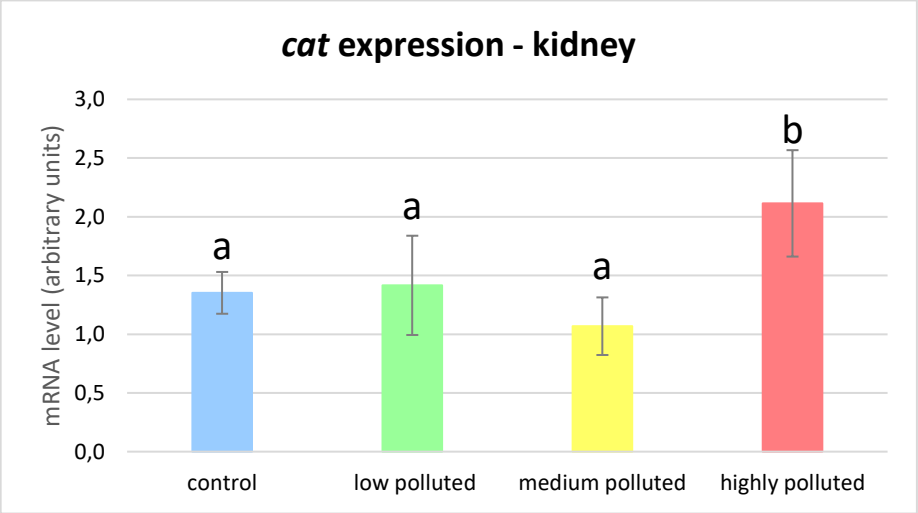

Figure 4.15) cat mRNA expression in the caudal kidney of specimens from the four sites, with the relative standard deviations (control site n=5, low-polluted site n=5, medium-polluted site n=6, highly-polluted site n=5). Different letters indicate statistically significant differences (p-value < 0.05) among sites.

Table 4.24). Levene's test result referred to cat mRNA expression levels in the caudal kidney. Variances show no statistically significant difference (p-value > 0.05) among sites.

Test for Equality of Variances (Levene's)

F	df1	df2	p
1.721	3.000	17.000	0.201

Table 4.25) ANOVA test result referred to cat mRNA expression levels in the caudal kidney. Means show statistically significant differences (p-value < 0.001) among sites.

ANOVA - 2^-ΔΔCt ▼

Cases	Sum of Squares	df	Mean Square	F	p
Site	3.127	3	1.042	9.026	< .001
Residuals	1.963	17	0.115		

Note. Type III Sum of Squares

Table 4.26). Tukey's test results referred to cat mRNA expression levels in the caudal kidney. The means for all the sites were compared to each other. (SE is the standard error while t is the fraction between the mean difference and SE).

Post Hoc Comparisons - Site

		Mean Difference	SE	t	p_{tukey}
Control	(Low-polluted)	−0.064	0.215	−0.297	0.991
	(Medium-polluted)	0.284	0.206	1.380	0.528
	(Highly-polluted)	−0.762	0.215	−3.545	0.012*
(Low-polluted)	(Medium-polluted)	0.348	0.206	1.691	0.359
	(Highly-polluted)	−0.698	0.215	−3.248	0.022*
(Medium-polluted)	(Highly-polluted)	−1.046	0.206	−5.083	< .001***

4.3.4 *ttp*

The expression levels of *ttp* in the liver are shown in Figure 4.16, with a statistically significant difference (p-value < 0.001) between the control site and the three polluted sites. In all the polluted sites, a decrease in the transcription levels with respect to the control site was measured: 74% for the low-polluted site, 69% for the medium-polluted site, and 80% for the highly-polluted site (Table 4.27). Also, in this case, Levene's test, no significant difference between the variances of the different sites was revealed, so the ANOVA was performed (Table 4.28 and Table 4.29).

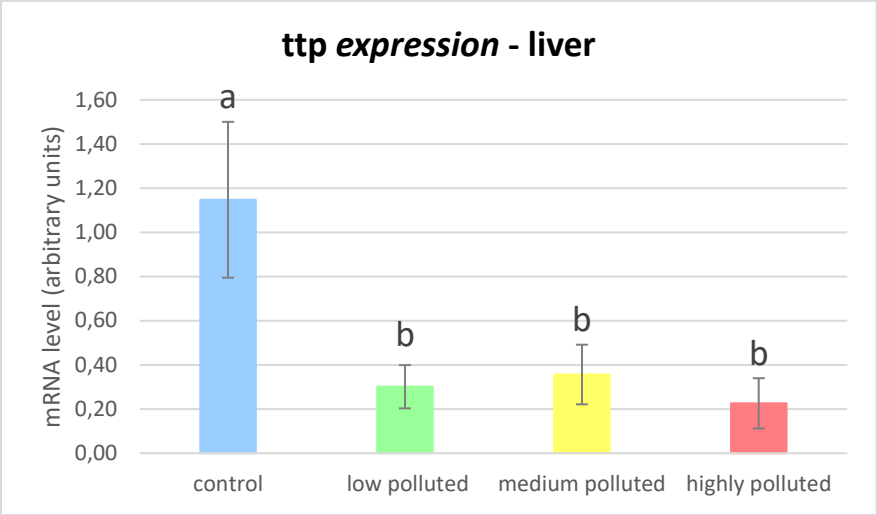

Figure 4.16) ttp mRNA expression in the liver of specimens from the four sites, with relative standard deviations (control site n=7, low-polluted site n=8, medium-polluted site n=6, highly-polluted site n=7). Different letters indicate statistically significant differences (p-value < 0.001) among sites.

Table 4.27) Levene's test result referred to ttp mRNA expression levels in the liver. Variances show no statistically significant difference (p-value > 0.05) among sites.

Test for Equality of Variances (Levene's) ▼

F	df1	df2	p
1.034	3.000	24.000	0.395

Table 4.28) ANOVA test result referred to ttp mRNA expression levels in the liver. Means show statistically significant differences (p-value < 0.001) among sites.

ANOVA - 2^-ΔΔCt ▼

Cases	Sum of Squares	df	Mean Square	F	p
Site	3.901	3	1.300	31.754	< .001
Residuals	0.983	24	0.041		

Table 4.29) Tukey's test results referred to ttp mRNA expression levels in the liver. The means for all the sites were compared to each other. (SE is the standard error while t is the fraction between the mean difference and SE).

Post Hoc Comparisons - Site

		Mean Difference	SE	t	p_{tukey}
Control	(Low-polluted)	0.846	0.105	8.082	< .001***
	(Medium-polluted)	0.791	0.113	7.028	< .001***
	(Highly-polluted)	0.922	0.108	8.521	< .001***
(Low-polluted)	(Medium-polluted)	−0.055	0.109	−0.505	0.957
	(Highly-polluted)	0.075	0.105	0.718	0.889
(Medium-polluted)	(Highly-polluted)	0.130	0.113	1.159	0.658

Results for *ttp* mRNA expression levels in the caudal kidney are reported in Figure 4.17. Also, in this case, a statistically significant (p-value < 0.01) decrease in the means for the low-polluted site and highly-polluted site (respectively 73% and 71%) compared to the control site was measured. Table 4.32 shows no statistically significant differences between the control site and the medium-polluted one.
The ANOVA test was performed (Table 4.31), considering that the p-value result according to Levene's test was > 0.05 (Table 4.30).

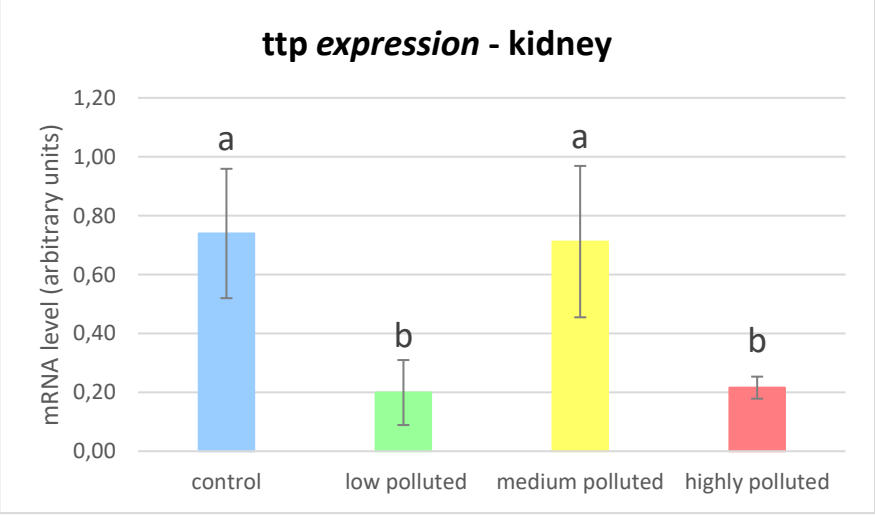

Figure 4.17) ttp mRNA expression in the caudal kidney of specimens from the four sites, with relative standard deviations (control site n=5, low-polluted site n=5, medium-polluted site n=5, highly-polluted site n=5). Different letters indicate statistically significant differences (p-value < 0.01) among sites.

Table 4.30) Levene's test result referred to ttp mRNA expression levels in the caudal kidney. Variances show no statistically significant difference (p-value > 0.05) among sites.

Test for Equality of Variances (Levene's)

F	df1	df2	p
1.719	3.000	16.000	0.203

Table 4.31) ANOVA test result referred to ttp mRNA expression levels in the caudal kidney. Means show statistically significant differences (p-value < 0.001) among sites.

ANOVA - 2^-ΔΔCt ▼

Cases	Sum of Squares	df	Mean Square	F	p
Site	1.345	3	0.448	14.013	< .001
Residuals	0.512	16	0.032		

Table 4.32) Tukey's test results referred to ttp mRNA expression levels in the caudal kidney. The means for all the sites were compared to each other. (SE is the standard error while t is the fraction between the mean difference and SE).

Post Hoc Comparisons - Site

		Mean Difference	SE	t	P_{tukey}
Control	(Low-polluted)	0.540	0.113	4.776	0.001**
	(Medium-polluted)	0.028	0.113	0.244	0.995
	(Highly-polluted)	0.524	0.113	4.629	0.001**
(Low-polluted)	(Medium-polluted)	−0.513	0.113	−4.532	0.002**
	(Highly-polluted)	−0.017	0.113	−0.147	0.999
(Medium-polluted)	(Highly-polluted)	0.496	0.113	4.385	0.002**

4.3.5 *g3bp*

The results of *g3bp* mRNA expression in the liver are shown in Figure 4.18. The Levene's test didn't indicate a statistically significant difference between the variances of the sites; therefore, the ANOVA was performed (Table 4.33 and Table 4.34). No statistically significant differences were found between the control site and the low-polluted/highly-polluted ones in the transcription levels; a statistically significant (p-value < 0.05) decrease of 90% in the medium-polluted site compared to the control one was measured (Table 4.35).

Figure 4.18) g3bp mRNA expression in the liver of specimens from the four sites, with relative standard deviations (control site n=5, low-polluted site n=5, medium-polluted site n=6, highly-polluted site n=5). Different letters indicate statistically significant differences (p-value < 0.05) among sites.

Table 4.33) Levene's test result referred to g3bp mRNA expression levels in the liver. Variances show no statistically significant difference (p-value > 0.05) among sites.

Test for Equality of Variances (Levene's)

F	df1	df2	p
3.120	3.000	18.000	0.052

Table 4.34) ANOVA test result referred to g3bp mRNA expression levels in the liver. Means show statistically significant differences (p-value < 0.001) among sites.

ANOVA - 2^-ΔΔCt

Cases	Sum of Squares	df	Mean Square	F	p
Site	5.875	3	1.958	15.652	< .001
Residuals	2.252	18	0.125		

Table 4.35) Tukey's test results referred to g3bp mRNA expression levels in the liver. The means for all the sites were compared to each other. (SE is the standard error while t is the fraction between the mean difference and SE).

Post Hoc Comparisons - Site

		Mean Difference	SE	t	p_{tukey}
Control	(Low-polluted)	−0.582	0.214	−2.718	0.062
	(Medium-polluted)	0.863	0.204	4.228	0.003**
	(Highly-polluted)	0.185	0.214	0.864	0.823
(Low-polluted)	(Medium-polluted)	1.446	0.214	6.749	< .001***
	(Highly-polluted)	0.767	0.224	3.429	0.014*
(Medium-polluted)	(Highly-polluted)	−0.679	0.214	−3.168	0.025*

Results for *g3bp* mRNA expression levels in the caudal kidney are reported in Figure 4.19. In this case, no statistically significant (p-value < 0.01) difference was measured between the means for the low-polluted and medium-polluted sites compared to the control sites. Table 4.38 shows a statistically significant difference between the control site and the highly-polluted one, and a decrease of 75.1% was measured in the polluted site.

The ANOVA test was performed (Table 4.37), considering that the p-value result according to Levene's test was > 0.05 (Table 4.36).

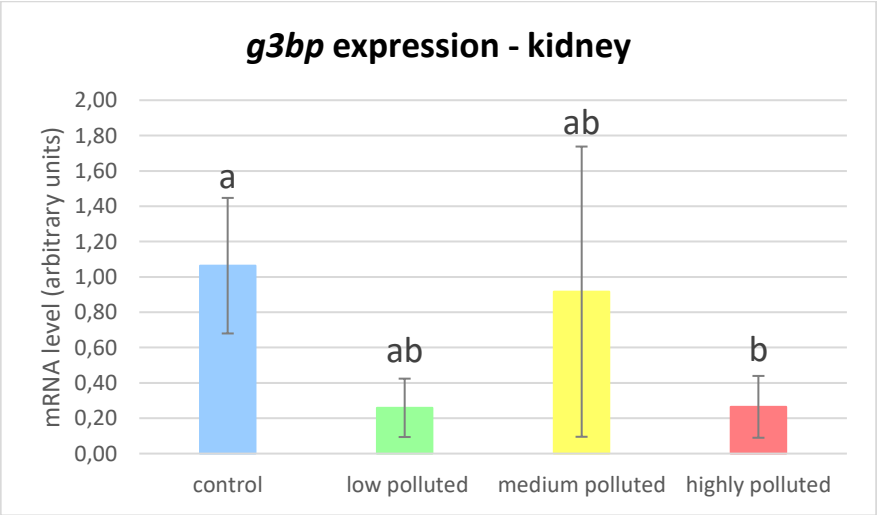

Figure 4.19) g3bp mRNA expression in the caudal kidney of specimens from the four sites, with relative standard deviations (control site n=5, low-polluted site n=5, medium-polluted site n=5, highly-polluted site n=6). Different letters indicate statistically significant differences (p-value < 0.05) among sites.

Table 4.36). Levene's test result referred to g3bp mRNA expression levels in the caudal kidney. Variances show no statistically significant difference (p-value > 0.05) among sites.

Test for Equality of Variances (Levene's)

F	df1	df2	p
3.142	3.000	17.000	0.052

Table 4.37) ANOVA test result referred to g3bp mRNA expression levels in the caudal kidney. Means show statistically significant differences (p-value < 0.001) among sites.

ANOVA - 2^-△△Ct

Cases	Sum of Squares	df	Mean Square	F	p
Site	2.830	3	0.943	4.519	0.017
Residuals	3.549	17	0.209		

Note. Type III Sum of Squares

Table 4.38). Tukey's test results referred to g3bp mRNA expression levels in the caudal kidney. The means for all the sites were compared to each other. (SE is the standard error while t is the fraction between the mean difference and SE).

Post Hoc Comparisons - Site

		Mean Difference	SE	t	P_{tukey}
Control	(Low-polluted)	0.805	0.289	2.784	0.056
	(Medium-polluted)	0.147	0.289	0.509	0.956
	(Highly-polluted)	0.799	0.277	2.888	0.046*
(Low-polluted)	(Medium-polluted)	−0.658	0.289	−2.275	0.143
	(Highly-polluted)	−0.006	0.277	−0.020	1.000
(Medium-polluted)	(Highly-polluted)	0.652	0.277	2.356	0.124

4.3.6 *tiar*

The results of *tiar* mRNA expression levels in the caudal kidney are shown in Figure 4.20. The Levene's test didn't indicate a statistically significant difference between the variances of the sites; therefore, the ANOVA test was performed (Table 4.39 and Table 4.40). No statistically significant difference was found between the control site and the polluted ones in transcription levels, according to the Tukey test, despite what resulted from the ANOVA test (p-value < 0.05) (Table 4.41).

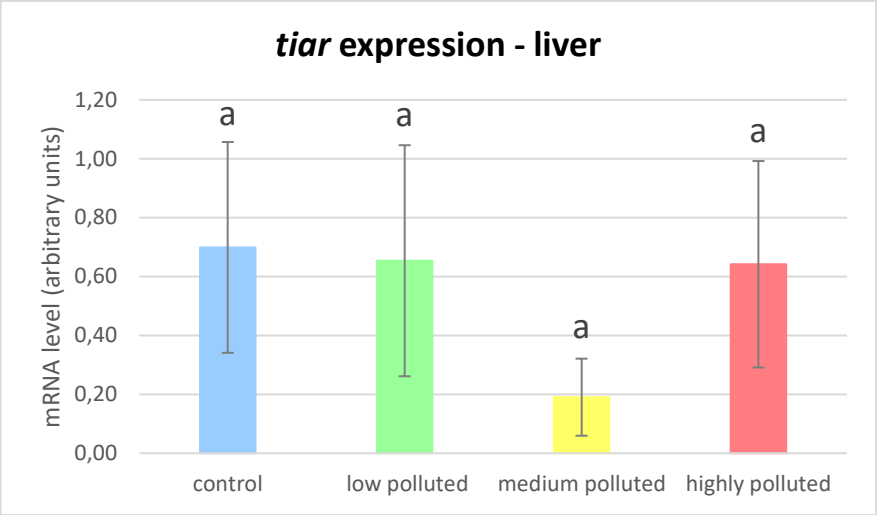

Figure 4.20) tiar mRNA expression in the liver of specimens from the four sites, with relative standard deviations (control site n=6, low-polluted site n=5, medium-polluted site n=6, highly-polluted site n=5). Different letters indicate no statistically significant differences (p-value > 0.05) among sites.

Table 4.39) Levene's test result referred to tiar mRNA expression levels in the liver. Variances show no statistically significant difference (p-value > 0,05) among sites.

Test for Equality of Variances (Levene's)

F	df1	df2	p
2.463	3.000	18.000	0.096

Table 4.40) ANOVA test result referred to tiar mRNA expression levels in the liver. Means show statistically significant differences (p-value < 0.05) among sites.

ANOVA - 2^-ΔΔCt

Cases	Sum of Squares	df	Mean Square	F	p
Site	1.001	3	0.334	3.277	0.045
Residuals	1.833	18	0.102		

Table 4.41) Tukey's test results referred to tiar mRNA expression levels in the liver. The means for all the sites were compared to each other. (SE is the standard error while t is the fraction between the mean difference and SE).

Post Hoc Comparisons - Site

		Mean Difference	SE	t	p_{tukey}
Control	(Low-polluted)	−0.582	0.214	−2.718	0.062
	(Medium-polluted)	0.863	0.204	4.228	0.003**
	(Highly-polluted)	0.185	0.214	0.864	0.823
(Low-polluted)	(Medium-polluted)	1.446	0.214	6.749	< .001***
	(Highly-polluted)	0.767	0.224	3.429	0.014*
(Medium-polluted)	(Highly-polluted)	−0.679	0.214	−3.168	0.025*

Results for *tiar* mRNA expression levels in the caudal kidney are reported in Figure 4.21. Also, in this case, no statistically significant (p-value < 0.01) difference was measured between the means for the polluted sites compared to the control site. The ANOVA test was performed (Table 4.43), considering that the p-value result according to Levene's test was > 0.05 (Table 4.42).

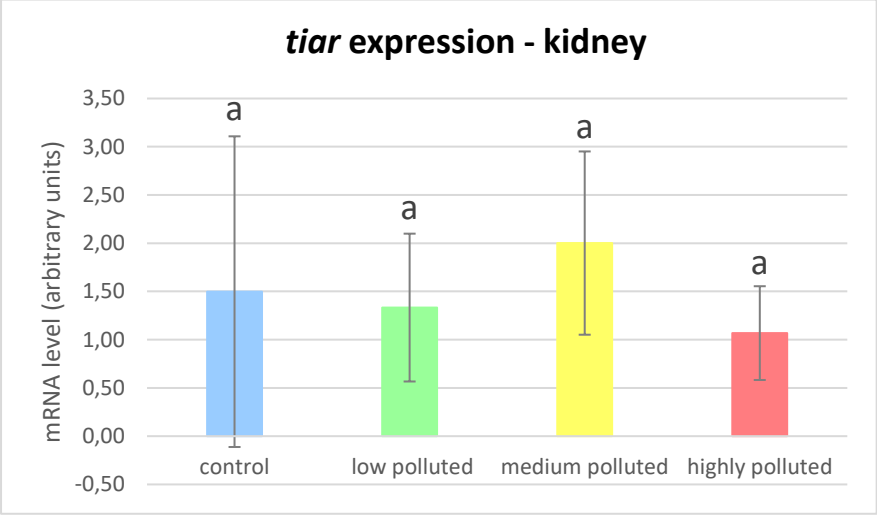

Figure 4.21) tiar mRNA expression in the caudal kidney of specimens from the four sites, with relative standard deviations (control site n=5, low-polluted site n=5, medium-polluted site n=5, highly-polluted site n=6). Different letters indicate no statistically significant differences (p-value > 0.05) among sites.

Table 4.42) Levene's test result referred to tiar mRNA expression levels in the caudal kidney. Variances show no statistically significant difference (p-value > 0,05) among sites.

Test for Equality of Variances (Levene's)

F	df1	df2	p
1.714	3.000	22.000	0.193

Table 4.43) ANOVA test result referred to tiar mRNA expression levels in the caudal kidney. Means show no statistically significant differences (p-value > 0.05) among sites.

Cases	Sum of Squares	df	Mean Square	F	p
Site	3.031	3	1.010	1.002	0.411
Residuals	22.187	22	1.009		

4.4 ENZYMATIC TISSUE ACTIVITY

Biochemical analyses compared the mRNA expression of the antioxidant enzymes CAT and GPx with their activity in liver and caudal kidney cell extract.

4.4.1 Se-GPx activity

Regarding the active Se-GPx total content inside the liver, a data transformation was necessary to perform the statistical tests. The Levene's test, ANOVA, and Tukey's test (Table 4.44, Table 4.45, and Table 4.46) were conducted on the logarithm of the values obtained with the biochemical assays. The results are depicted in Figure 4.22; the only statistically significant difference was observed between the low-polluted site and the medium-polluted one.

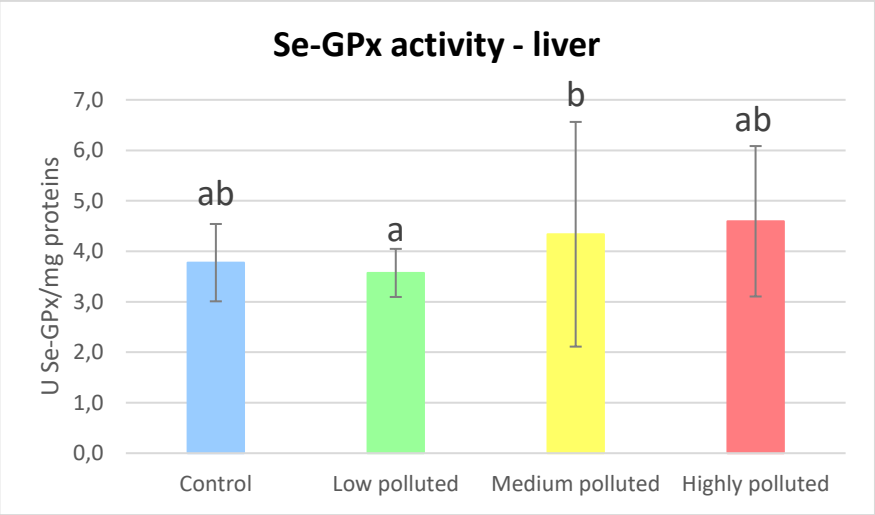

Figure 4.22) Means and standard deviations of the Se-GPx activity in the liver of specimens from the four sites (control site n=9, low-polluted site n=8, medium-polluted site n=9, highly-polluted site n=10). Different letters indicate statistically significant differences (p-value < 0,05).

Table 4.44) Levene's test resul treferred to Se-GPx activity levels in the liver. The variances of different sites have no statistically significant difference (p-value > 0,05).

Test for Equality of Variances (Levene's)

F	df1	df2	p
2.841	3.000	29.000	0.055

Table 4.45) ANOVA result treferred to Se-GPx activity levels in the liver. The means of different sites have statistically significant differences (p-value < 0,05).

ANOVA - Column 3 ▼

Cases	Sum of Squares	df	Mean Square	F	p
Column 4	0.131	3	0.044	3.284	0.035
Residuals	0.386	29	0.013		

Table 4.46) Tukey's test results treferred to Se-GPx activity levels in the liver. All site means were compared, and different results were obtained. (SE is the standard error

while t is the fraction between the mean difference and SE).

Post Hoc Comparisons - Column 4

		Mean Difference	SE	t	P_{tukey}
Control	(Low-pollution)	0.018	0.056	0.320	0.988
	(Medium-pollution)	−0.155	0.061	−2.550	0.073
	(Highly-pollution)	−0.074	0.053	−1.403	0.508
(Low-pollution)	(Medium-pollution)	−0.173	0.062	−2.776	0.045*
	(Highly-pollution)	−0.092	0.055	−1.686	0.349
(Medium-pollution)	(Highly-pollution)	0.081	0.060	1.355	0.537

In the case of the caudal kidney, it was unnecessary to transform the data to perform the statistical analysis (Table 4.47, Table 4.48, and Table 4.49). The results are shown in Figure 4.23. No statistically significant difference was observed between the control and medium-polluted sites. Conversely, an increase of 42% was observed in the low-polluted site and 35% in the highly-polluted site, compared to the control site.

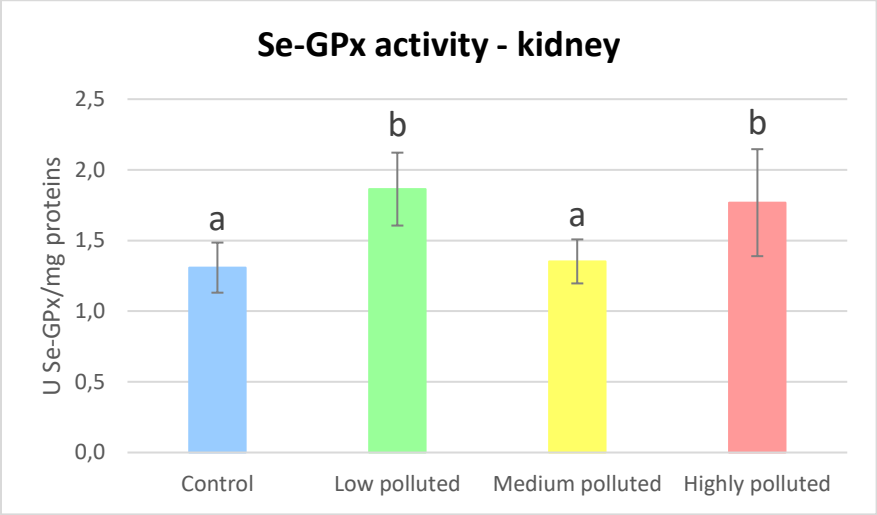

Figure 4.23) Means and standard deviations of the Se-GPx activity in the caudal kidney of specimens from the four sites (control site n=10, low-polluted site n=9, medium-polluted site n=7, highly-polluted site n=9). Different letters indicate statistically significant differences (p-value < 0,05).

Table 4.47) Levene's test result treferred to Se-GPx activity levels in the caudal kidney. The variances of different sites have no statistically significant difference (p-value > 0,05).

Test for Equality of Variances (Levene's)

F	df1	df2	p
2.131	3.000	31.000	0.116

Table 4.48) ANOVA result treferred to Se-GPx activity levels in the caudal kidney. The means of different sites have statistically significant differences (p-value < 0,001).

ANOVA - GPx (U GPX/ml) / (mg prot/ml) ▼

Cases	Sum of Squares	df	Mean Square	F	p
Site	2.155	3	0.718	10.559	< .001
Residuals	2.109	31	0.068		

Table 4.49) Tukey's test results treferred to Se-GPx activity levels in the caudal kidney. All site means were compared, and different results were obtained. (SE is the standard error while t is the fraction between the mean difference and SE).

Post Hoc Comparisons - Site

		Mean Difference	SE	t	P_{tukey}
Control	(Low-pollution)	−0.556	0.120	−4.643	< .001***
	(Medium-pollution)	−0.042	0.129	−0.327	0.988
	(Highly-pollution)	−0.460	0.120	−3.836	0.003**
(Low-pollution)	(Medium-pollution)	0.514	0.131	3.913	0.002**
	(Highly-pollution)	0.097	0.123	0.786	0.860
(Medium-pollution)	(Highly-pollution)	−0.418	0.131	−3.178	0.017*

4.4.2 CAT activity

The results of active CAT total content inside the liver are shown in Figure 4.24. ANOVA was performed after Levene's test (Table 4.50 and Table 4.51) to compare the means. No statistically significant differences were found between the control site and the polluted one, but there is a difference between the medium-polluted site and the low/highly-polluted ones (Table 4.52).

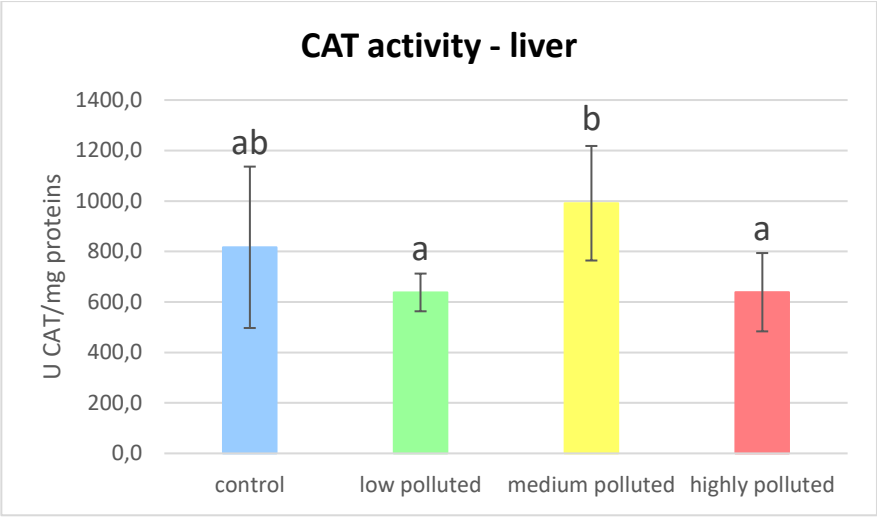

Figure 4.24) Means and standard deviations of the CAT activity in the liver of specimens from the four sites (control site n=7, low-polluted site n=9, medium-polluted site n=7,

highly-polluted site n=10). Different letters indicate statistically significant differences (p-value < 0,05).

Table 4.50) Levene's result treferred to CAT activity levels in the liver. The variances of different sites have no statistically significant difference (p-value > 0,05).

Test for Equality of Variances (Levene's) ▼

F	df1	df2	p
5.193	3.000	29.000	0.005

Table 4.51) ANOVA result treferred to CAT activity levels in the liver. The means of different sites have statistically significant differences (p-value < 0,01).

ANOVA - CAT (U GPX/ml) / (mg prot/ml) ▼

Cases	Sum of Squares	df	Mean Square	F	p
Site	675454.689	3	225151.563	5.516	0.004
Residuals	$1.184 \times 10^{+6}$	29	40819.830		

Table 4.52). Tukey's test result referred to CAT activity levels in the liver. All site means were compared, and different results were obtained. (SE is the standard error while t is the fraction between the mean difference and SE).

Post Hoc Comparisons - Site

		Mean Difference	SE	t	p_{tukey}
Control	(Low-polluted)	178.783	101.818	1.756	0.315
	(Medium-polluted)	−174.631	107.994	−1.617	0.385
	(Highly-polluted)	177.876	99.566	1.787	0.300
(Low-polluted)	(Medium-polluted)	−353.415	101.818	−3.471	0.008**
	(Highly-polluted)	−0.907	92.831	−0.010	1.000
(Medium-polluted)	(Highly-polluted)	352.507	99.566	3.540	0.007**

The active CAT total content inside the kidney is shown in Figure 4.25. In this case, the Levene's test and the ANOVA were also performed (Table 4.53 and Table 4.54). No statistical differences were observed between the control site and the low-polluted one. There is an increase in enzyme activity in the medium-polluted site (32%) and the highly-polluted one (39%) compared to the control site (Table 4.55).

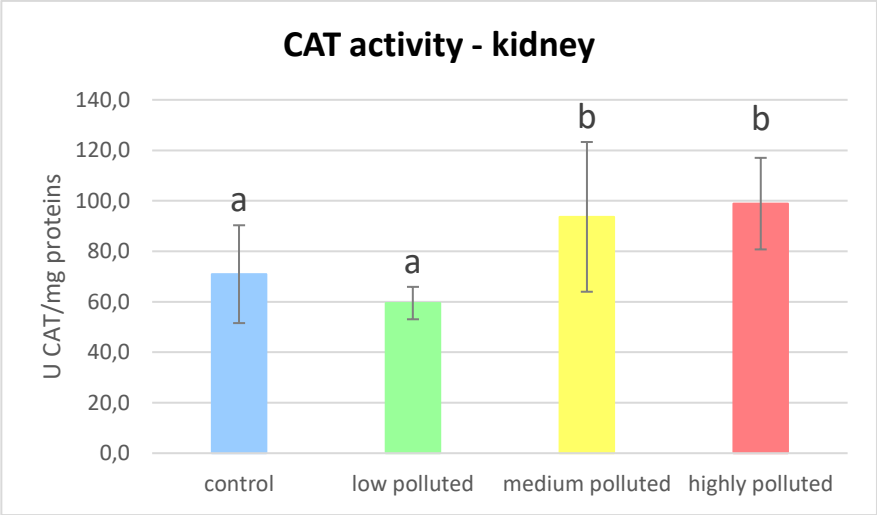

Figure 4.25) Means and standard deviations of the CAT activity in the caudal kidney of specimens from the four sites (control site n=9, low-polluted site n=9, medium-polluted site n=8, highly-polluted site n=9). Different letters indicate statistically significant differences (p-value < 0,05).

Table 4.53) Levene's test result referred to CAT activity levels in the caudal kidney. The variances of different sites have no statistically significant difference (p-value > 0,05).

Test for Equality of Variances (Levene's) ▼

F	df1	df2	p
2.212	3.000	31.000	0.106

Table 4.54) ANOVA result referred to CAT activity levels in the caudal kidney. The means of different sites have statistically significant differences (p-value < 0,001).

ANOVA - CAT (U GPX/ml) / (mg prot/ml)

Cases	Sum of Squares	df	Mean Square	F	p
Site	9218.416	3	3072.805	15.228	< .001
Residuals	6255.223	31	201.781		

Table 4.55) Tukey's test results referred to CAT activity levels in the caudal kidney. All site means were compared, and different results were obtained. (SE is the standard error while t is the fraction between the mean difference and SE).

Post Hoc Comparisons - Site

		Mean Difference	SE	t	P_{tukey}
Control	(Low-polluted)	11.444	6.696	1.709	0.336
	(Medium-polluted)	−22.702	6.902	−3.289	0.013*
	(Highly-polluted)	−27.951	6.696	−4.174	0.001**
(Low-polluted)	(Medium-polluted)	−34.146	6.902	−4.947	< .001***
	(Highly-polluted)	−39.396	6.696	−5.883	< .001***
(Medium-polluted)	(Highly-polluted)	−5.249	6.902	−0.761	0.871

5 DISCUSSION

As previously stated, the main focus of PFAS research is human health, whereas not much is known about the effect of this pollutant on freshwater fauna. Considering water as the main polluted matrix in the Veneto region, investigating the role of PFAS chronic exposure in *S. cephalus*, an endemic and cosmopolitan species in the region, can be interesting to understand the impact of those pollutants on the physiology of freshwater fauna and river's ecosystem.

Previous works in the laboratory where I did my master's thesis internship focused on studying the antioxidant responses to PFAS in *S. cephalus* (Vanzan, 2024). From those experiments, it was pointed out that there was an impairment between the mRNA levels of some analysed genes (*gpx1*, *gpx4*, and *cat*) and the activity of the corresponding enzymes in the kidney tissue. This impairment was not directly attributable to the different half-lives of the respective molecules. Therefore, it raised the hypothesis of a post-transcriptional regulation operated by some mRNA-mRNA binding protein complexes in the cells called SGs (Drago et al., 2021).

The results obtained in this research aim to understand more in-depth the physiological responses induced by PFAS at the level of the antioxidant system in *S. cephalus* and to evaluate a possible correlation between these responses and the presence of SGs, as previously detected in eukaryotic cells by another research group (Takahashi et al., 2013).

Initially, three somatic indices were evaluated to have a general idea of the well-being of the specimens of *S. cephalus* sampled in sites at different PFAS impacts.

Regarding the hepatosomatic index, liver size was increased in fish from medium and highly-polluted sites. This result aligns with previous studies, where lower PFAS concentrations were evaluated (Piva, 2021), so the hepatosomatic index probably grows proportionally to the pollutant concentration increase. The liver accumulates lipids in the hepatocytes during stress conditions, a condition known as "hepatic steatosis". Previous studies on mice (Attema et al., 2022) exposed to low PFAS concentration and zebrafish (Cheng et al., 2016) chronically exposed to PFOS detected hepatic steatosis.

Probably, the liver is not the only organ to be affected by a weight increase consequent to PFAS exposure, considering that Fulton's Condition Factor revealed,

in my studies, an increase also in total body weight in *S. cephalus* specimens collected from the medium and highly-polluted sites. An element in favour of the hypothesis on lipid accumulation in different organs is the downregulation of the peroxiredoxin 4 gene (*prdx4*) previously measured in my lab in *S. cephalus* kidney, chronically exposed to PFAS (Vanzan, 2024). This antioxidant enzyme inhibits lipid accumulation in the cell (Yamada and Guo, 2018). The downregulation of the *prdx4* transcription levels could be carried out by the cells to accumulate more lipids, reducing hydrophilicity and making the interaction between PFAS and proteins less probable. This would happen because those substances have more affinity with proteins (Han et al., 2003).

The results of the Spleen Somatic Index differ: the highest values were detected in fish from the low-polluted site and the lowest values in fish from the highly-polluted site. The spleen is particularly interesting because it has a major role in regulating immunity. Previous studies evidenced a spleen weight decrease in mice exposed to PFOS (Wang et al., 2011), a decrease connected with an increase in liver weight; it was, consequently, supposed to be an adverse effect of PFOS on the immune system. Similar results were also found in zebrafish exposed to PFOA (Zhong et al., 2020). The spleen is also involved in erythropoiesis, the process of erythrocyte formation; in humans, this activity is carried out by bone marrow, but fish do not have it, so the head kidney is the main organ responsible for it. Spleen has a minor role in erythropoiesis, acting predominantly when the O_2 demand increases (Witeska, 2013). An increase in the spleen weight in the low-polluted site is presumably due to a significant erythrocyte formation or an induction of the immune response. Considering the hypotheses, it is presumable that spleen weight increases in the low-polluted site as a primary response to contrast PFAS effect. When this effect becomes too excessive for the organism (medium-polluted and highly-polluted sites), the spleen goes under stress, decreasing its mass. With this hypothesis, the spleen seems to have a minor role in PFAS defence when the concentration is high; therefore, the liver and the general accumulation of lipids better play this role.

Partial sequences of some SG-related genes were characterised for the first time in *S. cephalus*. This result allowed me to design *ad hoc* primers to study the target species' expression of *ttp*, *g3bp*, and *tiar*. In the present study, the presence of SGs

has been directly correlated with the expression of the above genes, encoding critical proteins for forming these complexes in the cell's cytoplasm. This assumption is based on a previous study (Drago et al., 2023) that directly correlated *tiar* mRNA expression with the presence of the relative protein.

The expression of *gpx1*, *gpx4* and *cat* measured in the liver was compared between the four sites considered, whether polluted or not by PFAS, and evaluated with the amount of active protein at each site. Particularly at the low-polluted sites, a decrease in *cat* gene transcription was found, but an equally evident decrease did not match this in active protein. The maintenance of constant CAT activity is probably related to the implementation of translation of the respective mRNA stored in the SGs, the release of which is produced by inhibition of the *ttp* gene. A similar situation occurs for *gpx4* in the medium-polluted site, but this time, the downregulation of *ttp* is accompanied by that of *g3bp*. At the highly-polluted site, there is an increase in both *cat* and *gpx4* mRNA expression, but without a corresponding increase in enzyme activity. In this case, the role of *g3bp* and *tiar* appears to be predominant, as they are not blocked in their expression and thus ensure SG-operated blockade of translation.

Unlike in the liver, in the caudal kidney, exposure to polluted environments induces an increase in CAT and GPx enzyme activity. In the low-polluted site, there is only an increase in GPx activity due to an upregulation of the *gpx4* gene and disassembly of SGs due to inhibition of the *ttp* gene. At the medium-polluted site, there is only an increase in CAT activity, but this corresponds neither to an accumulation of *cat* mRNA nor a downregulation of any of the three SGs-related genes. This finding is at odds with the hypothesis and will require further investigation. At the highly-polluted site, both antioxidant enzymes are induced, due to both increased transcription of the respective genes (*cat* and *gpx4*) and downregulation of *ttp* and *g3bp*.

Previous data demonstrated that the kidney is the second organ concerning PFAS accumulation (Savoca and Pace, 2021). The high GPx and CAT activity for the highly-polluted site could indicate a prevalent presence of H_2O_2, the ROS species for which these two enzymes are scavengers. Similar results were pointed out in previous studies (Vanzan, 2024).

GPx activity also increases in the low-polluted site but not in the medium-polluted one. There is the possibility that other antioxidant enzymes, such as peroxiredoxins, operate in these conditions. Antioxidant defences work in a complementary manner to each other: Godin and Ganrett (1992) previously correlated a low GPx activity with a high CAT activity. The opposite condition was pointed out in the liver of two Antarctic fish species, where high Se-GPx activity corresponded to lower CAT activity (Santovito et al., 2012). CAT typically plays a minor role at low H_2O_2 concentrations but becomes useful when this ROS increases (Regoli et al., 2005b). The hypothesis could be that CAT activity is enhanced when the oxidative stress increases (medium-polluted site) and GPx decreases. In the highly-polluted site, the oxidative stress could be so high that both enzymes get activated to better contrast those conditions. This hypothesis could be confirmed by the fact that in the liver, *cat* and *gpx4* also present a higher mRNA expression in the highly-polluted site, so it can be deduced that the specimens collected in this site seem to enhance all their antioxidant defences.
The unchanged *gpx1* mRNA expression in the kidney and liver could be explained by the fact that, like other GPx isoforms, GPx1 is predominantly expressed inside the cytoplasm, while GPx4 is the only one present inside mitochondria (Poli et al., 2018), that is considered one of the PFAS targets in zebrafish (Hagenaars et al., 2013); therefore, GPx1 probably is not the most important isoform in response to the stress caused by these pollutants.

An intriguing final observation is that in all cases, *gpx4* and *cat* have higher transcript levels in the highly-polluted site. These may accumulate inside mitochondria (*gpx4*) and peroxisomes (*cat*), serving as a defence mechanism against high PFAS concentrations to be protected and regulated in translation inside SGs. This last point is of utmost importance, especially when we consider that in the highly-polluted site, the average PFAS concentration above 1000 ng/l is characterized by variability over time. The fish likely accumulate the *gpx4* and *cat* transcripts in chronic stress conditions to protect themselves from future PFAS damage. This finding is a significant contribution to our understanding of the effects of PFAS on freshwater fauna and the river ecosystem.

Taken together, these results show that the expression of the three SG components is not homogeneous, and different protein components of SGs may take a priority role in blocking or releasing specific mRNAs.

How SGs recruit mRNAs is still under study. mRNAs can be recognised thanks to their sequence. For example, TIA proteins and G3BP can recognise C-rich and AU-rich elements thanks to their RRM domains (Cruz-Gallardo et al., 2014; Kang et al., 2021), and TTP can recognise AU-rich elements thanks to its zinc finger domains (López de Silanes et at., 2005). Other hypotheses are that SGs can recognise mRNAs according to the length of the transcript (Khong et al., 2017) or the timing of transcript expression (Glauninger et al., 2024). Considering the first hypothesis, the *gpx4* transcript may also be recruited inside the SGs by other proteins, not just those encoded by the studied genes. This would explain, for example, the increase in CAT activity at the medium-polluted site.

6 CONCLUSION

Understanding the effects of human activities on the environment is not just important, it's essential. This understanding not only helps us grasp the dynamics that occur in the various matrices but also sheds light on the feedback effect of these activities on human life itself. PFAS are of particular concern as pollutants due to their worldwide presence, propensity for transport, bioaccumulation, environmental persistence and potential toxicity. Since the discovery of the harmful effects of these contaminants, numerous researches have been conducted to understand how they move inside the environment, at what concentration they result in danger to human health, and how they can be removed from various matrices, but knowledge is still incomplete. The purpose of the current study was to contribute to filling, in part, this knowledge gap by understanding the effects of PFAS on freshwater fauna, which is crucial to evaluate the impact of those contaminants on the river ecosystem. Our research underscores the significance of this purpose and the importance of our findings.

The results obtained in my thesis are partially in line with those expected. The chronic effect of PFAS on the antioxidant system of freshwater fish has been investigated, and the correlation between this and SG assembly/disassembly was partially detected. Liver and kidney tissues have been used to better understand this correlations. In both tissues, PFAS seems to trigger a response in the antioxidant system, with the involvement of *gpx4* and *cat* in *S. cephalus* specimens sampled from the highly-polluted site.

In these fish, the regulation of SG disassembly has been hypothesised, especially in the caudal kidney, with the decrease of *ttp* and *g3bp* mRNA levels and probably of the related protein.

During the dissection activity, other organs have been sampled. Therefore, future research could be focused on analysing the PFAS effect and SGs presence, for example, in the gills, which turned out to be one of the main organs in PFAS accumulation at low concentrations (Piva, 2022).

Only three SG-related genes have been considered in this study (*ttp*, *tiar* and *g3bp*), so, in the future, it will be interesting to evaluate the expression of other SG components, both at the transcriptional level and protein level. Concerning this last point, SGs could be visualised in *S. cephalus* liver and kidney by confocal/electron

microscopy with the colocalisation of antibodies specific for crucial protein components of SGs, including those mentioned in this study. Instead, *gpx4* and *cat* mRNAs inside SGs could be visualised using the in situ hybridisation technique.
For *ttp, tiar* and *g3bp,* partial nucleotide sequence was obtained for the first time in *S. cephalus* by sequencing, paving the way for future studies on the molecular evolution of these genes, for example, by phylogenetic analyses comparing orthologous sequences from different species.

In this study, two essential assumptions have been made. Firstly, we cannot exclude the presence of other stress sources in the sampled rivers, but we can say that the effects of other pollutants are supposed to be negligible. This affirmation is supported by ARPAV data, which did not detect other contaminants at relevant concentrations. Therefore, we can say that my results depend on PFAS contaminants. However, we cannot exclude that some other contaminants, even at very low concentrations, may have negatively affected fish. For this reason, future analyses in controlled laboratory conditions will be recommended. In those experiments, animals may be exposed to different concentrations of a single pollutant or a mix of various types. In this way, it will be possible to understand the effect of PFAS not influenced by the presence of other contaminants and also avoid the adverse effects of other environmental components, like pathogens and chemical-physical water characteristics (dissolved oxygen concentration, temperature, pH), on fish physiology. The second assumption is the direct correlation between river PFAS concentration and bioaccumulation inside organisms. Previous data (Piva et al., 2022) showed an impairment between PFAS concentration and bioaccumulation inside fish; therefore, analytical analysis will be performed on our samples to evaluate the accurate PFAS concentrations inside different organs. It is essential to directly correlate the induction of physiological responses in the organism to a stressor, particularly these specific pollutants.

7 REFERENCES

Anderson, P., & Kedersha, N. (2006). RNA granules. *Journal of Cell Biology*, *172*(6), 803–808.

Anderson, P., & Kedersha, N. (2009). RNA granules: Post-transcriptional and epigenetic modulators of gene expression. *Nature Reviews Molecular Cell Biology*, *10*(6), 430–436.

Arp, H. P. H., & Hale, S. E. (2022). Assessing the Persistence and Mobility of Organic Substances to Protect Freshwater Resources. *ACS Environmental Au*, *2*(6), 482–509.

Aruoma, O. I. (1998). Free radicals, oxidative stress, and antioxidants in human health and disease. *Journal of the American Oil Chemists' Society*, *75*(2), 199–212.

Attema, B., Janssen, A. W. F., Rijkers, D., van Schothorst, E. M., Hooiveld, G. J. E. J., & Kersten, S. (2022). Exposure to low-dose perfluorooctanoic acid promotes hepatic steatosis and disrupts the hepatic transcriptome in mice. *Molecular Metabolism*, *66*, 101602.

Ayala, A., Muñoz, M. F., & Argüelles, S. (2014). Lipid Peroxidation: Production, Metabolism, and Signaling Mechanisms of Malondialdehyde and 4-Hydroxy-2-Nonenal. *Oxidative Medicine and Cellular Longevity*, *2014*(1), 360438.

Balestrieri, A., Prigioni, C., Remonti, L., Sgrosso, S., & Priore, G. (2006). Feeding ecology of *Leuciscus cephalus* and *Rutilus rubilio* in southern Italy. *Italian Journal of Zoology*, *73*(2), 129–135.

Blackshear, P. J., Lai, W. S., Kennington, E. A., Brewer, G., Wilson, G. M., Guan, X., & Zhou, P. (2003). Characteristics of the Interaction of a Synthetic Human Tristetraprolin Tandem Zinc Finger Peptide with AU-rich Element-containing RNA Substrates. *Journal of Biological Chemistry*, *278*(22), 19947–19955.

Bohlin, T., Hamrin, S., Heggberget, T. G., Rasmussen, G., & Saltveit, S. J. (1989). Electrofishing—Theory and practice with special emphasis on salmonids. *Hydrobiologia*, *173*(1), 9–43.

Bonato, M., Corrà, F., Bellio, M., Guidolin, L., Tallandini, L., Irato, P., & Santovito, G. (2020). PFAS Environmental Pollution and Antioxidant Responses: An Overview of the Impact on Human Field. *International Journal of Environmental Research and Public Health*, *17*(21), Articolo 21.

Brigelius-Flohé, R., & Maiorino, M. (2013). Glutathione peroxidases. *Biochimica et Biophysica Acta (BBA) - General Subjects*, *1830*(5), 3289–3303.

Buchan, J. R., & Parker, R. (2009). Eukaryotic Stress Granules: The Ins and Outs of Translation. *Molecular Cell*, *36*(6), 932–941.

Buck, R. C., Franklin, J., Berger, U., Conder, J. M., Cousins, I. T., de Voogt, P., Jensen, A. A., Kannan, K., Mabury, S. A., & van Leeuwen, S. P. (2011). Perfluoroalkyl and polyfluoroalkyl substances in the environment: Terminology, classification, and origins. *Integrated Environmental Assessment and Management*, *7*(4), 513–541.

Burton, G. J., & Jauniaux, E. (2011). Oxidative stress. *Best Practice & Research Clinical Obstetrics & Gynaecology*, *25*(3), 287–299.

Chen, C. Y., Gherzi, R., Ong, S. E., Chan, E. L., Raijmakers, R., Pruijn, G. J., Stoecklin, G., Moroni, C., Mann, M., & Karin, M. (2001). AU binding proteins recruit the exosome to degrade ARE-containing mRNAs. *Cell*, *107*(4), 451–464.

Cheng, J., Lv, S., Nie, S., Liu, J., Tong, S., Kang, N., Xiao, Y., Dong, Q., Huang, C., & Yang, D. (2016). Chronic perfluorooctane sulfonate (PFOS) exposure induces hepatic steatosis in zebrafish. *Aquatic Toxicology*, *176*, 45–52.

Collard, F., Gasperi, J., Gilbert, B., Eppe, G., Azimi, S., Rocher, V., & Tassin, B. (2018). Anthropogenic particles in the stomach contents and liver of the freshwater fish *Squalius cephalus*. *Science of The Total Environment*, *643*, 1257–1264.

Cousins, I. T., DeWitt, J. C., Glüge, J., Goldenman, G., Herzke, D., Lohmann, R., Ng, C. A., Scheringer, M., & Wang, Z. (2020). The high persistence of PFAS is sufficient for their management as a chemical class. *Environmental Science. Processes & Impacts*, *22*(12), 2307–2312.

Cruz-Gallardo, I., Aroca, Á., Gunzburg, M. J., Sivakumaran, A., Yoon, J.-H., Angulo, J., Persson, C., Gorospe, M., Karlsson, B. G., Wilce, J. A., & Díaz-Moreno, I. (2014). The binding of TIA-1 to RNA C-rich sequences is driven by its C-terminal RRM domain. *RNA Biology*, *11*(6), 766–776.

Donnelly, N., Gorman, A. M., Gupta, S., & Samali, A. (2013). The eIF2α kinases: Their structures and functions. *Cellular and Molecular Life Sciences*, *70*(19), 3493–3511.

Drago, L., Perin, G., Santovito, G., & Ballarin, L. (2023). The stress granule component TIAR during the non-embryonic development of the colonial ascidian *Botryllus schlosseri*. *Fish & Shellfish Immunology*, *141*, 108999.

Drago, L., Anna, P., Nicola, F., Loriano, B., Rigers, B., & Gianfranco, S. (2021). Stress granules in *Ciona robusta*: First evidences of TIA-1-related nucleolysin and tristetraprolin gene expression under metal exposure. *Comparative Biochemistry and Physiology Part C: Toxicology & Pharmacology*, *243*, 108977.

Fenton, S. E., Ducatman, A., Boobis, A., DeWitt, J. C., Lau, C., Ng, C., Smith, J. S., & Roberts, S. M. (2021). Per- and Polyfluoroalkyl Substance Toxicity and Human Health Review: Current State of Knowledge and Strategies for Informing Future Research. *Environmental Toxicology and Chemistry*, *40*(3), 606–630.

Gamsjaeger, R., Liew, C. K., Loughlin, F. E., Crossley, M., & Mackay, J. P. (2007). Sticky fingers: Zinc-fingers as protein-recognition motifs. *Trends in Biochemical Sciences*, *32*(2), 63–70.

Giesy, J. P., & Kannan, K. (2001). Global distribution of perfluorooctane sulfonate in wildlife. *Environmental Science & Technology*, *35*(7), 1339–1342.

Glauninger, H., Bard, J. A. M., Wong Hickernell, C. J., Airoldi, E. M., Li, W., Singer, R. H., Paul, S., Fei, J., Sosnick, T. R., Wallace, E. W. J., & Drummond, D. A. (2024). Transcriptome-wide mRNA condensation precedes stress granule formation and excludes stress-induced transcripts. *bioRxiv*, 2024.04.15.589678

Glüge, J., Scheringer, M., T. Cousins, I., C. DeWitt, J., Goldenman, G., Herzke, D., Lohmann, R., A. Ng, C., Trier, X., & Wang, Z. (2020). An overview of the uses of per- and polyfluoroalkyl substances (PFAS). *Environmental Science: Processes & Impacts*, *22*(12), 2345–2373.

Godin, D. V., & Garnett, M. E. (1992). Species-related variations in tissue antioxidant status—I. Differences in antioxidant enzyme profiles. *Comparative Biochemistry and Physiology. B, Comparative Biochemistry*, *103*(3), 737–742.

Guillén-Boixet, J., Kopach, A., Holehouse, A. S., Wittmann, S., Jahnel, M., Schlüßler, R., Kim, K., Trussina, I. R. E. A., Wang, J., Mateju, D., Poser, I., Maharana, S., Ruer-Gruß, M., Richter, D., Zhang, X., Chang, Y.-T., Guck, J., Honigmann, A., Mahamid, J., Hyman, A. A., Pappu, R. V., Alberti, S., & Franzmann, T. M. (2020). RNA-Induced Conformational Switching and Clustering of G3BP Drive Stress Granule Assembly by Condensation. *Cell*, *181*(2), 346-361.e17.

Hagenaars, A., Vergauwen, L., Benoot, D., Laukens, K., & Knapen, D. (2013). Mechanistic toxicity study of perfluorooctanoic acid in zebrafish suggests mitochondrial dysfunction to play a key role in PFOA toxicity. *Chemosphere*, *91*(6), 844–856.

Hall, T. M. T. (2005). Multiple modes of RNA recognition by zinc finger proteins. *Current Opinion in Structural Biology*, *15*(3), 367–373.

Han, X., Snow, T. A., Kemper, R. A., & Jepson, G. W. (2003). Binding of Perfluorooctanoic Acid to Rat and Human Plasma Proteins. *Chemical Research in Toxicology*, *16*(6), 775–781.

Hirose, T., Ninomiya, K., Nakagawa, S., & Yamazaki, T. (2023). A guide to membraneless organelles and their various roles in gene regulation. *Nature Reviews Molecular Cell Biology*, *24*(4), 288–304.

Iqbal, M. J., Kabeer, A., Abbas, Z., Siddiqui, H. A., Calina, D., Sharifi-Rad, J., & Cho, W. C. (2024). Interplay of oxidative stress, cellular communication and signaling pathways in cancer. *Cell Communication and Signaling*, *22*(1), 7.

Ivanov, P., Kedersha, N., & Anderson, P. (2019). Stress Granules and Processing Bodies in Translational Control. *Cold Spring Harbor Perspectives in Biology*, *11*(5), a032813.

Jain, S., Wheeler, J. R., Walters, R. W., Agrawal, A., Barsic, A., & Parker, R. (2016). ATPase-Modulated Stress Granules Contain a Diverse Proteome and Substructure. *Cell*, *164*(3), 487–498.

Jomova, K., Raptova, R., Alomar, S. Y., Alwasel, S. H., Nepovimova, E., Kuca, K., & Valko, M. (2023). Reactive oxygen species, toxicity, oxidative stress, and antioxidants: Chronic diseases and aging. *Archives of Toxicology*, *97*(10), 2499–2574.

Kang, W., Wang, Y., Yang, W., Zhang, J., Zheng, H., & Li, D. (2021). Research Progress on the Structure and Function of G3BP. *Frontiers in Immunology*, *12*.

Kedersha, N., Chen, S., Gilks, N., Li, W., Miller, I. J., Stahl, J., & Anderson, P. (2002). Evidence that ternary complex (eIF2-GTP-tRNAiMet)-Deficient preinitiation complexes are core constituents of mammalian stress granules. *Molecular Biology of the Cell*, *13*(1), 195–210. Scopus.

Kedersha, N., Cho, M. R., Li, W., Yacono, P. W., Chen, S., Gilks, N., Golan, D. E., & Anderson, P. (2000). Dynamic shuttling of TIA-1 accompanies the recruitment of mRNA to mammalian stress granules. *The Journal of Cell Biology*, *151*(6), 1257–1268.

Kedersha, N. L., Gupta, M., Li, W., Miller, I., & Anderson, P. (1999). RNA-binding proteins TIA-1 and TIAR link the phosphorylation of eIF-2 alpha to the

assembly of mammalian stress granules. *The Journal of Cell Biology*, *147*(7), 1431–1442.

Khong, A., Matheny, T., Jain, S., Mitchell, S. F., Wheeler, J. R., & Parker, R. (2017). The Stress Granule Transcriptome Reveals Principles of mRNA Accumulation in Stress Granules. *Molecular Cell*, *68*(4), 808-820.e5.

Kim, H. S., Headey, S. J., Yoga, Y. M. K., Scanlon, M. J., Gorospe, M., Wilce, M. C. J., & Wilce, J. A. (2013). Distinct binding properties of TIAR RRMs and linker region. *RNA Biology*, *10*(4), 579–589.

Klug, A. (1999). Zinc finger peptides for the regulation of gene expression. *Journal of Molecular Biology*, *293*(2), 215–218.

Lai, W. S., Carballo, E., Strum, J. R., Kennington, E. A., Phillips, R. S., & Blackshear, P. J. (1999). Evidence that Tristetraprolin Binds to AU-Rich Elements and Promotes the Deadenylation and Destabilization of Tumor Necrosis Factor Alpha mRNA. *Molecular and Cellular Biology*, *19*(6), 4311–4323.

Lavut, A., & Raveh, D. (2012). Sequestration of highly expressed mRNAs in cytoplasmic granules, P-bodies, and stress granules enhances cell viability. *PLoS Genetics*, *8*(2), e1002527.

Lewis, A. J., Yun, X., Spooner, D. E., Kurz, M. J., McKenzie, E. R., & Sales, C. M. (2022). Exposure pathways and bioaccumulation of *per*- and polyfluoroalkyl substances in freshwater aquatic ecosystems: Key considerations. *Science of The Total Environment*, *822*, 153561.

Li, R., Jia, Z., & Trush, M. A. (2016). Defining ROS in Biology and Medicine. *Reactive oxygen species (Apex, N.C.)*, *1*(1), 9–21.

López de Silanes, I., Galbán, S., Martindale, J. L., Yang, X., Mazan-Mamczarz, K., Indig, F. E., Falco, G., Zhan, M., & Gorospe, M. (2005). Identification and functional outcome of mRNAs associated with RNA-binding protein TIA-1. *Molecular and Cellular Biology*, *25*(21), 9520–9531.

Lushchak, V. I. (2016). Contaminant-induced oxidative stress in fish: A mechanistic approach. *Fish Physiology and Biochemistry*, *42*(2), 711–747.

Lushchak, V. I., & Bagnyukova, T. V. (2006). Effects of different environmental oxygen levels on free radical processes in fish. *Comparative Biochemistry and Physiology Part B: Biochemistry and Molecular Biology*, *144*(3), 283–289.

Matsuki, H., Takahashi, M., Higuchi, M., Makokha, G. N., Oie, M., & Fujii, M. (2013). Both G3BP1 and G3BP2 contribute to stress granule formation. *Genes to Cells*, *18*(2), 135–146.

Mazroui, R., Sukarieh, R., Bordeleau, M.-E., Kaufman, R. J., Northcote, P., Tanaka, J., Gallouzi, I., & Pelletier, J. (2006). Inhibition of Ribosome Recruitment Induces Stress Granule Formation Independently of Eukaryotic Initiation Factor 2α Phosphorylation. *Molecular Biology of the Cell*, *17*(10), 4212–4219.

Murata, T., Yoshino, Y., Morita, N., & Kaneda, N. (2002). Identification of nuclear import and export signals within the structure of the zinc finger protein TIS11. *Biochemical and Biophysical Research Communications*, *293*(4), 1242–1247.

Nandi, A., Yan, L.-J., Jana, C. K., & Das, N. (2019). Role of Catalase in Oxidative Stress- and Age-Associated Degenerative Diseases. *Oxidative Medicine and Cellular Longevity*, *2019*, 9613090.

Noori, S. (2012). An Overview of Oxidative Stress and Antioxidant Defensive System. *Journal of Clinical & Cellular Immunology*, *01*.

Nover, L., Scharf, K. D., & Neumann, D. (1989). Cytoplasmic heat shock granules are formed from precursor particles and are associated with a specific set of mRNAs. *Molecular and Cellular Biology*, *9*(3), 1298–1308.

Panieri, E., Baralic, K., Djukic-Cosic, D., Buha Djordjevic, A., & Saso, L. (2022). PFAS Molecules: A Major Concern for the Human Health and the Environment. *Toxics*, *10*(2), 44.

Parker, F., Maurier, F., Delumeau, I., Duchesne, M., Faucher, D., Debussche, L., Dugue, A., Schweighoffer, F., & Tocque, B. (1996). A Ras-GTPase-Activating Protein SH3-Domain-Binding Protein. *Molecular and Cellular Biology*, *16*(6), 2561–2569.

Patrocinio, R. del V., & Europe, W. H. O. R. O. for. (2017). *Keeping our water clean: The case of water contamination in the Veneto Region, Italy*. World Health Organization. Regional Office for Europe.

Pellizzaro, A., Zaggia, A., Fant, M., Conte, L., & Falletti, L. (2018). Identification and quantification of linear and branched isomers of perfluorooctanoic and perfluorooctane sulfonic acids in contaminated groundwater in the veneto region. *Journal of Chromatography A*, *1533*, 143–154.

Pérez, F., Nadal, M., Navarro-Ortega, A., Fàbrega, F., Domingo, J. L., Barceló, D., & Farré, M. (2013). Accumulation of perfluoroalkyl substances in human tissues. *Environment International*, *59*, 354–362.

Pfaffl, M. W. (2001). A new mathematical model for relative quantification in real-time RT-PCR. *Nucleic Acids Research*, *29*(9), e45.

Pitter, G., Da Re, F., Canova, C., Barbieri, G., Zare Jeddi, M., Daprà, F., Manea, F., Zolin, R., Bettega, A. M., Stopazzolo, G., Vittorii, S., Zambelli, L., Martuzzi, M., Mantoan, D., & Russo, F. (2020). Serum Levels of Perfluoroalkyl Substances (PFAS) in Adolescents and Young Adults Exposed to Contaminated Drinking Water in the Veneto Region, Italy: A Cross-Sectional Study Based on a Health Surveillance Program. *Environmental Health Perspectives*, *128*(2), 27007.

Piva, E. (2021). Preliminary data on physiological responses induced by PFAS exposure in freshwater fish of the Veneto region. Master thesis, University of Padova.

Piva, E., Schumann, S., Dotteschini, S., Brocca, G., Radaelli, G., Marion, A., Irato, P., Bertotto, D., & Santovito, G. (2022). Antioxidant Responses Induced by PFAS Exposure in Freshwater Fish in the Veneto Region. *Antioxidants*, *11*(6), Articolo 6.

Poli, A., Fabbri, E., Agnisola, C., Calamita, G., Santovito, G., & Verri, T. (2018). Fisiologia animale. EdiSES.

Regoli, F., Nigro, M., Benedetti, M., Fattorini, D., & Gorbi, S. (2005). Antioxidant efficiency in early life stages of the Antarctic silverfish, *Pleuragramma antarcticum:* Responsiveness to pro-oxidant conditions of platelet ice and chemical exposure. *Aquatic Toxicology*, *75*(1), 43–52.

Reineke, L. C., & Lloyd, R. E. (2014). The Stress Granule Protein G3BP1 Recruits Protein Kinase R To Promote Multiple Innate Immune Antiviral Responses. *Journal of Virology*, *89*(5), 2575–2589.

Reineke, L. C., & Neilson, J. R. (2019). Differences between acute and chronic stress granules, and how these differences may impact function in human disease. *Biochemical Pharmacology*, *162*, 123–131.

Renfrew, D., & Pearson, T. W. (2021). The social life of the "forever chemical": PFAS pollution legacies and toxic events. *Environment and Society*, *12*(1), 146-163.

Santovito, G., Piccinni, E., Boldrin, F., & Irato, P. (2012). Comparative study on metal homeostasis and detoxification in two Antarctic teleosts. *Comparative Biochemistry and Physiology Part C: Toxicology & Pharmacology*, *155*(4), 580–586.

Santovito, G., Piccinni, E., Cassini, A., Irato, P., & Albergoni, V. (2005). Antioxidant responses of the Mediterranean mussel, *Mytilus galloprovincialis*, to environmental variability of dissolved oxygen. *Comparative Biochemistry and Physiology Part C: Toxicology & Pharmacology*, *140*(3), 321–329.

Sattin, G., Bakiu, R., Tolomeo, A. M., Carraro, A., Coppola, D., Ferro, D., Patarnello, T., & Santovito, G. (2015). Characterization and expression of a new cytoplasmic glutathione peroxidase 1 gene in the Antarctic fish *Trematomus bernacchii*. *Hydrobiologia*, *761*(1), 363–372.

Savoca, D., & Pace, A. (2021). Bioaccumulation, Biodistribution, Toxicology and Biomonitoring of Organofluorine Compounds in Aquatic Organisms. *International Journal of Molecular Sciences*, *22*(12), 6276.

Stoecklin, G., Stubbs, T., Kedersha, N., Wax, S., Rigby, W. F. C., Blackwell, T. K., & Anderson, P. (2004). MK2-induced tristetraprolin:14-3-3 Complexes prevent stress granule association and ARE-mRNA decay. *EMBO Journal*, *23*(6), 1313–1324.

Storey, K. B. (1996). Oxidative stress: Animal adaptations in nature. *Brazilian Journal of Medical and Biological Research = Revista Brasileira De Pesquisas Medicas E Biologicas*, *29*(12), 1715–1733.

Takahashi, M., Higuchi, M., Matsuki, H., Yoshita, M., Ohsawa, T., Oie, M., & Fujii, M. (2013). Stress Granules Inhibit Apoptosis by Reducing Reactive Oxygen Species Production. *Molecular and Cellular Biology*, *33*(4), 815–829.

Tourrière, H., Chebli, K., Zekri, L., Courselaud, B., Blanchard, J. M., Bertrand, E., & Tazi, J. (2023). The RasGAP-associated endoribonuclease G3BP mediates stress granule assembly. *The Journal of Cell Biology*, *222*(11).

Tourrière, H., Gallouzi, I. E., Chebli, K., Capony, J. P., Mouaikel, J., van der Geer, P., & Tazi, J. (2001). RasGAP-associated endoribonuclease G3Bp: Selective RNA degradation and phosphorylation-dependent localization. *Molecular and Cellular Biology*, *21*(22), 7747–7760.

Trenz, T. S., Delaix, C. L., Turchetto-Zolet, A. C., Zamocky, M., Lazzarotto, F., & Margis-Pinheiro, M. (2021). Going Forward and Back: The Complex Evolutionary History of the GPx. *Biology*, *10*(11), 1165.

Valko, M., Leibfritz, D., Moncol, J., Cronin, M. T. D., Mazur, M., & Telser, J. (2007). Free radicals and antioxidants in normal physiological functions and human disease. *The International Journal of Biochemistry & Cell Biology*, *39*(1), 44–84.

Vanzan, G. (2024). Antioxidant responses in kidney of *Squalius cephalus*, chronically exposed to PFAS in rivers of Veneto region. Master thesis, University of Padova.

Wang, Y., Wang, L., Liang, Y., Qiu, W., Zhang, J., Zhou, Q., & Jiang, G. (2011). Modulation of dietary fat on the toxicological effects in thymus and spleen

in BALB/c mice exposed to perfluorooctane sulfonate. *Toxicology Letters*, *204*(2), 174–182.

Wang, Z., DeWitt, J. C., Higgins, C. P., & Cousins, I. T. (2017). A Never-Ending Story of Per- and Polyfluoroalkyl Substances (PFASs)? *Environmental Science & Technology*, *51*(5), 2508–2518.

Waris, S., Wilce, M. C. J., & Wilce, J. A. (2014). RNA Recognition and Stress Granule Formation by TIA Proteins. *International Journal of Molecular Sciences*, *15*(12), 23377–23388.

Witeska, M. (2013). Erythrocytes in teleost fishes: A review. *Zoology and Ecology*, *23*(4), 275–281.

Xie, Z., & Kallenborn, R. (2023). Legacy and emerging per- and poly-fluoroalkyl substances in polar regions. *Current Opinion in Green and Sustainable Chemistry*, *42*, 100840.

Yamada, S., & Guo, X. (2018). Peroxiredoxin 4 (PRDX4): Its critical in vivo roles in animal models of metabolic syndrome ranging from atherosclerosis to nonalcoholic fatty liver disease. *Pathology International*, *68*(2), 91–101.

Yang, P., Mathieu, C., Kolaitis, R.-M., Zhang, P., Messing, J., Yurtsever, U., Yang, Z., Wu, J., Li, Y., Pan, Q., Yu, J., Martin, E. W., Mittag, T., Kim, H. J., & Taylor, J. P. (2020). G3BP1 Is a Tunable Switch that Triggers Phase Separation to Assemble Stress Granules. *Cell*, *181*(2), 325-345.e28.

Zareitalabad, P., Siemens, J., Hamer, M., & Amelung, W. (2013). Perfluorooctanoic acid (PFOA) and perfluorooctanesulfonic acid (PFOS) in surface waters, sediments, soils and wastewater – A review on concentrations and distribution coefficients. *Chemosphere*, *91*(6), 725–732.

Zhong, Y., Shen, L., Ye, X., Zhou, D., He, Y., & Zhang, H. (2020). Mechanism of immunosuppression in zebrafish (*Danio rerio*) spleen induced by environmentally relevant concentrations of perfluorooctanoic acid. *Chemosphere*, *249*, 126200.

8 WEBSITE REFERENCES

Secretariat of the Stockholm Convention (2022). Text od the Stockholm Convention.
https://www.pops.int/TheConvention/Overview/TextoftheConvention/tabid/2232/Default.aspx

Fishbase https://www.fishbase.se/summary/Squalius-cephalus.html

Fish.uk https://www.fish-uk.com/species_chub.htm

International Union for Conservation of Nature. IUCN.
https://www.iucnredlist.org/species/61205/19009224#habitat-ecology

Organisation for Economic Co-operation and Development. Terminoloygy of per- and polyfluoroalkyl substances

https://www.oecd.org/chemicalsafety/portal-perfluorinated chemicals/terminology-per-and-polyfluoroalkyl-substances.pdf

Regione del Veneto https://www.regione.veneto.it/web/sanita/pfas